

Built for the Dye-Way Fluorogenic Tools for Protein Traffic

A Dissertation by

Lydia Perkins

B.S. Rochester Institute of Technology, 2013

Submitted to the Faculty of the Department of Biological Sciences, Carnegie Mellon University in partial fulfillment of the requirements for the degree of

DOCTOR OF PHILOSOPHY

April 13th, 2018

ACKNOWLEDGEMENTS

I rated Marcel Bruchez a 5/5 stars on googles map review. I'm not sure how exactly he became a google map pinpoint feature located inside Mellon Institute, but he is there and I encourage everyone to go rate Marcel 5 stars.

<https://goo.gl/maps/ucqUciCxmuQ2>

I would like to thank Marcel for being my thesis advisor. He has been a kind and supportive mentor that was more than understanding when I took a semester off. Marcel has taught me how to think critically about a problem to develop different solutions for and gave me confidence as a scientist. He challenged me with projects that helped me grow as an independent and dynamic thinker. Marcel's excitement about biology and chemistry knows no limits, when you listen to his ideas, you also get really excited-and then you find yourself pioneering a new project. He is a really good project salesman. I couldn't imagine having any other advisor, Dr. Marcel Bruchez has been a great mentor.

I want to thank Greg a ton for working with me throughout my study, being my marathon running coach, and friend. He has been a big motivator. This all would not be possible without him.

I am thankful and happy to have been a part of the Bruchez lab and MBIC. A big thanks to Cheryl, who helped with direction on projects and was a huge support. Iris and Dima have been wonderful peers and friends. I am thankful for having the MBIC scientists as valuable research resources and as very good friends. I would like to thank the whole lab and MBIC, past and present:

Dr. Marcel Bruchez

Dr. Yi Wang	Dr. Cheryl Telmer	Dr. Greg Fisher	Dr. Haibing Teng
Dr. Saumya Saurabh	Iris Yang	Dr. Jon Jarvik	Yehuda Creeger
Dr. Chris Pratt	Dmytro Kolodieznyi	Dr. Byron Ballou	Donna Smith
Dr. Qi Yan	Alex Carpenter	Dr. Brigitte Schmidt	Robert Bodnar
Dr Jianjun He	Dan Ackerman	Dr. Chris Szent-Gyorgyi	
Dr. Matha Naganbabu	Dr. Xiaohong Tan	Sue Andreko	
Dr. Ming Zhang	Hauxia Shi	Dr. Alan Waggoner	
Dr. Taylor Canady			

I would like to thank my thesis committee members, Drs. Jon Jarvik, Manoj Puthenveedu, and Fred Lanni.

I am extremely grateful for my sisters' motivation and support. Mariah and Stephanie have always been encouraging me. My parents, Brian and Susan, have been big role models in my life and have helped me get this far.

I would like to thank Sara Wirth and Stacy Lambour for helping me become a stronger person.

Thanks to all my close friends outside of the lab: Steve Szymczak, Jill Secrest, Kathy Beyerle, Brian Baum, Gunnar Atli Sigurdsson, Kit Ham, Rory Eutsey, and Brendan Redler.

ABSTRACT

The fluorescent toolbox is expanding, and Fluorogen Activating Protein Technology (FAP) is contributing by providing tools for collecting direct real-time, live cell protein trafficking measurements. Chapter I includes a brief overview of current fluorescent and fluorogenic labeling approaches. After the review of labeling methods, FAP Technology is presented as a well suited tool for cell surface protein trafficking investigations. Core strengths of the developed fluorogenic dyes are highlighted. This chapter is a discussion on using FAP labeling strategies to quantify cell surface protein translocation, particularly addressing the needs for a direct, quick, and high-throughput adaptable protein trafficking detection assay for GPCRs and Ion channels. Chapter I concludes with introducing new methods for assessing intracellular trafficking of protein pools in the cell. Chapter II entails the development of a new pH sensor tool that can quantify pH related changes associated with protein trafficking from the surface to the endosomal network, and how it was applied to observe B2AR differential agonist induced trafficking behavior. Chapter III describes the development of a high-throughput assay for identifying potential kinase targets that enhance VX-809 corrector ability to rescue the mutant $\Delta F508$ cystic fibrosis transmembrane conductance regulator (CFTR). The screen was based on a FAP approach that uses both surface and total protein fluorescence measurements collected from a plate reader. Chapter IV presents the current work on creating a lysosomal FAP construct that will function as a test-bed for monitoring protein trafficking related to lysosomal dysfunction.

TABLE OF CONTENTS

CHAPTER I: Fluorogen Activating Protein Tools Fit for Protein Trafficking Measurements

Review of Protein and Chemical Labeling Approaches: From Fluorophores to Fluorogens.....	1.
Fluorogen Activating Protein Technology for Protein Trafficking Measurements.....	4.
GPCRS	7.
Ion Channels.....	11.
Conclusion and Future Directions.....	15.
References.....	16.

CHAPTER II: Genetically Targeted Ratiometric and Activated pH Indicator Complexes (TRApHIC) for Receptor Trafficking

Abstract and Introduction.....	21.
Results.....	24.
Discussion and Future Directions.....	34.
Methods.....	34.
References.....	39.
Supporting Information.....	42.

CHAPTER III: High-content Surface and Total Expression siRNA Kinase Library Screen with VX-809 Treatment Reveals Kinase Targets that Enhance F508del-CFTR Rescue

Abstract and Introduction.....	54.
Results.....	57.
Discussion and Future Directions.....	69.
Methods.....	70.
References.....	74.
Supporting information.....	77.

CHAPTER IV: Lysosomal Protein FAP Construct Validation and Application

Abstract and Introduction.....	88.
Results.....	90.
Discussion and Future Directions.....	102.
Methods.....	102.
References.....	105.

CHAPTER V: Down the Road

On The Drug Discovery Route: Seeing the Results.....	107.
Potential Lab Studies on Protein Trafficking.....	108.
Advancing the Tools.....	110.
References.....	111.

CHAPTER I

Fluorogen Activating Protein Tools Fit for Protein Trafficking Measurements

ABSTRACT: There is a large, growing array of fluorescent protein and chemical labeling methods currently available, and throughout the past decade the list of Fluorogen Activating Proteins (FAPs) and reporter dyes has grown to support a variety of methods to investigate protein trafficking events. The platform's capabilities have been demonstrated in several systems expanded, and commercialized for widespread use. The FAP labeling techniques have been applied to basic science research studies and high-throughput screens using microscopy, flow-cytometry, and plate readers.

Review of Protein and Chemical Labeling Approaches: From Fluorophores to Fluorogens

Live cell imaging involving the dynamics of organelles and proteins is enabled by fluorescent protein (FP) tags and chemical, fluorescent labeling techniques which are continuously evolving to answer complicated biological questions. Addressing FP and chemical labeling limitations and expanding their capabilities for more sophisticated temporal and spatial protein measurements has come hand in hand with the advancement of microscopy and experimental throughput, commanding more dynamic, brighter, and more photostable fluorescent probes. Fluorescent labeling optimization and development has produced diverse labeling strategies that enable quantitative analysis of biological processes or events, increasing the number of tools in the fluorescent toolkit.

FP tags are among the first and most commonly used, as they provide straightforward specific, genetically encoded protein labels that offer a wide selection of FP colors and biosensors. FP tags originated from the discovery of *Aequorea victoria* green fluorescent protein (GFP). The fluorescent property of GFP comes from its own protein folding that creates a chromophore through interactions within its β -barrel structure, (Chalfie et al., 1994; Tsien, 1998) which has been mutagenized and remodeled to produce numerous variants that are brighter, fluoresce in different colors from blue to yellow, and serve as functional reporter probes. (Heim and Tsien, 1996; Shaner et al., 2005) Exploring other marine species also added blue to far-red spectrum colored FPs to the arsenal. (Rodriguez et al., 2017; Shaner et al., 2004) While there have been considerable improvements with FP modification, engineering brighter and photostable FPs is a tricky challenge due to their buried chromophores that are not amenable to chemical modification, and their environment sensitivity i.e. fluorescence quenching at low pH. (Rodriguez et al., 2017) Yet, there is a continuous effort to find new FPs from different organisms. A significant limitation of any FP tag is the ubiquitous fluorescence of the FP tagged protein, hindering investigation of distinct populations of the protein. For example, G-protein coupled receptor (GPCR) dimerization studies in the early 2000s were limited by being unable to distinguish between cell-surface and intracellular receptors. (Goddard and Watts, 2012; Milligan et al., 2003)

Chemical probe labeling techniques, also called semi-synthetic labeling, feature genetically encoded peptide tags that associate with customized synthetic dyes to suit different experimental needs, offering a powerful approach for specifically and selectively labeling proteins of interest, coupled with the power of synthetic chemistry to limit the sites accessed by the labeling dye. The first of these used dye labeling methods arrived in the early 2000s. Johnsson's lab in 2003 produced the most recognized, prominent chemical labeling-tag technology, the SNAP tag. (Keppler et al., 2003) The SNAP tag is derived from the human DNA repair protein, O⁶-alkylguanine-DNA alkyltransferase (hAGT). The 20 kDa fusion tag transfers the alkyl group on the O⁶ position of benzyl-guanine (BG) to its reactive cysteine site, causing BG to covalently bind to the hAGT protein. (Keppler et al., 2003) BG derivatives can be designed with different fluorescent elements, which do not interfere with BG binding to hAGT. CLIP tag is the 33 kDa brother to SNAP-tag; developed in 2008 from a different mutant variant of hAGT, the CLIP tag covalently reacts with benzyl-cytosine (BC). (Gautier et al., 2008) SNAP-tag and CLIP tags can function as orthogonal partners in the same cell, allowing for multicolor labeling and ability to detect protein-protein interactions through cross-linking of a BG-BC substrate hybrid joined together by a fluorophore. (Gautier et al., 2008) A similar functioning 33 kDa probe established in 2007, the Halo-tag, is a mutant form of a bacterial enzyme that can covalently bind to the alkyl group of chloroalkynes conjugated to fluorophores. (Los and Wood, 2007) In addition, the trimethoprim, TMP-tag, is a designed high-affinity, non-covalent interaction probe between trimethoprim (with fluorophores attached), and the 18 kDa E. coli dihydrofolate reductase (2005). (Jing and Cornish, 2013; Miller et al., 2005) However, a weakness of fluorophore-based synthetic compounds is the presence of background fluorescence with dye addition, requiring the need for wash-steps to remove unbound fluorescent dye, adding another experimental variable, while also interfering with real-time biological measurements.

The ability to activate specific fluorescence on-demand is desirable for improving signal to background noise, and providing more experimental design options. Fluorogenic approaches have been developed to achieve fluorescence only upon dye-protein tag binding. Tsien's group, who had initiated the development of multicolored FPs, also pioneered the first fluorogenic chemical label in 1998. (Griffin et al., 1998) The fluorogenic reagents use an arsenic scaffold with green fluorescein (FIAsH) or red resorufin (ReAsh) that bind to a small tetracysteine sequence (TC) protein tag. Both FIAsH and ReAsh are essentially non-fluorescent when associated with EDT, Bis-1,2-ethanedithiol, but after EDT is replaced by TC binding, the TC-FIAsH or TC-ReAsh complex displays bright fluorescence. (Luedtke et al., 2007) Yet, several pitfalls exist with FIAsH and ReAsh labeling. The TC tag can only bind the reagents in a reducing environment, and due to the reagents arsenic property, there can be nonspecific protein binding, in addition to low signal-to-noise with weak expression of TC-tagged proteins. (Hoffmann et al., 2010)

In 2008 Fluorogen Activating Protein (FAP) technology was introduced as a new class of protein-dye reporters, combining the selectivity of genetically encoded single chain antibody 25 kDa tag (FAP) with specific fluorogenic dyes, which are non-fluorescent until bound to their cognate FAP. (Szent-Gyorgyi et al., 2008a) There are several dyes available that emit in the far-red spectrum, reducing background autofluorescence, and provide photostability for super-resolution microscopy. FAP technology will be discussed in more detail in the following section. A year later the 14 kDa photoactive yellow protein (PYP) tag was published after its discovery in bacteria as a blue light receptor. (Hori et al., 2009; Kort et al., 1996)

The Cys-69 residue within the PYP active center covalently binds with coumarin and cinnamic acid thioester derivatives by transthioesterification. The PYP dyes are non-fluorescent in polar environments, but become fluorescent within the PYPs' nonpolar active center.(Hori et al., 2013) With directed evolution, PYP was later reengineered to Y-FAST (yellow fluorescence-activating and absorption shifting tag) in 2016.(Plamont et al., 2016) This new fluorogenic tag non-covalently binds hydroxybenzylidene rhodamine dyes of different colors. Y-FASTs binding affinity provides the option to washout dyes to turn off fluorescence when desired.(Plamont et al., 2016) A different fluorogenic probe tactic was inspired by the absorptive properties of vision chromophores, where cellular retinoic acid binding protein II (CRABP II) was investigated as a 15.6 kDa fluorogenic probe tag in 2015. The CRABP II tag is paired with a non-fluorescent cyanine dye precursor to achieve bright, far-red emission fluorescence that is pH stable.(Yapici et al., 2015)

Only more recently has SNAP, CLIP, Halo, and TMP tags adopted fluorogenic or activatable dye probes.(Jing and Cornish, 2013; Leng et al., 2017; Liu et al., 2017; Prifti et al., 2014; Sun et al.) Silicon-rhodamine (siR) dyes were created by Johnsson and colleagues as a near-infrared, cell permeable fluorogenic probe compatible with the popular SNAP, CLIP, and Halo tags.(Lukinavičius et al., 2012) The photostable siR substrates have proved to be invaluable for super-resolution microscopy, and there continues to be evaluation of silicon rhodamine, rhodamine, and carbopyronine dyes for super resolution application.(Butkevich et al., 2016; Grimm et al., 2016a) To improve spatial resolution with single molecule microscopy in live-cells, the Lavis lab at Janelia developed a strategy to enhance the brightness of cell-permeable fluorophores by minimal structural adjustments. They reported increased quantum yield of tetramethylrhodamine by replacing the N,N-dialkyl groups with azetidine rings, and expanded it to several other fluorophores: coumarin, naphthalimide, acridine, rhodol, carborhodamine, oxazine and Si-rhodamine classes. (Grimm et al., 2015) These adjusted versatile fluorophores, known as Janelia Fluor (JF) dyes, have also been made photoactivatable, compatible with super resolution PALM microscopy and are currently the best “light up” labels for the Halo and SNAP tag. (Grimm et al., 2016b, 2017)

There is a large, growing catalog of protein-fluorogenic labeling techniques for biologists to use; however picking which one is best suited for individual research needs, on the small or large scale, is not a simple choice. A single genetically encoded tag, labeled with distinct chemical dyes, can perform different “functional” measurements. Hence, design of the right dye for the measurement, and use of the right dye and labeling protocol, provides a new experimental avenue for specific information collection.

There have been several recent reviews on fluorescent and fluorogenic labeling techniques(Bruchez, 2015; Jullien and Gautier, 2015; Li et al., 2017; Rodriguez et al., 2017; Thorn, 2017; Xu and Hu, 2018; Yan and Bruchez, 2015) (Shengnan Xu and Hai-Yu Hu, 2018; Rodriguez *et al.*, 2017; Li *et al.*, 2017; Thorn, 2017; Jullien and Gautier, 2015; Qi and Bruchez, 2015; Bruchez, 2015), which describe strengths and weaknesses of different methods. Qi and Bruchez, and more recently Xu and Hu have already provided an extensive background and perspective of FAP technology. Here, I will be discussing FAP labeling strategies for measuring cell surface protein trafficking adaptable for high-throughput assays.

Fluorogen Activating Protein Technology for Protein Trafficking Measurements

Important cell surface proteins, such as receptors and ion channels, are finely controlled in their bioavailability at the cell surface, where they perform significant physiological functions and responses. Aberrant cellular trafficking can lead to altered activity and thereby pathological disease states. Understanding the trafficking mechanism of these crucial surface proteins is important for elucidating function and correcting disease conditions. Studying plasma membrane (PM) protein dynamics has been revolutionized by using fluorescence, either by labeling with fluorophore conjugated antibodies, pH sensitive GFP tags, or use of chemical tags to specifically and quantitatively label surface proteins. However, there is a clinical urgency for drugs to treat their associated disorders, and high-throughput drug discovery screens have been on-going to find “hits” that have a desirable effect on a specific disease state. Yet, due to the constraints of direct trafficking detection methods, the most common approach to determine a target effect is through using tools to measure functional changes in protein activity. These drug screens do not necessarily differentiate between a direct effect on protein activity or protein trafficking. Activity is dependent on both the properties of the protein and the density of protein at the cell surface, and being able to distinguish between activity and trafficking provides a significant perspective of mechanistic action (Figure 1). To include this measurement in screens, detection methods have to be readily adaptable to large scale assays, without prohibitive costs or lengthy multi-step procedures. These requirements are met by the fluorogen activating protein platform, and strategies have been developed for large-scale measurements of cell surface protein transit.

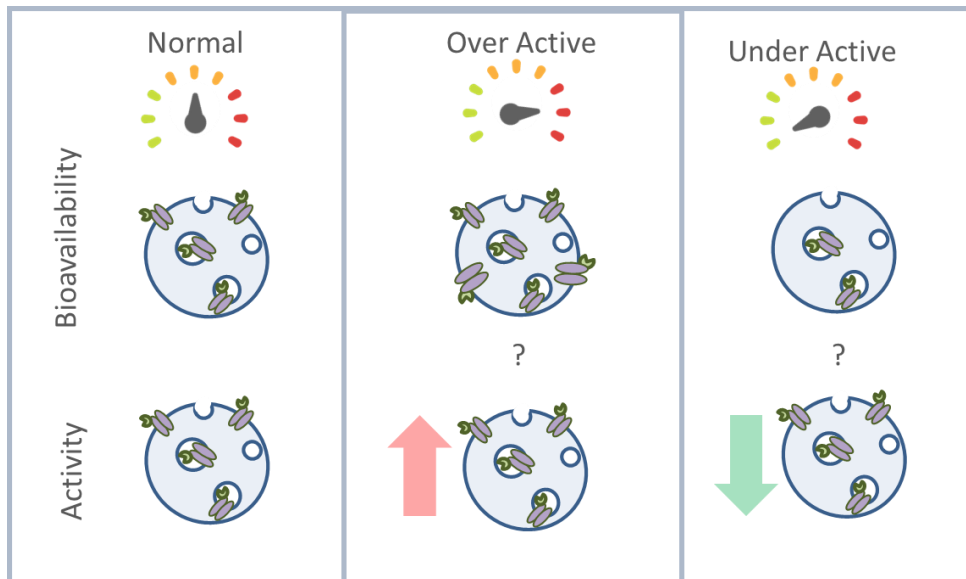


Figure 1. Overall activity can be either caused by altered bioavailability or altered direct protein activity.

Assessing protein trafficking in live cells is a core strength of FAP technology. The rapid and specific labeling of a tagged protein of interest (POI), intracellular or surface, with far-red malachite green derivatives creates a toolbox suitable for scalable, dynamic multi-color imaging experiments and direct quantitative trafficking-related measurements. Over the past several years, a library of distinct fluorogenic dye ligands has been demonstrated to bind to a common, well-folded FAP tag, the dL5** FAP. These dye variants include variants of cell excluded and cell permeable fluorogens (Figure 2,3,4) Limiting labeling to extracellular FAP tagged protein on the plasma membrane (PM) is advantageous for selectively observing endocytosis and endosomal trafficking without confounding signal from intracellular POI. Still, labeling all tagged protein (inside and out) can be a useful tactic for relating the amount of protein at the cell surface with total amount of protein. Either a matched or a different color cell-permeable dye can be used sequentially after surface labeling to give a surface/total POI measurement that increases overall assay sensitivity. The fluoromodule activating system continues to gain new designer dyes, tagged-proteins, and innovative experimental methods to improve detection of protein itineraries that can be adapted to a high-throughput format.

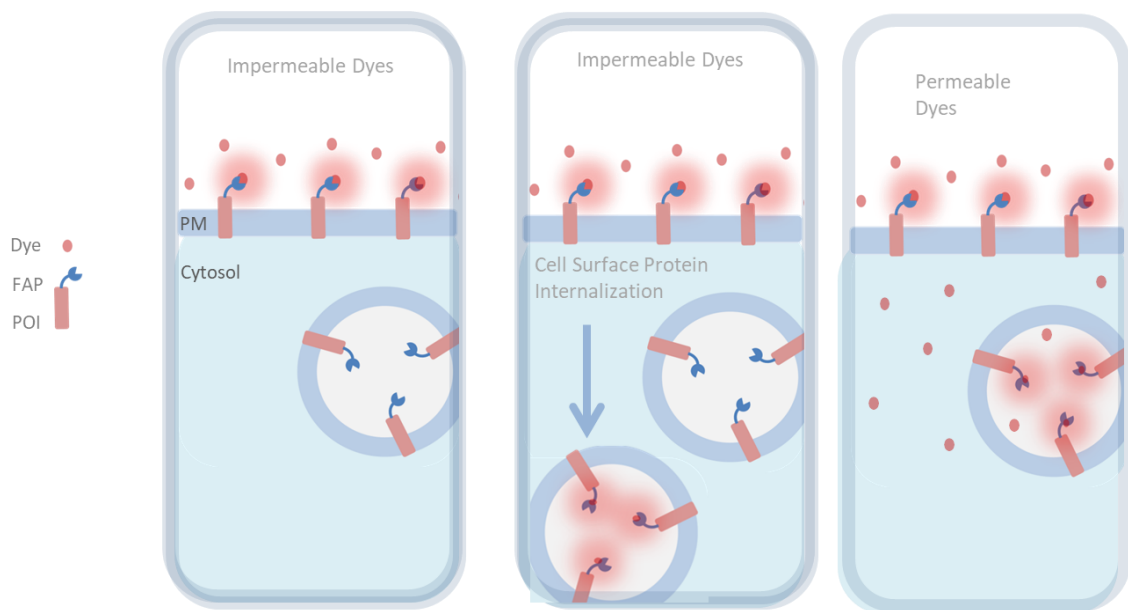
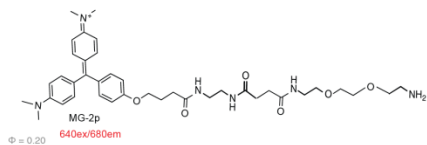
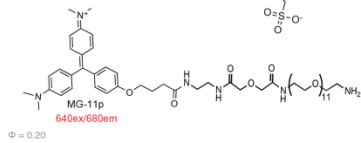
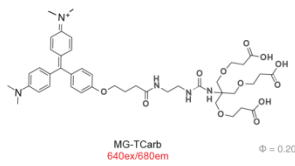
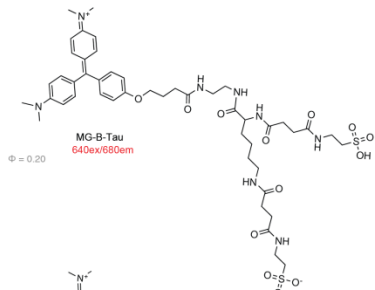
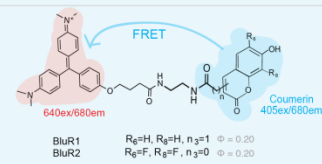
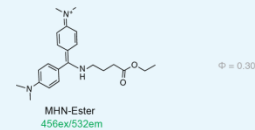
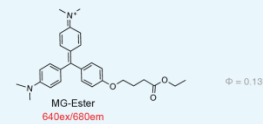
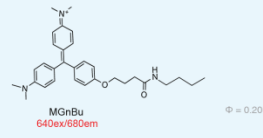


Figure 2. A Snapshot of FAP-POI labeled with cell excluded or permeable dye.

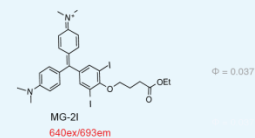
dL5** Cell Impermeable Dyes



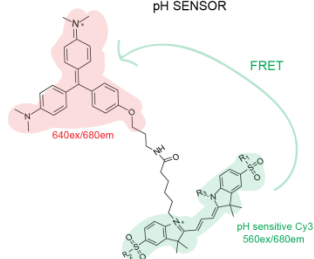
dL5** Cell Permeable Dyes



Photosensitizer

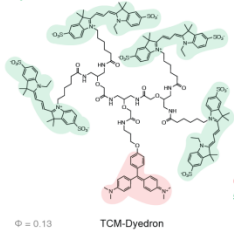


pH SENSOR



	pH 5	pH 8
Cy3pH(S/S)-MG	$\Phi = 0.21$	$\Phi = 0.17$
Cy3pH(S/SA)-MG	$\Phi = 0.22$	$\Phi = 0.13$
Cy3pH(SA/SA)-MG	$\Phi = 0.21$	$\Phi = 0.10$
Cy3-MG	$\Phi = 0.25$	$\Phi = 0.18$

Cy3 - MG FRET



Cy3 - MG FRET

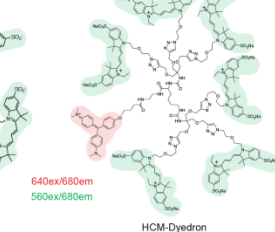


Figure 3. Fluorogenic dyes bound by dL5**. Cell excluded and permeable to the mammalian PM.

AM2.2 Cell Impermeable Dyes

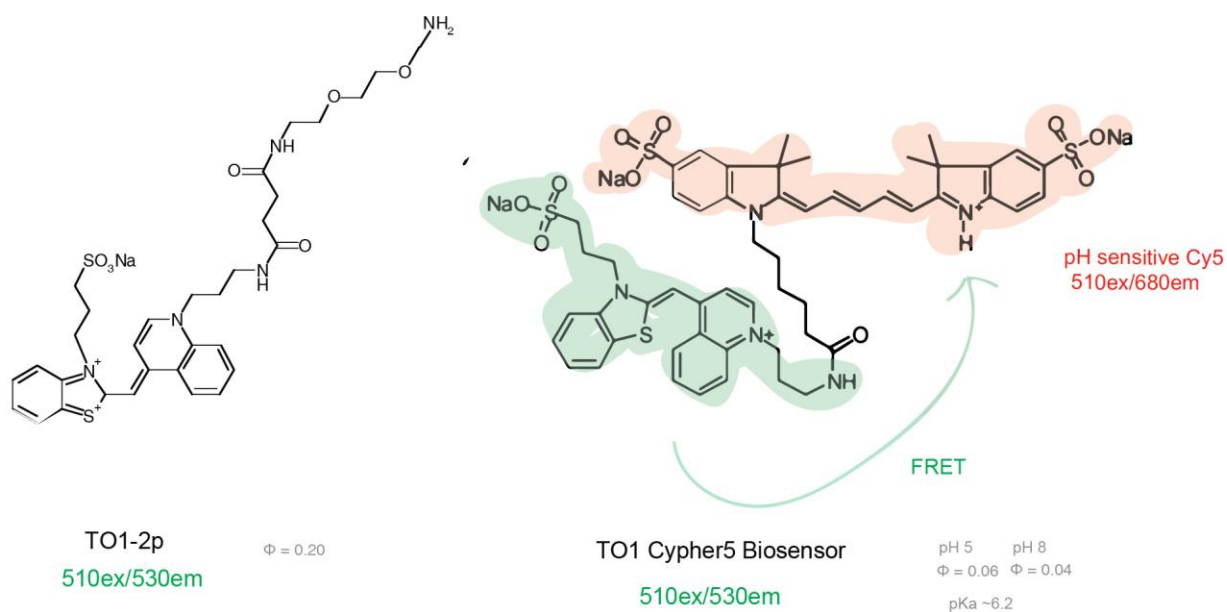


Figure 4. Fluorogenic dyes specific for AM2.2. Cell excluded to mammalian PM

GPCRS

GPCRS are the largest, overarching class of surface signaling protein. Their important physiological roles make them the most heavily investigated drug targets. The surface receptors can be activated by many different ligands, and pair to intracellular G-proteins, which relay signals and a biological effect downstream of receptor activation. (Hill, 2006) GPCRs are generally only ligand-activated on the cell surface, and are desensitized through their removal from the plasma membrane. After GPCR internalization, they are either degraded or sent through the recycling endosomal network to the cell surface. The careful regulation of GPCR traffic to and from the plasma membrane controls their activity and overall biological role. (Hanyaloglu and Zastrow, 2008) Thus, having fluorescent labeling techniques that can report receptor localization and trafficking is crucial for elucidating GPCR specific therapeutic mechanisms. (Hislop and Von Zastrow, 2011) GPCRs tagged with FP at the intracellular c-terminus has been used as a general observation technique, yet lacks the ability to determine distinct surface signal from collective signal. (Barak et al., 1997) Cell surface receptor labeling with GPCR ligands or antibodies conjugated with fluorophores has been a long-standing classical approach for internalization and recycling measurements, although it is unclear whether or not antibodies or ligands remain bound downstream after internalization. (Kumagai et al., 2015) These techniques can also entail long incubation periods and multiple wash-steps, constraining the scale of the experiment. The extracellular n-terminus of GPCRs can be fused with a small peptide tag if it does not interfere with activity, allowing for GPCR fusions with different extracellular tags such as the SNAP tag, Halo tag, FAP tag, or FLAG (antibody epitope tag). As an

extracellular tag, the fluorogenic FAP complex is particularly advantageous due to its simplicity and core strength for quick, selective cell surface protein labeling and detecting trafficking events. The development of the FAP-GPCR platform is described below.

B2AR

A specific protein of interest in the first category has been the prototypical GPCR, beta-2-adrenergic receptor (B2AR), which has widely been used as a foundation for understanding complex GPCRs, and as a classic GPCR test-bed for new assays.(Saunders et al., 2012)

The FAP platform was developed by screening and selecting small scFv tags based on affinity and activation of to two fluorogenic dyes, malachite green (MG) and sulfonated thiazole orange (TO1). The dL5** and AM2.2 FAP tags non-covalently bind MG and TO1 dye derivatives respectively (Figure 3 and Figure 4). FAP-dye binding suppresses some dye bond-rotations in the electronic excited state, thereby rigidizing the chemical structure and causing fluorescence activation. The first synthesized dyes, MG-2p, MG-11p, and TO1-2p, possess an amphiphilic diethylene glycol diamine, resulting in a +2 charge that prevents these dyes from passively crossing the plasma membrane (PM) and entering the cell. (Szent-Gyorgyi et al., 2008b)

The MG-11p and TO1-2p dyes were first used to create a framework to detect and quantify GPCR internalization that could be translated to a high-throughput design.(Fisher et al., 2010; Holleran et al., 2010) There are different FAP-B2AR labeling strategies to measure changes in cell surface density. Fluorogen labeling can be done before agonist activation to visualize post-activation internalization, or after surface removal to measure the loss in signal as an indicator of overall FAP-B2AR endocytosis. To detect recycling after agonist induced internalization, agonist can be removed and dye added to quantify any increase in cell surface signal. FAP technology was able to quantifiable and reproducibly detect translocation of cell surface proteins using, imaging, and flow cytometry.(Holleran et al., 2010; Saunders et al., 2012)

Another assay was designed to measure receptor desensitization and resensitization with two different cell excluded dyes, TO1-2p-Cy5 and TO1-2p. TO1-2p has a higher binding affinity than TO1-2p-Cy5, allowing bound fluorogen displacement by the higher affinity dye. AM2.2 FAP-B2AR was labeled on the surface with TO1-2p-Cy5, measured as a red signal, and after agonist incubation, TO1-2p (green) was added, without or with antagonist. Without antagonist addition, red labeled receptors are present on the cell surface and in endosomal vesicles, and the red surface fluorescence is quickly displaced by TO1-2p green signal, providing a measurement of overall intracellular accumulation in the red channel. With antagonist addition, red labeled receptors are recycled to the cell surface, where the bound red fluorogen is displaced by the second, green, dye, as a measurement of resensitization.(Fisher et al., 2014)

More recently, another cell excluded dye, MG-B-Tau, was developed that is the current go-to standard for labeling cell surface proteins. MG-B-Tau's two sulfonated groups (net charge of -1) and short hydrophilic linker make it substantially more cell impermeable than the precursor MG dye derivatives. MG-B-Tau demonstrated proficiency to rapidly and selectively label dL5** FAP-B2AR for quantitative trafficking using flow cytometry and microscopy.(Yan et al., 2015)

The FAP platform has grown to include ratiometric physiological pH indicator fluoromolecules. A cell impermeable tandem dye molecule, TO1-Cypher5, was designed by coupling a pH sensitive Cy5 analog with TO1. This reporter uses FRET with two separate emission channels (TO1 510ex/530em and pH dependent FRET 510ex/680em), and functions as a ratiometric pH biosensor. TO1-Cypher5 surface labeling was used as an approach to detect the local changes associated with AM2.2 FAP-B2AR trafficking. (Grover et al., 2012) Recently, a new far-red, genetically Targetable, Ratiometric, Activatable Physiological Indicator Complex (TRApHIC) was developed. The pH sensor uses FRET with one emission channel (MG 640ex/680em and pH dependent FRET 560ex/680em), and the paradigm is pictured in Figure 5. Cy3(S/SA)-MG was shown to quantifiably monitor dL5** FAP-B2AR internalization and recycling in response to different agonists, and demonstrated compatibility with super resolution microscopy. (Perkins et al., 2017)

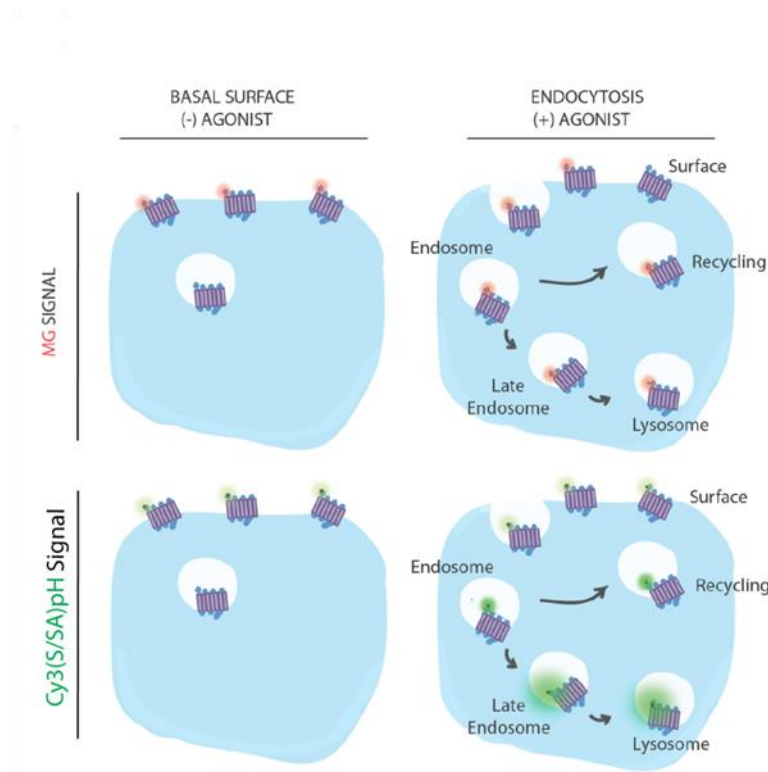


Figure 5. Diagram to show the signal changes related to different steps of Cy3(S/SA)pH-MG labeled FAP-B2AR internalization. MG signal (640ex/680em) stays consistent over the time course and changes in pH sensitive FRET signal (640ex/680em) intensity is dependent on the local pH environment.

FAP-GPCR Assay Timeline:

2010

- Detection and quantification of beta2AR internalization in living cells using FAP-based biosensor technology. Fisher GW *et al.*
- Fluorogen-Activating Proteins as Biosensors of Cell-Surface Proteins in Living Cells. Holleran JP *et al.*

2012

- Fluorogen activating proteins in flow cytometry for the study of surface molecules and receptors. Saunders MJ *et al.*
- Inhibitors of FAP-fluorogen interaction as a multiplex assay tool compound for receptor internalization assays. Wu Y *et al.*
- Genetically encoded pH sensor for tracking surface proteins through endocytosis. Grover A *et al.*

2013

- High-throughput Flow Cytometry Compatible Biosensor Based on Fluorogen Activating Protein Technology Saunders MJ *et al.*

2014

- Self-Checking Cell-Based Assays for GPCR Desensitization and Resensitization Fisher GW *et al.*

2015

- Near-instant surface-selective fluorogenic protein quantification using sulfonated triarylmethane dyes and fluorogen activating proteins. Yan Q *et al.*

2017

- Genetically Targeted Ratiometric and Activated pH Indicator Complexes (TRApHIC) for Receptor Trafficking Perkins LA *et al.*

Ion Channels

Ion channels are responsible for the regulated and selective transport of ions across the membrane. The critical functions of ion channels span across a range of pathologies, making them key therapeutic targets, and the second largest class of drug targets after GPCRs.(Overington et al., 2006) Their movements to and from the cell surface regulates their overall function, and changes in trafficking can have drastic impacts on homeostasis. Controlled ion channel activity at the cell surface is important for regulating heartbeat, blood pressure, muscle excitation, cell proliferation, and salt and water balance. (Ashcroft, 2006) Thus, detecting ion channel trafficking gives important mechanistic insights and therapeutic significance. The development of fluorescent labeling techniques caused an advent of visualizing ion channel dynamics at the plasma membrane that allowed for complementary measurements to biochemical assays.(Smyth and Shaw, 2008) However, designing genetically encoded tagged ion channels is difficult due to potential interference with native channel function, which has greatly limited the development of ion channel assays with genetic chemical labels.(Bocksteins et al., 2012; Zheng, 2015) Given the minimal ion channel chemical labeling options, ion channel FAP-platforms that exhibit native function represents a valuable new tool for labeling cell surface ion channels to assess trafficking.

The ion channels that have been studied with the dL5** FAP platform are the cystic fibrosis transmembrane conductance regulator (CFTR), the large conductance, voltage-and calcium-activated potassium (BK) channels, and recently the γ -Aminobutyric acid (GABA) type A receptors (GABA_ARs). This section is divided by channel for individual strategies to address the specific trafficking questions.

CFTR

The trafficking defective chloride channel, the mutant Δ F508-CFTR, fails to be exported to the cell surface where it functions. The Δ F508 mutation is the most prevalent cause of Cystic Fibrosis (CF), a genetic disease that results in mucus build-up in the lungs, causing severe breathing difficulties, chronic bacterial lung infections, and reduced life expectancy.(Ratjen and Döring, 2003) Most CF therapies available, only treat the symptoms, and finding therapies to treat the underlying cause of the disease has been extremely challenging. Δ F508-CFTR is misfolded in the endoplasmic reticulum (ER) and flagged by the quality control machinery and sent for proteosomal degradation.(Kopito, 1999) However, the mutant protein can form a functional channel if delivered to the cell surface. Therapeutic screens are searching for compounds or targets that can rescue the trafficking defective CFTR by delivering it to the PM. Most corrector HT screens rely on functional CFTR measurements due the prohibitive costs, time, and steps that come with quantifying CFTR at the PM in a large-scale format, usually by cellular fractionation and western blotting. FAP technology has mitigated other labeling assay limitations by only needing a simple, quick dye addition to label cell surface CFTR. FAP fusion Δ F508-CFTR has been shown to be accessible to high-throughput assay development utilizing different measurement approaches, including imaging, flow cytometry and multi-well fluorescent quantitation.

Holleran et al., developed dL5** FAP-WT CFTR and dL5** FAP- Δ F508-CFTR constructs and established a novel detection platform. Initial work used MG-11p as a single, fast surface CFTR labeling

fluorogen measurable by flow-cytometry and microscopy.(Holleran et al., 2010) The streamlined system was validated by using corrector compounds to rescue FAP- Δ F508-CFTR to the cell surface.(Holleran et al., 2012) The detection system developed was later used with high-temporal resolution microscopy to visualize internalization and accumulation of CFTR from the PM, and demonstrated that treatment with, C4 or C18 correctors, can redirect FAP- Δ F508-CFTR trafficking from a degradation route to recycling pathway.(Holleran et al., 2013) More recently a 96-well format, HT microscopy based, no wash method was developed as a platform for drug discovery. This platform uses MG-B-Tau to selectively label FAP- Δ F508-CFTR at the PM.(Larsen et al., 2016) To improve experimental sensitivity, we have now included the capability to measure direct CFTR traffic efficiency through measuring both cell surface protein and total protein. A surface and total protein HT measurement assay was developed on a plate reader, but could also be implemented using high-throughput flow-cytometry or microscopy. This assay first labels CFTR at the cell surface with MG-B-Tau, then after measuring surface signal, a second dye that is cell permeable is added to wells. The second dye, MGnBu, is a new MG dye derivative that has the same brightness as MG-B-Tau allowing for quantitative collection of the combined signal of MG-B-Tau labeling on the surface plus MGnBu intracellular labeling with the same excitation and emission wavelengths. This FAP approach was used to investigate potential kinase targets that could enhance CFTR corrector, VX-809, rescue of Δ F508-CFTR.(Perkins et al., 2018) The versatility of FAP across microscopy, plate reader, and flow-cytometry instruments has allowed for diverse strategies of measuring CFTR trafficking and rescue to the plasma membrane.

BK

The BK channel is expressed throughout the central nervous system (CNS), kidney, and smooth muscle. (Wu and Marx, 2010) Reduced function in the CNS can cause epilepsy and seizures.(N'Gouemo, 2011) Changes to the density of cell surface BK channels can have significant influences on its ability to regulate neurotransmitter release. (Faber and Sah, 2003)To investigate BK channel trafficking, the BK α channel was tagged with dL5** FAP and surface labeled with MG-2p or all expressed FAP-BK α was labeled with cell-permeable dye, MG-Ester. Assessing the signal of BK α at the PM in comparison to observing its intracellular localization, showed that co-transfecting its beta-4 subunit regulated it.

s cell surface presence. This study showed that the beta-4 subunit expression plays a role in reducing BK α s PM density.(Shruti et al., 2012) Pratt et. al., created a method to quantify surface and internal BK channel pools by using a two color dye FAP labeling system. The fluorogenic Green-Inside Red-Outside (GIRO) labeling strategy uses MG-B-Tau in combination with a cell permeable green dye, MHN-Ester. GIRO labeling was able to detect BK α channel surface expression dynamics. This approach recapitulated surface and internal immunofluorescence labeling, with FAP clearly being advantageous over immunofluorescence methods by detecting real-time changes in live cells, with labeling within minutes.(Pratt et al., 2015) Using microscopy and flow-cytometry, the GIRO method reported BK α channel stability, with a long cell surface half-life, and that forskolin induced activation of adenylyl cyclase reduced BK α PM density.(Pratt et al., 2015) Recently Pratt et al., demonstrated CRISPR insertion of dL5** FAP- BK α in mouse brain tissue, creating a novel mouse model for studying BK channels in live or fixed brain tissue.(Pratt et al., 2017) In this project, MG-TCarb became one of the newest dye additions to the cell excluded category. MG-TCarb utilizes a negatively charged moiety configuration to reduce background

nuclear DNA dye binding in fixed brain tissue. The new mouse FAP platform was used to reveal BK channel clustering with beta-4 subunit expression in the cerebellum, and shows promise for future BK channel trafficking studies.(Pratt et al., 2017)

GABA

A new FAP tool was designed to track multistage synaptic GABA_A Receptor internalization and trafficking, extendable for future use in drug related HT screens.(Lorenz-Guertin et al., 2017) These receptors function as ligand gated chloride channels involved in inhibitory neurotransmission in the brain. (Luscher et al., 2011) GABA_AR primarily consist of two subunits, with the $\gamma 2$ subunit being heavily involved in GABA_AR function-being critical for receptor synaptic targeting and cluster maintenance.(Schweizer et al., 2003) The mechanisms of GABA_AR trafficking in response to endogenous and pharmacological molecules has not been fully investigated, which has led Lorzen-Guertin et al. to develop dL5** $\gamma 2$ pHFAP GABA_ARs as a versatile trafficking sensor. This tool has largely employed the previously described Cy3(S/SA)-MG dye as a monitor the trafficking itinerary of $\gamma 2$ pHFAP GABA_ARs, providing vesicle-level pH measurements. The platform has established a trafficking paradigm of GABA_ARs that can be used to assess trafficking changes caused by different agents.(Lorenz-Guertin et al., 2017)

FAP-Ion Channel Assay Timeline:

2010

- Fluorogen-Activating Proteins as Biosensors of Cell-Surface Proteins in Living Cells.
Holleran JP *et al.*

2012

- The brain-specific Beta4 subunit downregulates BK channel cell surface expression.
Shruti S *et al.*
- Pharmacological rescue of the mutant cystic fibrosis transmembrane conductance regulator (CFTR) detected by use of a novel fluorescence platform.
Holleran JP *et al.*

2013

- Regulated recycling of mutant CFTR is partially restored by pharmacological treatment.
Holleran JP *et al.*

2015

- Fluorogenic Green-Inside Red-Outside (GIRO) Labeling Approach Reveals Adenylyl Cyclase-Dependent Control of BK α Surface Expression.
Pratt, CP *et al.*

2016

- Simple image-based no-wash method for quantitative detection of surface expressed CFTR.
Larsen MB *et al.*

2017

- A versatile optical tool for studying synaptic GABAA receptor trafficking
Lorenz-Guertin, JM
- Tagging of Endogenous BK Channels with a Fluorogen-Activating Peptide Reveals β 4-Mediated Control of Channel Clustering in Cerebellum.
Pratt CP, *et al.*

2018

- High-Content Surface and Total Expression siRNA Kinase Library Screen with VX-809 Treatment Reveals Kinase Targets that Enhance F508del-CFTR Rescue.
Perkins LA, *et al.*

Discussion and Future Directions

We have shown different assays and strategies for cell surface protein detection that have been validated in several different systems and show promising use as high-throughput methods utilizing fluorescence and various measuring instruments. Intracellular dye labeling is another component that was discussed as a means to relate overall protein amounts with PM traffic efficiency. Recently Shiwarski et al., introduced a dL5** FAP delta opioid receptor construct for a quick labeling scheme with cell permeable dye MG-Ester. The assay design took advantage of the far-red properties of MG for multicolored imaging with GFP, and worked as a simple, live cell assessment of delta opioid receptor localization in the golgi vs cell surface. (Shiwarski et al., 2017)

We are currently expanding our protein trafficking measurement capabilities inside the cell for detecting lysosomal protein delivery. Dysfunctional lysosomal trafficking is responsible for several neurological diseases, and the functions of most lysosomal proteins remain unknown. (Aridor and Hannan, 2000; Schwake et al., 2013) A FAP tool could be useful for pulse-chase lysosomal trafficking observation and lysosomal proteolysis activity measurements. Developing a lysosomal based FAP platform may provide a new method for therapeutic drug screens for diseases caused by aberrant lysosomal trafficking, such as Niemann Pick C.

The non-covalent dye-binding nature of FAP technology is a feature that can allow dye exchanges, like the AM2.2 TO1-2p and TO1-Cy5 paradigm, and could potentially permit dye washouts. The current developed dL5** MG dyes have subnanomolar Kds, taking hours for dye dissociation. Developing new dyes with higher Kds would be another tool for creating dynamic assays and pulse-chase labeling strategies. The molecular biosensor imaging center (MBIC) and Bruchez group has designed and created the current list of dyes, and recently another lab, Hu and colleagues, has started to develop several new malachite green derivatives.(Zhang et al., 2017) The FAP toolbox is continuously growing with the exploration of new fluorogen dyes, whether improvement on current existing dyes or creating new biosensors, that provides new opportunities for protein labeling methods.

The FAP toolbox is expanding by improving existing dyes and modifying properties to create biosensors and improve the arsenal for tackling the next generation of scientific problems.

REFERENCES:

- Aridor, M., and Hannan, L. a (2000). Traffic jam: a compendium of human diseases that affect intracellular transport processes. *Traffic* 1, 836–851.
- Ashcroft, F.M. (2006). From molecule to malady. *Nature* 440, 440–447.
- Barak, L.S., Ferguson, S.S., Zhang, J., Martenson, C., Meyer, T., and Caron, M.G. (1997). Internal trafficking and surface mobility of a functionally intact beta2-adrenergic receptor-green fluorescent protein conjugate. *Mol Pharmacol* 51.
- Bocksteins, E., J., A., P., D., and J., D. (2012). Immunostaining of Voltage-Gated Ion Channels in Cell Lines and Neurons – Key Concepts and Potential Pitfalls. In *Applications of Immunocytochemistry*, (InTech), p.
- Bruchez, M.P. (2015). Dark dyes-bright complexes: Fluorogenic protein labeling. *Curr. Opin. Chem. Biol.* 27, 18–23.
- Butkevich, A.N., Mitronova, G.Y., Sidenstein, S.C., Klocke, J.L., Kamin, D., Meineke, D.N.H., D’Este, E., Kraemer, P.-T., Danzl, J.G., Belov, V.N., et al. (2016). Fluorescent Rhodamines and Fluorogenic Carbopyronines for Super-Resolution STED Microscopy in Living Cells. *Angew. Chemie Int. Ed.* 55, 3290–3294.
- Chalfie, M., Tu, Y., Euskirchen, G., Ward, W.W., and Prasher, D.C. (1994). Green fluorescent protein as a marker for gene expression. *Science* (80-.). 263.
- Faber, E.S.L., and Sah, P. (2003). Calcium-Activated Potassium Channels: Multiple Contributions to Neuronal Function. *Neurosci.* 9, 181–194.
- Fisher, G.W., Adler, S. a, Fuhrman, M.H., Waggoner, A.S., Bruchez, M.P., and Jarvik, J.W. (2010). Detection and quantification of beta2AR internalization in living cells using FAP-based biosensor technology. *J. Biomol. Screen. Off. J. Soc. Biomol. Screen.* 15, 703–709.
- Fisher, G.W., Fuhrman, M.H., Adler, S.A., Szent-Gyorgyi, C., Waggoner, A.S., and Jarvik, J.W. (2014). Self-checking cell-based assays for GPCR desensitization and resensitization. *J. Biomol. Screen.*
- Gautier, A., Juillerat, A., Heinis, C., Corrêa, I.R., Kindermann, M., Beaufils, F., and Johnsson, K. (2008). An Engineered Protein Tag for Multiprotein Labeling in Living Cells. *Chem. Biol.* 15, 128–136.
- Goddard, A.D., and Watts, A. (2012). Contributions of fluorescence techniques to understanding G protein-coupled receptor dimerisation. *Biophys. Rev.* 4, 291–298.
- Griffin, B.A., Adams, S.R., and Tsien, R.Y. (1998). Specific covalent labeling of recombinant protein molecules inside live cells. *Science* (80-.). 281.
- Grimm, J.B., English, B.P., Chen, J., Slaughter, J.P., Zhang, Z., Revyakin, A., Patel, R., Macklin, J.J., Normanno, D., Singer, R.H., et al. (2015). A general method to improve fluorophores for live-cell and single-molecule microscopy. *Nat. Methods* 12, 244–250.
- Grimm, J.B., Klein, T., Kopek, B.G., Shtengel, G., Hess, H.F., Sauer, M., and Lavis, L.D. (2016a). Synthesis of a Far-Red Photoactivatable Silicon-Containing Rhodamine for Super-Resolution Microscopy. *Angew. Chemie Int. Ed.* 55, 1723–1727.

Grimm, J.B., English, B.P., Choi, H., Muthusamy, A.K., Mehl, B.P., Dong, P., Brown, T.A., Lippincott-Schwartz, J., Liu, Z., Lionnet, T., et al. (2016b). Bright photoactivatable fluorophores for single-molecule imaging. *Nat. Methods* *13*, 985–988.

Grimm, J.B., Muthusamy, A.K., Liang, Y., Brown, T.A., Lemon, W.C., Patel, R., Lu, R., Macklin, J.J., Keller, P.J., Ji, N., et al. (2017). A general method to fine-tune fluorophores for live-cell and in vivo imaging. *Nat. Methods*.

Grover, A., Schmidt, B.F., Salter, R.D., Watkins, S.C., Waggoner, A.S., and Bruchez, M.P. (2012). Genetically Encoded pH Sensor for Tracking Surface Proteins through Endocytosis. *Angew. Chemie Int. Ed.* *51*, 4838–4842.

Hanyaloglu, A.C., and Zastrow, M. von (2008). Regulation of GPCRs by Endocytic Membrane Trafficking and Its Potential Implications. *Annu. Rev. Pharmacol. Toxicol.* *48*, 537–568.

Heim, R., and Tsien, R.Y. (1996). Engineering green fluorescent protein for improved brightness, longer wavelengths and fluorescence resonance energy transfer. *Curr. Biol.* *6*, 178–182.

Hill, S.J. (2006). G-protein-coupled receptors: past, present and future. *Br. J. Pharmacol.* *147 Suppl*, S27–S37.

Hislop, J.N., and Von Zastrow, M. (2011). Analysis of GPCR localization and trafficking. *Methods Mol. Biol.* *746*, 425–440.

Hoffmann, C., Gaietta, G., Zürn, A., Adams, S.R., Terrillon, S., Ellisman, M.H., Tsien, R.Y., and Lohse, M.J. (2010). Fluorescent labeling of tetracysteine-tagged proteins in intact cells. *Nat. Protoc.* *5*, 1666–1677.

Holleran, J., Brown, D., Fuhrman, M.H., Adler, S.A., Fisher, G.W., and Jarvik, J.W. (2010). Fluorogen-Activating Proteins as Biosensors of Cell-Surface Proteins in Living Cells. *Cytom. A* *76*, 1358–1375.

Holleran, J.P., Glover, M.L., Peters, K.W., Bertrand, C.A., Watkins, S.C., Jarvik, J.W., and Frizzell, R.A. (2012). Pharmacological rescue of the mutant cystic fibrosis transmembrane conductance regulator (CFTR) detected by use of a novel fluorescence platform. *Mol. Med.* *18*, 685–696.

Holleran, J.P., Zeng, J., Frizzell, R. a, and Watkins, S.C. (2013). Regulated recycling of mutant CFTR is partially restored by pharmacological treatment. *J. Cell Sci.* *126*, 2692–2703.

Hori, Y., Ueno, H., Mizukami, S., and Kikuchi, K. Photoactive Yellow Protein-Based Protein Labeling System with Turn-On Fluorescence Intensity.

Hori, Y., Ueno, H., Mizukami, S., and Kikuchi, K. (2009). Photoactive Yellow Protein-Based Protein Labeling System with Turn-On Fluorescence Intensity. *J. Am. Chem. Soc.* *131*, 16610–16611.

Hori, Y., Norinobu, T., Sato, M., Arita, K., Shirakawa, M., and Kikuchi, K. (2013). Development of Fluorogenic Probes for Quick No-Wash Live-Cell Imaging of Intracellular Proteins. *J. Am. Chem. Soc.* *135*, 12360–12365.

Jing, C., and Cornish, V.W. (2013). A fluorogenic TMP-tag for high signal-to-background intracellular live cell imaging. *ACS Chem. Biol.* *8*, 1704–1712.

Jullien, L., and Gautier, A. (2015). Fluorogen-based reporters for fluorescence imaging: a review. *Methods Appl. Fluoresc.* *3*, 42007.

- Keppler, A., Gendreizig, S., Gronemeyer, T., Pick, H., Vogel, H., and Johnsson, K. (2003). A general method for the covalent labeling of fusion proteins with small molecules in vivo. *Nat Biotechnol* 21.
- Kopito, R.R. (1999). Biosynthesis and Degradation of CFTR. *Physiol Rev* 79, S167-173.
- Kort, R., Hoff, W.D., Van West, M., Kroon, A.R., Hoffer, S.M., Vlieg, K.H., Crielaand, W., Van Beeumen, J.J., and Hellingwerf, K.J. (1996). The xanthopsins: a new family of eubacterial blue-light photoreceptors. *EMBO J.* 15, 3209–3218.
- Kumagai, H., Ikeda, Y., Motozawa, Y., Fujishiro, M., Okamura, T., Fujio, K., Okazaki, H., Nomura, S., Takeda, N., Harada, M., et al. (2015). Quantitative measurement of GPCR endocytosis via pulse-chase covalent labeling. *PLoS One* 10.
- Larsen, M.B., Hu, J., Frizzell, R.A., and Watkins, S.C. (2016). Simple image-based no-wash method for quantitative detection of surface expressed CFTR. *Methods* 96, 40–45.
- Leng, S., Qiao, Q.-L., Gao, Y., Miao, L., Deng, W.-G., and Xu, Z.-C. (2017). SNAP-tag fluorogenic probes for wash free protein labeling.
- Li, C., Tebo, A., and Gautier, A. (2017). Fluorogenic Labeling Strategies for Biological Imaging. *Int. J. Mol. Sci.* 18, 1473.
- Liu, W., Fu Li, H., Chen, X., Hou, J., Yi, L., and Wu, Y.-W. A Rapid and Fluorogenic TMP-AcBOPDIPY Probe for Covalent Labeling of Proteins in Live Cells.
- Liu, Y., Miao, K., Dunham, N.P., Liu, H., Fares, M., Boal, A.K., Li, X., and Zhang, X. (2017). The Cation- π Interaction Enables a Halo-Tag Fluorogenic Probe for Fast No-Wash Live Cell Imaging and Gel-Free Protein Quantification. *Biochemistry* 56, 1585–1595.
- Lorenz-Guertin, J.M., Wilcox, M.R., Zhang, M., Larsen, M.B., Pilli, J., Schmidt, B.F., Bruchez, M.P., Johnson, J.W., Waggoner, A.S., Watkins, S.C., et al. (2017). A versatile optical tool for studying synaptic GABAA receptor trafficking. *J. Cell Sci.* 130, 3933–3945.
- Los, G. V, and Wood, K. (2007). The HaloTag: a novel technology for cell imaging and protein analysis. *Methods Mol Biol* 356.
- Luedtke, N.W., Dexter, R.J., Fried, D.B., and Schepartz, A. (2007). Surveying polypeptide and protein domain conformation and association with FIAsh and ReAsH. *Nat. Chem. Biol.* 3, 779–784.
- Lukinavičius, G., Umezawa, K., Olivier, N., Honigsmann, A., Yang, G., Plass, T., Mueller, V., Reymond, L., Corrêa Jr, I.R., Luo, Z.-G., et al. (2012). A near-infrared fluorophore for live-cell super-resolution microscopy of cellular proteins.
- Luscher, B., Fuchs, T., and Kilpatrick, C.L. (2011). GABAAR Receptor Trafficking-Mediated Plasticity of Inhibitory Synapses. *Neuron* 70, 385–409.
- Miller, L.W., Cai, Y., Sheetz, M.P., and Cornish, V.W. (2005). In vivo protein labeling with trimethoprim conjugates: a flexible chemical tag. *Nat. Methods* 2, 255–257.
- Milligan, G., Ramsay, D., Pascal, G., and Carrillo, J.J. (2003). GPCR dimerisation. *Life Sci.* 74, 181–188.
- N’Gouemo, P. (2011). Targeting BK (big potassium) channels in epilepsy. *Expert Opin. Ther. Targets* 15,

1283–1295.

Overington, J.P., Overington, J.P., Al-Lazikani, B., Al-Lazikani, B., Hopkins, A.L., and Hopkins, A.L. (2006). How many drug targets are there? *Nat. Rev. Drug Discov.* *5*, 993–996.

Perkins, L.A., Yan, Q., Schmidt, B.F., Kolodieznyi, D., Saurabh, S., Larsen, M.B., Watkins, S., Kremer, L., and Bruchez, M.P. (2017). Genetically Targeted Ratiometric and Activated pH Indicator Complexes (TRAPHIC) for Receptor Trafficking. *Biochemistry* *acs.biochem.7b01135*.

Perkins, L.A., Fisher, G.W., Naganbabu, M., Schmidt, B.F., Mun, F., and Bruchez, M.P. (2018). High-Content Surface and Total Expression siRNA Kinase Library Screen with VX-809 Treatment Reveals Kinase Targets that Enhance F508del-CFTR Rescue. *Mol. Pharm.* *15*, 759–767.

Plamont, M.-A., Billon-Denis, E., Maurin, S., Gauron, C., Pimenta, F.M., Specht, C.G., Shi, J., Quérard, J., Pan, B., Rossignol, J., et al. (2016). Small fluorescence-activating and absorption-shifting tag for tunable protein imaging in vivo. *Proc. Natl. Acad. Sci. U. S. A.* *113*, 497–502.

Pratt, C.P., He, J., Wang, Y., Barth, A.L., and Bruchez, M.P. (2015). Fluorogenic Green-Inside Red-Outside (GIRO) Labeling Approach Reveals Adenylyl Cyclase-Dependent Control of BK α Surface Expression. *Bioconjug. Chem.* *26*, 1963–1971.

Pratt, C.P., Kuljis, D.A., Homanics, G.E., He, J., Kolodieznyi, D., Dudem, S., Hollywood, M.A., Barth, A.L., and Bruchez, M.P. (2017). Tagging of Endogenous BK Channels with a Fluorogen-Activating Peptide Reveals β 4-Mediated Control of Channel Clustering in Cerebellum. *Front. Cell. Neurosci.* *11*, 337.

Prifti, E., Reymond, L., Umebayashi, M., Hovius, R., Riezman, H., and Johnsson, K. (2014). A Fluorogenic Probe for SNAP-Tagged Plasma Membrane Proteins Based on the Solvatochromic Molecule Nile Red. *ACS Chem. Biol.* *9*, 606–612.

Ratjen, F., and Döring, G. (2003). Cystic fibrosis. *Lancet* *361*, 681–689.

Rodriguez, E.A., Campbell, R.E., Lin, J.Y., Lin, M.Z., Miyawaki, A., Palmer, A.E., Shu, X., Zhang, J., and Tsien, R.Y. (2017). The Growing and Glowing Toolbox of Fluorescent and Photoactive Proteins. *Trends Biochem. Sci.* *42*, 111–129.

Saunders, M.J., Szent-Gyorgyi, C., Fisher, G.W., Jarvik, J.W., Bruchez, M.P., and Waggoner, A.S. (2012). Fluorogen Activating Proteins in Flow Cytometry for the Study of Surface Molecules and Receptors. *Methods* *57*, 308–317.

Schwake, M., Schröder, B., and Saftig, P. (2013). Lysosomal Membrane Proteins and Their Central Role in Physiology. *Traffic* *14*, 739–748.

Schweizer, C., Balsiger, S., Bluethmann, H., Mansuy, I.M., Fritschy, J.-M., Mohler, H., and Lüscher, B. (2003). The γ 2 subunit of GABAA receptors is required for maintenance of receptors at mature synapses. *Mol. Cell. Neurosci.* *24*, 442–450.

Shaner, N.C., Campbell, R.E., Steinbach, P.A., Giepmans, B.N., Palmer, A.E., and Tsien, R.Y. (2004). Improved monomeric red, orange and yellow fluorescent proteins derived from *Discosoma* sp. red fluorescent protein. *Nat Biotechnol* *22*.

Shaner, N.C., Steinbach, P.A., and Tsien, R.Y. (2005). A guide to choosing fluorescent proteins. *Nat*

Methods 2.

- Shiwarski, D.J., Darr, M., Telmer, C.A., Bruchez, M.P., and Puthenveedu, M.A. (2017). PI3K class II α regulates δ -opioid receptor export from the trans-Golgi network. *Mol. Biol. Cell* 28, 2202–2219.
- Shruti, S., Urban-Ciecko, J., Fitzpatrick, J. a, Brenner, R., Bruchez, M.P., and Barth, A.L. (2012). The brain-specific Beta4 subunit downregulates BK channel cell surface expression. *PLoS One* 7, e33429.
- Smyth, J.W., and Shaw, R.M. (2008). Visualizing ion channel dynamics at the plasma membrane. *Heart Rhythm* 5, S7-11.
- Sun, X., Zhang, A., Baker, B., Sun, L., Howard, A., Buswell, J., Maurel, D., Masharina, A., Johnsson, K., Noren, C.J., et al. Development of SNAP-Tag Fluorogenic Probes for Wash- Free Fluorescence Imaging.
- Szent-Gyorgyi, C., Schmidt, B.F., Schmidt, B. a, Creeger, Y., Fisher, G.W., Zakel, K.L., Adler, S., Fitzpatrick, J. a J., Woolford, C. a, Yan, Q., et al. (2008a). Fluorogen-activating single-chain antibodies for imaging cell surface proteins. *Nat. Biotechnol.* 26, 235–240.
- Szent-Gyorgyi, C., Schmidt, B.F., Creeger, Y., Fisher, G.W., Zakel, K.L., Adler, S., Fitzpatrick, J.A.J., Woolford, C.A., Yan, Q., Vasilev, K. V, et al. (2008b). Fluorogen-activating single-chain antibodies for imaging cell surface proteins. *Nat Biotech* 26, 235–240.
- Thorn, K. (2017). Genetically encoded fluorescent tags. *Mol. Biol. Cell* 28, 848–857.
- Tsien, R.Y. (1998). The green fluorescent protein. *Annu Rev Biochem* 67.
- Wu, R.S., and Marx, S.O. (2010). The BK potassium channel in the vascular smooth muscle and kidney: α - and β -subunits. *Kidney Int.* 78, 963–974.
- Xu, S., and Hu, H.-Y. (2018). Fluorogen-activating proteins: beyond classical fluorescent proteins. *Acta Pharm. Sin. B.*
- Yan, Q., and Bruchez, M.P. (2015). Advances in chemical labeling of proteins in living cells. *Cell Tissue Res.* 360, 179–194.
- Yan, Q., Schmidt, B.F., Perkins, L. a., Naganbabu, M., Saurabh, S., Andreko, S.K., and Bruchez, M.P. (2015). Near-instant surface-selective fluorogenic protein quantification using sulfonated triarylmethane dyes and fluorogen activating proteins. *Org. Biomol. Chem.* 13, 2078–2086.
- Yapici, I., Lee, K.S.S., Berbasova, T., Nosrati, M., Jia, X., Vasileiou, C., Wang, W., Santos, E.M., Geiger, J.H., and Borhan, B. (2015). “Turn-on ” protein fluorescence: In situ formation of cyanine dyes. *J. Am. Chem. Soc.* 137, 1073–1080.
- Zhang, Q., Wang, Q., Sun, Y., Zuo, L., Fetz, V., and Hu, H.Y. (2017). Superior Fluorogen-Activating Protein Probes Based on 3-Indole-Malachite Green. *Org. Lett.* 19, 4496–4499.
- Zheng, J. (2015). *Handbook of ion channels* (CRC Press).

CHAPTER II

Genetically Targeted Ratiometric and Activated pH Indicator Complexes (TRApHIC) for Receptor Trafficking

Published December 2017 in ACS Biochemistry

Reprinted (adapted) with permission from:

Perkins, L. A., Yan, Q., Schmidt, B. F., Kolodieznyi, D., Saurabh, S., Larsen, M. B., Watkins, S., Kremer, L., and Bruchez, M. P. (2017) Genetically Targeted Ratiometric and Activated pH Indicator Complexes (TRApHIC) for Receptor Trafficking. *Biochemistry* acs.biochem.7b01135. Copyright 2018 American Chemical Society.

Author Contributions:

L.A.P performed imaging experiments, data analysis, and wrote the paper. Q.Y. performed imaging, photobleaching experiments, initial data analysis, and wrote the paper. B.F.S synthesized TO1-Cypher5, Cy3-MG, Cy3pH(S/S)-MG, Cy3pH(S/SA)-MG, and Cy3pH(SA/SA)-MG. D.K. developed quick pipeline for organizing large single-vesicle time-course data sets for Prism, performed spectroscopy data collection, and helped with methods. M.B.L. performed pH calibration and data analysis. S.C.W. did data analysis and provided assistance with STED microscopy. L.K. and S.S. performed emission and excitation spectra of Cy3pH(S/S)-MG, Cy3pH(S/SA)-MG, and Cy3pH(SA/SA)-MG. M.P.B. designed sensors, experiments, and wrote the paper.

ABSTRACT: Fluorescent protein based pH sensors are a useful tool for measuring protein trafficking through pH changes associated with endo- and exocytosis. However, commonly used pH sensing probes are ubiquitously expressed with their protein of interest throughout the cell, hindering the ability to focus on specific trafficking pools of proteins. We developed a family of excitation-ratiometric, activatable pH responsive tandem dyes, consisting of a pH sensitive Cy3 donor linked to a fluorogenic malachite green acceptor. These cell-excluded dyes are targeted and activated upon binding to a genetically expressed fluorogen activating protein, and are suitable for selective labeling of surface proteins for analysis of endocytosis and recycling in live cells using both confocal and superresolution microscopy. Quantitative profiling of the endocytosis and recycling of tagged β 2-adrenergic receptor (B2AR) at a single vesicle level revealed differences among B2AR agonists, consistent with more detailed pharmacological profiling.

INTRODUCTION: G-protein coupled receptors (GPCRs) comprise the largest family of membrane signaling receptors.(Pierce et al., 2002) These cell surface receptors play an important role in controlling homeostasis and cellular phenotypes by relaying extracellular stimuli to intracellular downstream targets. Defects in GPCR signaling and trafficking are associated with many human diseases, such as drug addiction and heart disease.(Yao et al., 2003; Salazar et al., 2007) This class of receptors is the dominant class among all drug targets.(Hopkins and Groom, 2002) The search for new GPCR drug candidates has demonstrated that different agonists can exhibit bias towards different cell signaling pathways.(Liu et al., 2012) The pharmaceutical significance of ligand bias has altered the methods of therapeutic screens and drug candidate evaluation.(Kenakin and Christopoulos, 2013) GPCR desensitization through endocytosis and its intracellular sorting, recycling, or degradation, are important mechanistic features that are associated with GPCR signaling.(Drake et al., 2006; Hanyaloglu and Zastrow, 2008) B2AR has been extensively studied, and is a classic test-bed for developing new procedures for drug classification, including the influence of drugs on B2AR's endocytic itinerary. The measurement of trafficking of GPCRs and other membrane proteins under the influence of various chemical and biological ligands is now an area that requires robust tools to establish quantitative trafficking phenotypes.

To tackle these challenges, fluorescent protein (FP) based sensors have been developed to study intracellular pH changes. (Super-)ecliptic pHluorin exhibits low fluorescence signal at pH < 6 and therefore has been widely used to investigate secretory vesicle exocytosis, internalization, and recycling.(Miesenbock et al., 1998; Sankaranarayanan et al., 2000; Diril et al., 2006; Xu et al., 2011) Ratiometric pHluorin produces a characteristic ratio with two excitation wavelengths and has been employed to measure the pH of various organelles.(Bizzarri et al., 2008) An enhanced, ratiometric pHluorin2(Mahon, 2011) was developed with increased fluorescence in acidic compartments. These characteristics made it a useful probe to study protein dynamics in endocytosis and recycling. While undergoing trafficking, the surface proteins are exposed to local environments with measurable pH changes that can be used to assess trafficking pathways. As an alternative to pH sensitive GFP, a Förster Resonant Energy Transfer (FRET)-based protein pH sensor family, pHlameleons(Esposito et al.), were established using FRET from a pH insensitive CFP to various pH sensitive YFP variants. To further advance multicolor imaging capabilities, a ratiometric red fluorescent protein pH sensor, pHRed, was developed, and was shown to detect pH changes in the cytosol and mitochondria.(Tantama et al., 2011) In addition, a pH sensitive, red fluorescent protein, pHTomtato(Li and Tsien, 2012), was engineered as a synaptic probe to report vesicle exocytosis in tandem with a GFP based calcium indicator. Subsequently, pHuji(Shen et al., 2014), an alternative red fluorescent protein pH sensor, with increased pH sensitivity, was demonstrated in parallel with pHluorin to image exocytosis and endocytosis of the transferrin receptor and B2AR simultaneously, exhibiting its utility as a second color pH probe.

A general weakness of FP based pH sensors, however, is that they label the total expressed pool of the protein of interest. After endocytosis the internalized pH sensitive FP-tagged receptors become indistinguishable from the resident intracellular pool of FP-tagged receptors, and contribute to background signal from incompletely quenched FPs or previously internalized protein in various acidic compartments. Discrimination of the surface pool from biosynthetic pools, which are also in neutral compartments, poses a fundamental limit for many FP pH sensor tags. Although FP methods have been

developed to distinguish surface receptor localization vs. intracellular by using a surface FRET based assay(Drake et al., 2008), this method only provides enhanced surface measurements without investigating individual vesicle trafficking after receptor activation.

Several non-FP methods have been developed to measure the pH of endosomal pathways and pH alterations in compartments. Programmable pH sensitive DNA nanomachines have been used as a tool to map endocytic pathways by tagging select trafficking proteins,(Modi et al., 2013) and cysteine cathepsin selective cell-permeable bifunctional probes have been designed to detect specific combinations of pH and protein activity.(Sanman et al., 2016) However, for the purpose of selectively studying GPCR trafficking itineraries, using chemo-selective methods that selectively visualize cell surface receptors, rather than the active site binders or ligands that bind the receptor, is necessary to achieve high-contrast labeling of the plasma-membrane resident protein fraction, suitable for robust trafficking analysis under a variety of manipulations.

Current pH sensitive chemo-selective labeling methods either use expressed epitope tags for antibody binding, labeled-ligand binding, peptide tags that covalently link to modified fluorophores (such as SNAP-tag(Mollwitz et al., 2012) and Halo tag(Los and Wood, 2007)), or coiled-coil tag probes.(Böhme and Beck-Sickinger, 2009; Takeda et al., 2012) A recently developed red-shifted pH sensitive fluorophore showed utility as a semisynthetic sensor platform with both SNAP-tag and protein specific antibodies, leading to a new genetically encoded long-wavelength pH indicator and provided an option for no protein expression modification in studying endo/exocytosis. However, the many chemo-selective methods can involve lengthy incubation times for optimal labeling, and multiple wash steps to remove any unbound fluorophores or ligands, which can lead to higher background signal.

Recent fluorogenic labeling applications reduced these challenges by using activatable “dark” fluorogens or fluorophores and show promising opportunities for superresolution microscopy.(Li et al., 2017) Development of far-red fluorogenic probes for superresolution imaging has improved the available photostability and brightness.(Grimm et al., 2015)(Butkevich et al., 2016)

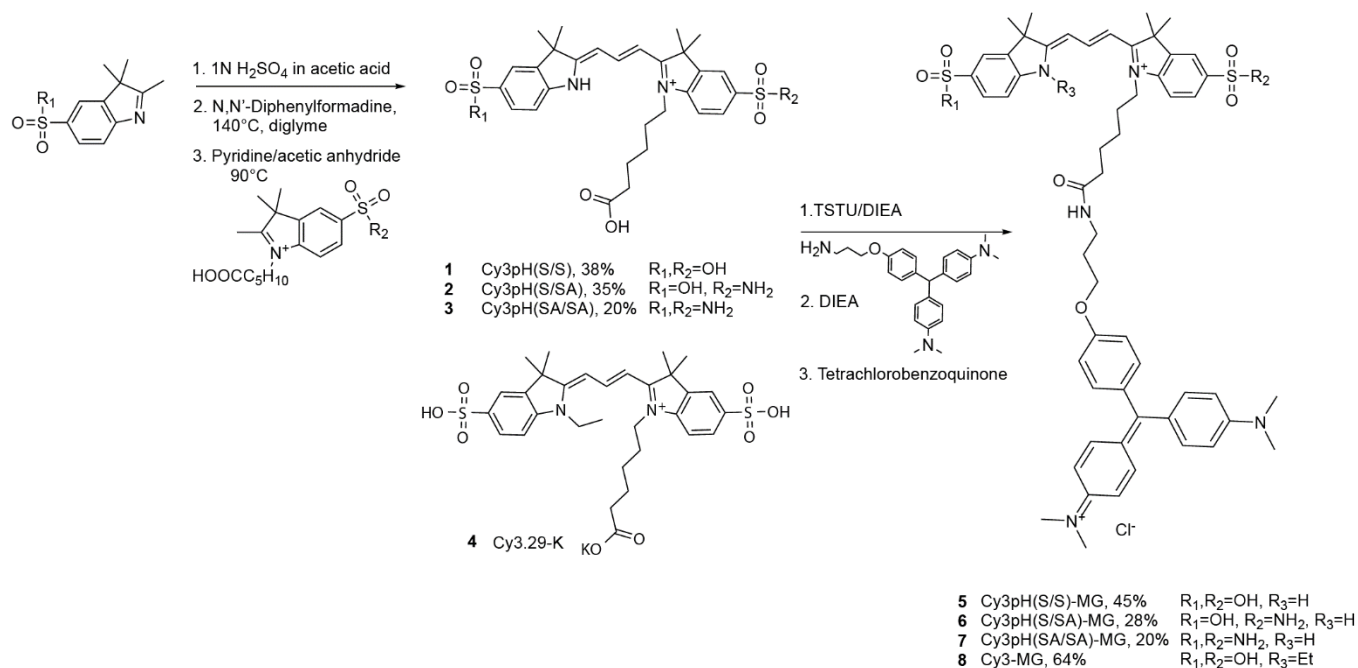
We recently demonstrated rapid labeling of fluorogen activating protein (FAP) tagged B2AR at the cell surface using a cell-excluded fluorogenic ligand based on the far-red triarylmethane dye malachite green (MG-B-Tau).(Yan et al., 2015) FAP technology utilizes a single chain antibody fragment that specifically binds and activates fluorogenic dyes that are otherwise non-fluorescent.(Szent-Gyorgyi et al., 2008) This FAP-dye labeling approach allows for high specificity, rapid dye labeling, and does not require wash steps to remove unbound (dark) dye. While the cell-excluded fluorogenic dye, MG-B-Tau, enabled detection of FAP-fused surface proteins, there remains a need for a robust method for dynamic imaging of receptor trafficking and pH changes during active endocytosis and recycling.

Here we demonstrate a family of far-red, genetically targetable, ratiometric, activatable pH indicator complexes (TRApHIC), based on a pH sensitive Cy3 indicator dye linked to the pH independent fluorogen malachite green, bound to the dL5** FAP. In the absence of FAP binding, the MG moiety quenches emission from the cell-excluded tandem dye, but upon binding of MG to FAP the indicator complex is formed, displaying dual fluorescence excitation with far-red emission, and an excitation ratio

that depends on the pH of the local environment. A family of pH sensitive Cy3 analogs provided a range of pKa values suitable for measurement of extracellular pH changes or changes in the endocytic/recycling pathway. The pH probe was validated in studies of endocytosis and recycling of a model GPCR, the β 2-adrenergic receptor, in both confocal and Stimulated Emission Depletion (STED)-based superresolution imaging, confirming reported differences between agonists in induced endocytosis and revealing differences in recycling after agonist removal.

RESULTS:

pH Sensor Development: Previously, a FAP-based TO1-cypHer5 pH sensor (Grover et al., 2012) was established. When bound to the cognate FAP, the cell impermeable tandem dye based on thiazole orange and cypher5 displays pH dependent FRET and an increased ratio in the acceptor to donor emission signal. This sensor was used to study receptor trafficking endpoints and antigen transfer in dendritic cells. In this sensor system, the acceptor shows fluorescence signal at low pH in the absence of FAP, resulting in a modest, 10-fold fluorogenic activation upon binding and the potential for significant off-target fluorescence due to cellular uptake into acidic compartments. TO1-cypHer5 is an emission-based ratiometric sensor, requiring the separation of the two emission channels during image acquisition and careful evaluation of photobleaching of the independent channels to provide robust pH measurements. To overcome these limitations, we developed a new tandem dye sensor using malachite green (MG) as a fluorogenic acceptor, and a pH dependent Cy3-based donor. This sensor is a variant of our previously demonstrated Cy3-MG tandem dyes (Yushchenko et al., 2012) employed for signal enhancement, and establishes a genetically targetable, highly fluorogenic, excitation-based ratiometric pH reporter that enables quantitative measurement of physiologic pH changes during endocytosis and recycling, dynamically in living cells.



Scheme 1. Synthesis of pH dependent cyanine-malachite green tandem dyes. Detailed synthesis and yields are provided in the supplementary material.

A new series of unsymmetrical Cy3-based pH sensitive donors (**1-3**), prepared as active esters were coupled to an amine-modified MG analog to produce a series of pH sensor tandem dyes (**5-7**) (Scheme 1). In the same fashion, the pH-insensitive analog (**8**) was made from the potassium salt of Cy3.29, a bis-alkylated Cy3 analog (**4**). Upon binding of the MG fluorogen moiety to a FAP (dL5**), the quenched tandem dye becomes activated (Figure S1; Figure S2). In both free and FAP-bound states, the Cy3 signal is efficiently quenched, and the excitation is transferred to the free MG, which acts as a quencher, or to the MG-FAP fluorescent complex, which displays FRET-sensitized emission. At low pH, protonation of the indole nitrogen of the pH sensitive Cy3 moiety extends the resonant aromatic system, increasing the donor absorption and energy transfer signal. While detecting emission from the MG-FAP complex (680 nm), the excitation contribution of the pH sensitive moiety (**1-3**) increases monotonically with respect to pH, whereas MG direct excitation is relatively pH independent (illustrated in Figure 1a and shown in Figure 1b).

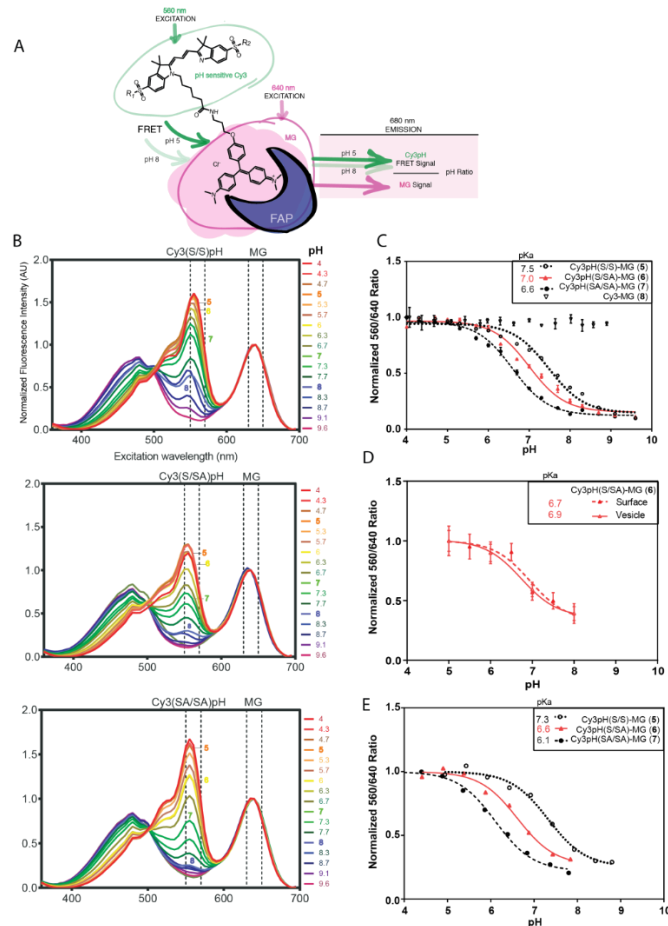


Figure 1. TRAPhIC labeling results in pKa tunable, pH responsive ratiometric probes. **A.** Illustration of dye structure pH sensitivity and the excitation-based ratiometric pH response. **B.** Excitation spectra of Cy3(S/S)pH-MG, Cy3(S/SA)pH-MG, and Cy3(SA/SA)pH-MG from pH 4.0 to pH 9.6, complexed with dL5**[†]. Emission was recorded at 710 nm in TECAN Infinite M1000 plate reader. **C.** Ratiometric characterization of dyes (5-8) response to pH in vitro. The normalized ratio of the fluorescence emission of the dye-protein complex in solution was measured using two excitation wavelengths (560 nm and 640 nm, 710 nm emission in TECAN Infinite M1000 plate reader) was plotted against the solution pH. Mean results were fitted to a non-linear sigmoidal curve, error bars are shown as S.D. TRAPhIC pKas were determined from curve fitting. **D.** Live FAP-B2AR expressing HEK cells were incubated with Cy3(S/SA)pH-MG and calibrated vs pH by nigericin/high K⁺ clamping. Data is shown as surface object measurements (no drug added) and vesicle object measurements (ISO induced endocytosis). The normalized ratio of the fluorescence emission from two excitation wavelengths (560 nm and 640 nm) was plotted against the solution pH. Mean results were fitted to a non-linear sigmoidal curve, error bars are shown as S.D. Dye pKas were determined from curve fitting. **E.** Live FAP-CFTR expressing HEK cells were incubated with each dye and the normalized ratio of the fluorescence emission from two excitation wavelengths (560 nm and 640 nm) was plotted against the solution pH. Results were fitted to a non-linear sigmoidal curve, pKas were determined from curve fitting.

The excitation ratio (560 nm/640 nm) of the family of dyes responds to pH changes with a characteristic sigmoidal curve, showing a ~5-fold change in the ratio from pH 5 to pH 8 when complexed with purified dL5** protein in solution (Figure 1c). The pK_a of the mono-sulfonamide analog (Cy3pH(S/SA)-MG (6), pK_a = 7.0) is better suited for studying endocytosis and recycling than the bis-sulfonate analog (Cy3pH(S/S)-MG (5), pK_a = 7.5), which shows less response throughout the physiological range and significant FRET at neutral pH. In addition, (6) is more useful than the bis-sulfonamide analog (Cy3pH(SA/SA)-MG (7), pK_a = 6.6), showing the greatest response at moderately acidic conditions, typically sampled by recycling receptors. However, the bis-alkylated Cy3 donor (Cy3-MG, 8), is unresponsive to pH changes.

All sensors tightly bind to the same FAP, providing a pH sensitive response that depends only on the dye. These dyes do not fluoresce in the absence of FAP and are cell impermeable (Figure S3; Figure S4). The availability of sensors with tunable pK_a is useful for studying physiology in various contexts with a common genetically encoded tag. These probes bind to dL5** with high affinity (K_ds < 10 nM), suitable for imaging on timescales from minutes to hours, and possess similar quantum yields (Table 1).

Table 1. Dye comparisons (5-8) in the presence of dL5**, with reported % quantum yield (QY), fold activation, R_{max}/R_{min}, pK_a, and K_d.

Dye	Quantum Yield (%)		Fold Activation		R _{max} /R _{min}	pK _a	(nM)
	pH = 5	pH = 8	pH = 5	pH = 8			
Cy3(S/S)pH-MG (5)	21.2	17.4	321	116	2.6	7.5	< 10
Cy3(S/SA)pH-MG (6)	21.8	13	91	122	3.9	7	< 10
Cy3(SA/SA)pH-MG (7)	21.2	10.4	67	49	7.1	6.6	< 10
Cy3-MG (8)	25.1	16.2	136	110	1	NA	< 10

R_{max}/R_{min} is the dynamic range of the dyes. Normalized 560/640 Ratio pH 5/ Normalized 560/640 Ratio pH 8 from Figure 1c.

Cellular Calibration: To calibrate the sensor-FAP complex across physiological pH changes during receptor trafficking, the nigericin clamping method(Thomas et al., 1979) was used in live human embryonic kidney (HEK-293) cells stably expressing a dL5** FAP fused to the N-terminus of B2AR. The sensor (6) was first added to these cells to label B2AR on the plasma membrane through specific interaction with the extracellular dL5**. Cells were subsequently treated with 10 μM isoproterenol (ISO), a potent B2AR agonist, to induce endocytosis (vesicle measurements), or left untreated (surface measurements), followed by switching from the culture media to the nigericin calibration buffer with a high concentration of KCl. This treatment clamps the intracellular pH to the media pH, allowing ratiometric calibration of pH

measurements in a living cellular milieu, whether on the surface or internalized into cellular compartments. The pH responsiveness of sensor (6) bound to dL5**⁺-B2AR on the surface or vesicles analyzed by confocal microscopy both show the same sigmoidal titration curve as the *in vitro* analysis using dL5**⁺ complex with (6) in solution (Fig. 1d). Dyes (5-7) showed distinct vesicular calibration responses in living HEK293 cells expressing a dL5**⁺-CFTR(Holleran et al., 2012) construct that paralleled the pKa values seen in the *in vitro* titrations, although shifted slightly lower in absolute fit pKa (Fig. 1e). The pH titrations of the proteins in cells hence parallel the response seen free in solution, demonstrating the tuning and cellular compatibility of this family of pH sensor dyes.

We evaluated a variety of imaging protocols to assess photobleaching during the imaging time course, recognizing there is a tradeoff between exposure time, intracellular dynamics, experimental duration, and ratiometric quantitation. After (6) surface labeling, B2AR endocytosis was induced with 10 μ M isoproterenol (ISO) for 15 min, and then nigericin pH clamped in different pH buffers. Cells were imaged with exposure times of 100 ms or 500 ms (Supplementary Fig. 5) for 60 frames. Objects ≤ 1 μ M diameter were identified, and quantified for excitation ratio (560 nm/640 nm) with a common emission filter and camera settings. 60 imaging cycles with 500 ms exposure for each channel (60s total illumination) resulted in a 10% change only at pH 5, potentially a result of the increased extinction coefficient of the donor at low pH coupled with the longer exposure. To eliminate potential photobleaching artifacts, using a short exposure time is preferred in live, real-time imaging ≥ 60 frames. Although the endocytosed vesicles are relatively immobile in the nigericin photobleaching experiments and endpoint experiment imaging, vesicles are more mobile during real-time receptor endocytosis and recycling, which may result in motion artifacts upon longer exposures that skews the ratio analysis without further image analysis and correction. In super resolution STED imaging with live cells (*vide infra*), endpoint imaging is optimal for reducing the total of repeated high intensity laser exposure, vesicle motion, and focal drift.

B2AR Agonist-Induced Trafficking: Upon addition of the sensor dye, cells showed strong fluorescence staining on the plasma membrane in the 640 nm excitation channel. The surface 560/640 ratio reported the pH as 7-8, showing pH 7.5 as the average of the fitted Gaussian peak of object ratios (Fig. 2c), consistent with the pH of the imaging media (Opti-MEM pH 7.4). Soon after exposure to the agonists isoproterenol (ISO) or epinephrine (EPI), endocytic vesicles started to emerge from the cell surface and move inward (Supplementary Video 1, 2; Fig. 2 a,b ISO and EPI). The intensity of the plasma membrane decreased significantly and punctate vesicular structures gradually accumulated in the cytoplasm. Fluorescence intensities of the vesicles rose rapidly in both channels, consistent with an enrichment of the receptors in the vesicle following receptor clustering and fusion of endocytosed vesicles during vesicle trafficking. In addition, observable pH changes accompanied the redistribution of the receptors following endocytosis. ~ 15 minutes into endocytosis, the majority of plasma membrane signal had dropped below the detection threshold. At this point, most of the detected objects were receptors in vesicular compartments. After 30.5 minutes, the pH of internalized vesicles covered a broad range, but had significantly decreased to an average of pH 6 for both ISO and EPI conditions (Fig. 2c ISO and EPI). This pH drop suggests continuous acidification of the population of vesicles in the sustained presence of an agonist. Due to the 30 second inter-frame interval, it was not possible to track single vesicles to assess temporal changes in pH, although

such studies may be possible when a narrower time window is utilized for imaging. NorEPI displayed a different endocytic behavior than ISO and EPI, with a widespread population of receptors on the plasma membrane and a lesser amount in endocytosed vesicles by time point 30.5 min. (Supplementary Video 3; Fig. 2 a,b,c NorEPI). Over the complete time course, ISO and EPI had a higher population % in pH ≤ 6 than NorEPI treated cells and the negative controls (Figure 2b). Overall, the calculated $t_{1/2}$ median endocytotic rate was ISO 5.76 (+/- 0.10) min, statistically indistinguishable from EPI at 5.58 (+/- 0.08) min, and lastly NorEPI at 11.8 (+/- 0.25) min (Table 2). The negative controls showed no signs of endocytosis with $\geq 80\%$ objects at pH 7 and $\geq 12\%$ at pH 8, and no significant shift from initiation to 30.5 min (Supplementary Video 4, 5; Fig. 2a,b,c ALP and DMSO).

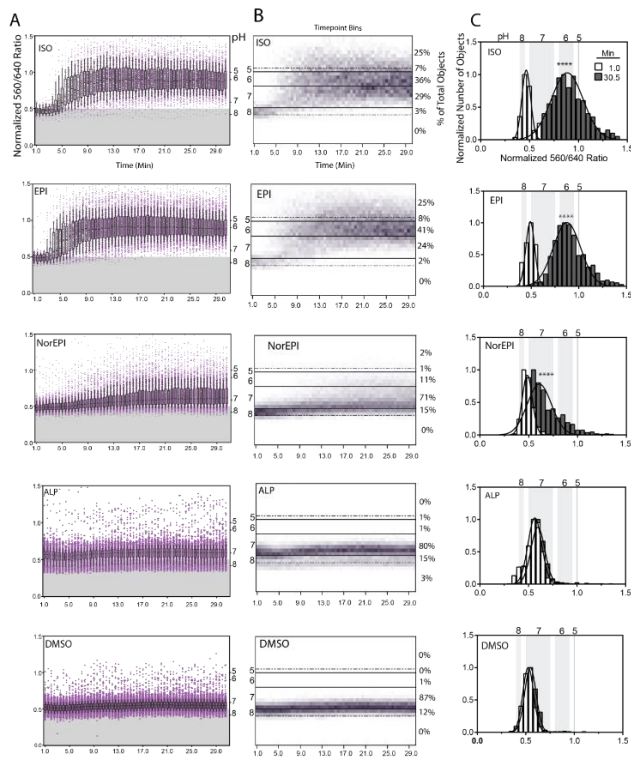


Figure 2. TRAPHiC labeling highlights differences among B2AR agonists in endocytosis rates by single vesicle measurements. A. Analysis of individual vesicles from dL5***-tagged B2AR in real time. Each point represents a single vesicle. The normalized ratio of the emission fluorescence from the two-excitation wavelengths (560 nm and 640 nm) of single vesicles is shown on the left Y-axis and the pH from the single vesicle calibration on the right Y-axis. For the endocytosis experiment, either cells were dosed with 10 μM ISO, 10 μM EPI, 300 μM NorEPI, 10 μM ALP, or 1:1000 DMSO. 1 minute after addition, endocytosis was observed for 30.5 min with 30 sec intervals. Data includes boxplots representing 90th, 75th, median, 25th, and 10th percentile. B. Heat-map and time point bins of vesicle results in A. pH bins are listed on the left Y-axis. Over the whole imaging time period, the total % objects at different pHs are listed on the right Y-axis. C. Histograms of time point 1 min and time 30.5 min vesicle ratios, curves are Gaussian fitted. The average Gaussian fit of each time point was compared. (T-test two tailed) ****P \leq 0.0001; ***P \leq 0.001; **P \leq 0.01; *P \leq 0.05. No indicator P-value $>$ 0.05

Recycling was observed after washing out agonist and adding antagonist, Alprenolol (ALP) (10 μ M), which halted residual endocytosis. At the beginning of exocytosis, ISO was visible as 2 distinct populations, with an average of pH 6.6 and pH 5 (Supplementary Video 6; Fig. 3c ISO). EPI had a broad spread with an average of pH 6 (Supplementary Video 7; Fig. 3c EPI). During the recycling phase, the pH shifted back towards baseline pH (Fig. 3a,b,c ISO and EPI). As the vesicles moved back and fused with the plasma membrane, the plasma membrane regained its fluorescence signal and signal ratio associated with neutral pH. However, EPI showed 2 populations, one remaining with an average of pH 6, and the other restored to pH 7 (Fig. 3c EPI). NorEPI exhibited markedly different exocytosis behavior (Supplementary Video 8). At the start of NorEPI exocytosis, a large population of objects was detected in the pH 7 range (a sum of 2 Gaussian fitted curve with an average of 7.3 and 6.6) (Fig. 3c NorEPI). Over the exocytosis time course, the more acidic population quickly returned to neutral pH 7.2.(Fig. 3b,c). The $t_{1/2}$ average exocytosis rates are shown in Table 2. Throughout the exocytosis imaging period, DMSO and ALP negative controls showed no significant change after washout and addition of ALP (Supplementary Video 9,10; Fig. 3a,b,c). The NorEPI treated cells showed significantly faster exocytosis and slower endocytosis than other agonists, suggesting that the agonist effect of the NorEPI may result in distinct signaling pathways that regulate internalization, intracellular signaling, and recycling.(Reiner et al., 2010)

Table 2. Endocytosis and exocytosis $t_{1/2}$ rates for B2AR agonists.

Drug	$t_{1/2}$ (Minutes)	
	Endocytosis	Exocytosis
ISO	5.76 \pm 0.10	18.14 \pm 0.32
EPI	5.58 \pm 0.08	18.32 \pm 0.33
NorEPI	11.80 \pm 0.25	3.04 \pm 0.46

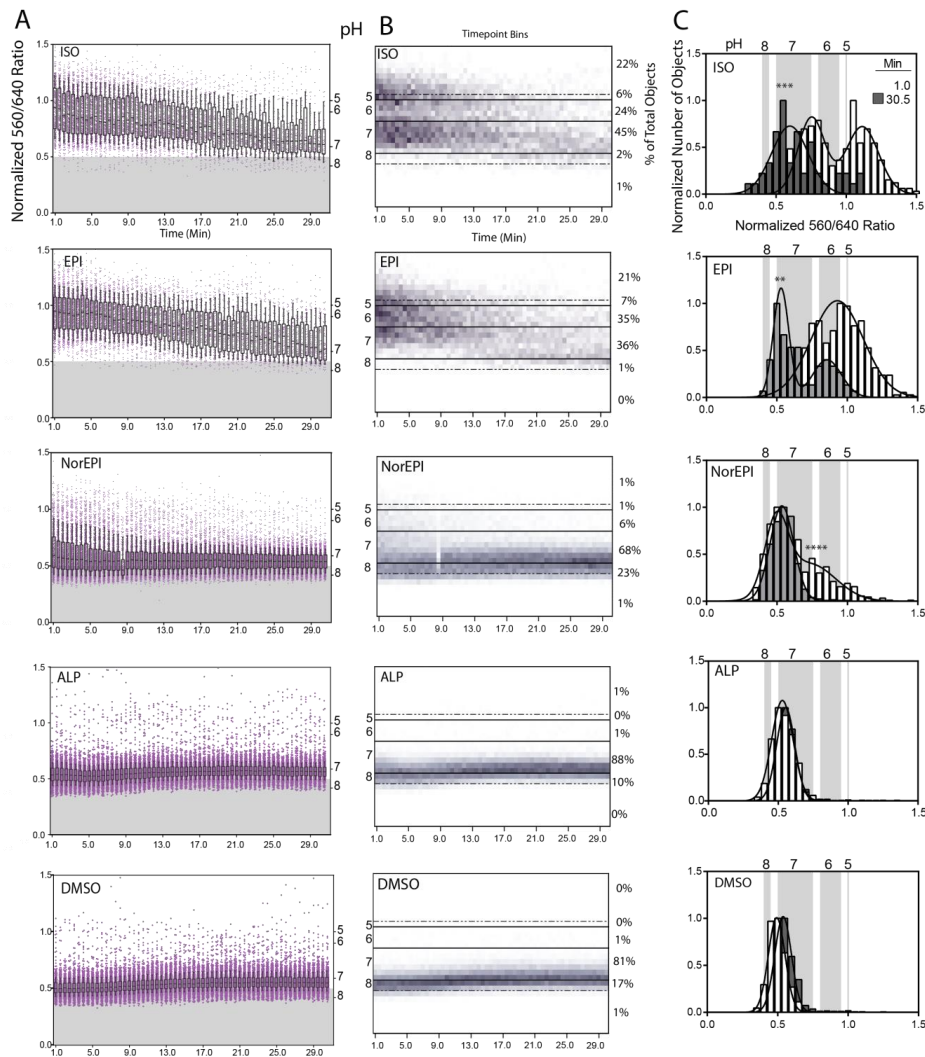


Figure 3. TRAPHC labeling highlights differences among B2AR agonists in recycling rates after drug removal and antagonist treatment by single vesicle measurements. A. Analysis of individual vesicles from dL5**⁺-tagged B2AR in real time. Each point represents a single vesicle. The normalized ratio of the emission fluorescence from the two-excitation wavelengths (560 nm and 640 nm) of single vesicles is shown on the left Y-axis and the pH from the single vesicle calibration on the right Y-axis. After endocytosis imaging, drug was washed out and 10 μ M ALP was added to the cells and time lapse imaging started again to capture the receptor recycling process. Images were acquired every 30 sec for a duration of 30 min. Data includes boxplots representing 90th, 75th, median, 25th, and 10th percentile. B. Heatmap and time point bins of vesicle results in A. pH bins are listed on the left Y-axis. Over the whole imaging time period, the total % objects at different pHs are listed on the right Y-axis. C. Histograms of time point 1 min and time 30.5 min results, curves are Gaussian fitted. The average Gaussian fit of each time point was compared. (T-test two tailed). For results with 2 different populations for a timepoint, One-Way ANOVA multiple comparisons test was performed. ****P \leq 0.0001; ***P \leq 0.001; **P \leq 0.01; *P \leq 0.05. No indicator P-value > 0.05

Superresolution Ratiometric Physiological Imaging: Because the emission of the tandem dye occurs through the MG fluorogen regardless of excitation, we thought it probable that STED could be used to achieve superresolution pH measurements using dual excitation and a single depletion wavelength (775 nm), suitable for depletion of the MG fluorogen (Supplementary Fig. 6). Exclusively using the 775 nm depletion laser is ideal for reducing cellular damage, autofluorescence, light scattering, and photobleaching. (Butkevich et al., 2016) We used a commercially available Leica STED system with dual excitation and 775 nm depletion for both excitation channels, and examined the resolution enhancement and ratiometric properties of FAP-B2AR labeled with tandem dye (**6**) in living cells. Figure 4a shows a confocal vs STED single frame image of endocytosed FAP-B2AR 20 min after dye labeling and ISO addition. The confocal and STED images show clear resolution differences that are more pronounced in select endosomal line plots (Fig. 4b). The line plots of the 560 and 640 ex channels in the confocal and STED channels show different ratiometric intensities, attributed to the differences in laser power between microscopy methods, required for optimal image quality. Simple raw confocal and STED object 560/640 ratios were obtained and plotted against each other, showing a positive linear correlation ($R^2 = .6$), suggesting a robust ratiometric pH sensor response for both confocal and STED modalities. (Fig. 4c)

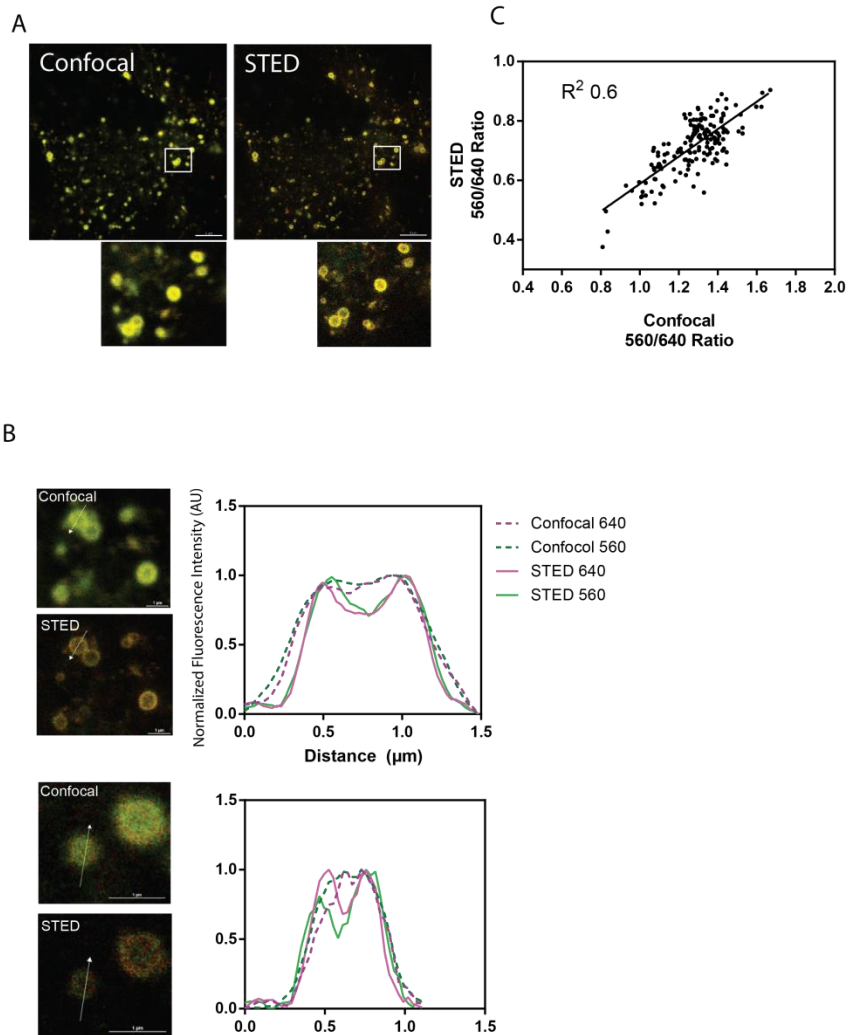


Figure 4. TRAPHiC labeling is compatible with ratiometric STED-based superresolution imaging. A. Confocal and STED image of Cy3(S/SA)pH-MG labeled FAP-B2AR. Scale bar 5 μm. B. Line plots across individual endosomal objects in 560 and 640 excitation channels, show pronounced resolution enhancement under STED excitation. Scale bar 1 μm. C. STED endosomal object 560/640 ratio plotted against the confocal 560/640 ratio. The resulting ratios show a ($R^2 = .6$) positive linear correlation with each other. (objects were collected from 3 different fields of view)

DISCUSSION AND FUTURE DIRECTIONS:

We devised a new approach to develop highly fluorogenic tandem dye sensors, and demonstrated the utility of the approach using a series of tuned pH sensors to visualize for receptor trafficking. These sensor dyes are activated on binding with high affinity to a cognate FAP, genetically fused to a target protein, generating FRET based excitation ratiometric properties. These pH sensors are well-suited for monitoring the pH dynamics associated with endocytosis and recycling of receptors or other cell surface proteins. Surface exposed receptor labeling is achieved by adding the dye to the cells in media without washing, where the cell-impermeant dye selectively labels proteins at the plasma membrane. We demonstrated this labeling approach using agonist-mediated internalization of B2AR, providing a new approach to studying real time trafficking of membrane proteins in living cells and demonstrating the first excitation-ratiometric physiological indicator useful in STED microscopy. B2AR physiology

These probes are well-suited for measuring a range of pH changes in receptor trafficking, or measuring pH changes in the extracellular and pericellular space. The dyes used as physiological indicators in our sensor platform are chromogenic and fluorescent in low pH environments, permitting a pH sensitive excitation channel as a result of physiological changes. It is possible that other reversible or reaction-based indicators could also be paired with a quenching fluorogen acceptor to produce new targeted, ratiometric, activatable physiological sensors for use in living cells. Although the pH sensitive probes demonstrated here are cell-excluded, other sensor dyes could yield cell-permeant physiological sensors, although the overall molecular weight may limit the ability of some sensor dyes to access intracellular targets.

METHODS:

Plasmid and Cell Line Generation: pBabe-dL5**-β2-AR was generated previously²⁴ and plasmid is available at Addgene (ID 101253). Stable HEK293 cells were generated by transfecting HEK293 cells with pBabe-dL5**-β2-AR followed by drug selection (1 mg ml⁻¹ puromycin, Invitrogen) and FACS enrichment (Becton Dickinson FACS Vantage flow cytometer. Excitation: 633 nm; emission: 685/35 nm).

Cell Culture: HEK cells were cultured in Dulbecco's Modified Eagle Medium. Cultures were supplied with 10% fetal bovine serum and incubated at 37 °C in 5% CO₂.

pH Calibration Buffer for In-vitro Measurements: In order to keep ion composition of the pH buffers the same across the whole range of the pH that should be covered several weak acids were used. 4.8g of glacial acetic acid, 7.84 g of phosphoric acid and 4.95g of boric acid were dissolved in 150mL of DI

water and brought up to 200 mL total making the stock acidic solution. For each pH buffer 12.5 mL of the acidic stock was transferred to 50 mL tube titrated with 2M NaOH to the desired pH and brought to 50 mL total.

Spectroscopic Analysis: UV-Vis absorption: roughly 0.1 mg Cy3pH(S/SA)-MG was dissolved in ethanol with 1% acetic acid to prevent carbinol formation of MG. The tandem dye concentration was measured by the absorbance peak of MG at 606 nm ($\epsilon = 91,600 \text{ M}^{-1}\text{cm}^{-1}$) in acidic ethanol using a UV-Vis spectrophotometer (PerkinElmer).

Excitation Spectra: Dyes with 5-fold excess of dL5 were precomplexed in pH buffers from pH 5 to pH 9 keeping sample absorption below 0.4 at main absorption peaks. Excitation scan was performed from 400 nm to 680 nm with the emission recorded at 710 nm and measured on a TECAN Infinite M1000 fluorescence plate reader.

Fluorescence Titration: Secretion and purification of soluble dL5 was as described previously.(Wang et al., 2015) Binding affinity to soluble dL5 was measured on a TECAN Infinite M1000 fluorescence plate reader. 1 nM dL5 was mixed with varying concentrations of dye at neutral pH (7.4) in PBS. The FAP+dye complex fluorescence was corrected by subtracting the fluorescence of a dye only sample. The data was fitted using a binary ligand depletion equilibrium model in Prism 6.0, which reported kD. Data points are the mean \pm S.D. from triplicate measurements.

Live Cell Spinning Disk Confocal Microscopy: 500 nM Cy3pH(S/SA)-MG (**6**) was added to cells to label dL5**⁻B2AR for 15 min. Then either 10 μM isoproterenol (ISO) (Cayman Chemicals), 10 μM epinephrine (EPI) (Cayman Chemicals), 300 μM norepinephrine (NorEPI) (Cayman Chemicals), 10 μM alprenolol (ALP) (Cayman Chemicals), or vehicle DMSO, was added to the cells and time lapse imaging started 1 minute after the addition of drug. Images were acquired every 30 sec for a duration of 30.5 min. Then drug was washed off by rinsing cells with at least 4 volumes of imaging medium, Opti-MEM (Invitrogen). After washout, 10 μM ALP was added to the cells and time lapse imaging started again to capture the recycling process. Images were acquired every 30 sec for a duration of 30.5 min. During imaging, cells were cultured in Opti-MEM in Mattek dishes (MatTek Corp.) and kept in an imaging chamber at 37 °C with 5% CO₂ supply (Pathology devices). Cells were imaged on an Andor Revolution XD system (Andor technology) with a Yokogawa CSU-X1 spinning disk confocal unit (Yokogawa Industries). Cells were imaged with a 60x, 1.49 TIRF objective (Nikon) and excited with a 640 nm and a 560 nm laser sequentially. Emission was collected with a 685/70 band pass for both channels. EM gain was set at 300.

Live Cell Leica STED and Confocal Microscopy: 500 nM Cy3pH(S/SA)-MG in Opti-MEM was added to cells to label dL5^{***}-B2-AR for 15 min. Then 10 μ M isoproterenol (ISO) (Cayman Chemicals) was added to the cells and imaging started 20 min after addition. Imaging was done on Leica microscope with 100x/1.40 HC PL APO oil objective. Cells were excited with 561 nm and 633 nm laser excitation using a white-light laser and the acousto-optic beam splitter respectively, while emission was detected at 660 nm - 725 nm (gain 100, time gate of 0.5 ns- 6.5 ns). STED imaging utilized 775 nm depletion laser (power 100%) for both excitation channels. Confocal laser power: 561ex (56%), 633 ex (12%); STED laser power: 561 ex (100%), 633 ex (64%). During imaging, cells were cultured in Opti-MEM (Invitrogen) in Mattek dishes (MatTek Corp.) and kept in an imaging chamber at 37 °C with 5% CO₂ supply.

pH Calibration with Nigericin Clamping: Nigericin calibration buffers contained 140 mM KCl, 5 mM α -D-glucose, 0.5 mM CaCl₂·2H₂O, 1 mM MgCl₂ and the pH (pH 5 to pH 8) of the mixture was adjusted using 20 mM MES and 20 mM Tris base, where MES and Tris base were added in different ratios to generate different pH buffers.(Chow and Hedley, 2001) Cells were treated with the calibration buffer with 10 μ M Nigericin (Sigma) for 10 min prior to imaging.

Single Object Ratio Analysis: Analysis was carried out using Imaris software. Objects were identified with spot detection and background subtraction in the 640 nm channel. After identifying objects, they were automatically thresholded based on the “average center intensity” in the 640 nm channel using default settings. The resulting object’s average intensity measurements were determined in the Cy3pH(S/SA) FRET (560 nm ex) and MG (640 nm ex) channels. For each identified object, the average 560/640 ratio was plotted vs. time after treatment for endocytosis and recycling conditions (Fig. 2a; Fig. 3a). The 75th, median, and 25th percentile were calculated at every time point and median was fitted to a sigmoidal curve to determine the $t_{1/2}$ values (curve not shown, all curves $R^2 > .85$). The boxplot whiskers represent the 90th and 10th percentile. The experimental data was also binned to .05 intervals from 0 - 1.5 (normalized 560/640 ratio) for each time point. Collectively, a heat map was generated, which displays the consensus and what percentage of all identified objects are in a pH range (Fig. 2b; Fig. 3b). The first time point (1 min) and last time point (30.5 min) bins for both endo- and exocytosis experiments, were plotted as a histogram and fitted to a robust Gaussian, or sum of 2 Gaussians, curve (Fig. 2c; Fig. 3c). The histogram fitted curves demonstrate if there was a significant population shift in pH between selected time points. Data analysis was performed with Prism 6.0. ****P \leq 0.0001; ***P \leq 0.001; **P \leq 0.01; *P \leq 0.05. No indicator P-value $>$ 0.05

pH Calibration Analysis: Expressing cells were labeled with 500 nM Cy3pH(S/SA)-MG for 15 min and then subjected to either 10 μ M ISO (vesicle) for 15 min or no drug (surface). In both conditions, nigericin clamping was done at each pH (from pH 5 to pH 8), at least 6 pairs of images (640 nm excitation followed by 560 nm excitation, both 680 emission) were taken for the ratio analysis. Exposure time was 100 ms for both channels. Objects were combined from all the images and binned histograms representing

the distribution of the ratio were generated by single Gaussian peak fitting. The best-fit average values were used for plots and non-linear sigmoid fitting using Prism 6.0. Data points are the mean \pm S.D. from the fit.

Photostability Measurement: Cells were labeled with 300 nM Cy3pH(S/SA)-MG and exposed to 10 μ M ISO for 15 min. Then the cells were subjected to nigericin clamping. Following Nigericin clamping, the cells were imaged with 640 nm excitation and 560 nm excitation sequentially for 60 cycles with an exposure time of 100 ms or 500 ms for both channels. The data is expressed as the mean \pm S.E.M. of 3 different fields of view.

Statistical Analysis: All statistics were performed by GraphPad Prism 6.0 and are either described in methods or in figure legends.

Data Availability: Synthesis and NMR of the final products is available in the supporting information. Cy3(S/SA)pH-MG cell impermeability and specificity is shown in supporting information. All data presented are available from the corresponding author upon request.

Supporting Information.

Dye activation with dL5 illustrated by emission spectra for dyes with or without protein (excitation at 610 nm (MG excitation) or 532 nm (Cy3 excitation) (Figure S1). Excitation spectra of dyes and their complexes at different pH with emission collected at 690 nm (Figure S2). Cy3(S/SA)pH-MG dye is FAP specific (Figure S3). Cy3(S/SA)pH-MG dye is cell impermeable (Figure S4). Photobleaching analysis of Cy3(S/SA)pH-MG when pH is clamped by nigericin (Figure S5). STED spectral depletion (Figure S6). Detailed synthesis of dyes is in chemistry supplemental information section. B2AR agonist endocytosis and exocytosis movies (Movie S1-S10)

FUNDING RESOURCES:

NMR instrumentation at CMU was partially supported by NSF (CHE-0130903 and CHE-1039870). The STED microscope was acquired under the NIH shared instrument grant program S10OD021540. This work was supported in part by NIH grants R01EB017268 and U54GM103529.

ACKNOWLEDGEMENTS:

We thank Dr. Manojkumar Puthenveedu and Zara Y. Weinberg for advice with B2AR trafficking, Ulf Schwarz for assistance with STED microscopy, and Dr. Cheryl Telmer for helpful discussion.

AUTHOR INFORMATION:

Author Contributions

L.A.P performed imaging experiments, data analysis, and wrote the paper. Q.Y. performed imaging, photobleaching experiments, initial data analysis, and wrote the paper. B.F.S synthesized TO1-Cypher5, Cy3-MG, Cy3pH(S/S)-MG, Cy3pH(S/SA)-MG, and Cy3pH(SA/SA)-MG. D.K. developed quick pipeline for organizing large single-vesicle time-course data sets for Prism, performed spectroscopy data collection, and helped with methods. M.B.L. performed pH calibration and data analysis. S.C.W. did data analysis and provided assistance with STED microscopy. L.K. and S.S. performed emission and excitation spectra of Cy3pH(S/S)-MG, Cy3pH(S/SA)-MG, and Cy3pH(SA/SA)-MG. M.P.B. designed sensors, experiments, and wrote the paper.

Corresponding author

Correspondence to Marcel P. Bruchez

COMPETING INTERESTS: M.P.B. is founder and Chief Scientific Officer at Sharp Edge Labs, Inc., a licensee commercially utilizing the FAP-fluorogen technology.

REFERENCES:

- Bizzarri, R., Serresi, M., Luin, S., and Beltram, F. (2008). Green fluorescent protein based pH indicators for in vivo use: a review. *Anal. Bioanal. Chem.* *393*, 1107.
- Böhme, I., and Beck-Sickinger, A.G. (2009). Illuminating the life of GPCRs. *Cell Commun. Signal.* *7*, 16.
- Butkevich, A.N., Mitronova, G.Y., Sidenstein, S.C., Klocke, J.L., Kamin, D., Meineke, D.N.H., D'Este, E., Kraemer, P.-T., Danzl, J.G., Belov, V.N., et al. (2016). Fluorescent Rhodamines and Fluorogenic Carbopyronines for Super-Resolution STED Microscopy in Living Cells. *Angew. Chemie Int. Ed.* *55*, 3290–3294.
- Chow, S., and Hedley, D. (2001). Flow Cytometric Measurement of Intracellular pH. *Curr. Protoc. Cytom.* *1–10*.
- Diril, M.K., Wienisch, M., Jung, N., Klingauf, J., and Haucke, V. (2006). Stonin 2 Is an AP-2-Dependent Endocytic Sorting Adaptor for Synaptotagmin Internalization and Recycling. *Dev. Cell* *10*, 233–244.
- Drake, M.T., Shenoy, S.K., and Lefkowitz, R.J. (2006). Trafficking of G Protein–Coupled Receptors. *Circ. Res.* *99*, 570 LP-582.
- Drake, M.T., Violin, J.D., Whalen, E.J., Wisler, J.W., Shenoy, S.K., and Lefkowitz, R.J. (2008). beta-arrestin-biased agonism at the beta2-adrenergic receptor. *J. Biol. Chem.* *283*, 5669–5676.
- Esposito, A., Gralle, M., Angela Dani, M.C., Lange, D., and Wouters, F.S. pHlameleons: A Family of FRET-Based Protein Sensors for Quantitative pH Imaging.
- Grimm, J.B., English, B.P., Chen, J., Slaughter, J.P., Zhang, Z., Revyakin, A., Patel, R., Macklin, J.J., Normanno, D., Singer, R.H., et al. (2015). A general method to improve fluorophores for live-cell and single-molecule microscopy. *Nat. Methods* *12*, 244–250.
- Grover, A., Schmidt, B.F., Salter, R.D., Watkins, S.C., Waggoner, A.S., and Bruchez, M.P. (2012). Genetically encoded pH sensor for tracking surface proteins through endocytosis. *Angew. Chemie - Int. Ed.* *51*, 4838–4842.
- Hanyaloglu, A.C., and Zastrow, M. von (2008). Regulation of GPCRs by Endocytic Membrane Trafficking and Its Potential Implications. *Annu. Rev. Pharmacol. Toxicol.* *48*, 537–568.
- Holleran, J.P., Glover, M.L., Peters, K.W., Bertrand, C. a, Watkins, S.C., Jarvik, J.W., and Frizzell, R. a (2012). Pharmacological rescue of the mutant cystic fibrosis transmembrane conductance regulator (CFTR) detected by use of a novel fluorescence platform. *Mol. Med.* *18*, 685–696.
- Hopkins, A.L., and Groom, C.R. (2002). The druggable genome. *Nat Rev Drug Discov* *1*, 727–730.
- Kenakin, T., and Christopoulos, A. (2013). Signalling bias in new drug discovery: detection, quantification and therapeutic impact. *Nat Rev Drug Discov* *12*, 205–216.

- Li, Y., and Tsien, R.W. (2012). pHTomato, a red, genetically encoded indicator that enables multiplex interrogation of synaptic activity. *Nat. Neurosci.* *15*, 1047–1053.
- Li, C., Tebo, G.A., and Gautier, A. (2017). Fluorogenic Labeling Strategies for Biological Imaging. *Int. J. Mol. Sci.* *18*.
- Liu, J.J., Horst, R., Katritch, V., Stevens, R.C., and Wüthrich, K. (2012). Biased signaling pathways in $\beta(2)$ -adrenergic receptor characterized by $(19)\text{F-NMR}$. *Science* *335*, 1106–1110.
- Los, G. V, and Wood, K. (2007). The HaloTag: a novel technology for cell imaging and protein analysis. *Methods Mol Biol* *356*.
- Mahon, M.J. (2011). pHluorin2: an enhanced, ratiometric, pH-sensitive green fluorescent protein. *Adv. Biosci. Biotechnol.* *2*, 132–137.
- Miesenbock, G., De Angelis, D.A., and Rothman, J.E. (1998). Visualizing secretion and synaptic transmission with pH-sensitive green fluorescent proteins. *Nature* *394*, 192–195.
- Modi, S., Nizak, C., Surana, S., Halder, S., and Krishnan, Y. (2013). Two DNA nanomachines map pH changes along intersecting endocytic pathways inside the same cell. *Nat. Nanotechnol.* *8*, 459–467.
- Mollwitz, B., Brunk, E., Schmitt, S., Pojer, F., Bannwarth, M., Schiltz, M., Rothlisberger, U., and Johnsson, K. (2012). Directed Evolution of the Suicide Protein O^6 -Alkylguanine-DNA Alkyltransferase for Increased Reactivity Results in an Alkylated Protein with Exceptional Stability. *Biochemistry* *51*, 986–994.
- Pierce, K.L., Premont, R.T., and Lefkowitz, R.J. (2002). Seven-transmembrane receptors. *Nat Rev Mol Cell Biol* *3*, 639–650.
- Reiner, S., Ambrosio, M., Hoffmann, C., and Lohse, M.J. (2010). Differential Signaling of the Endogenous Agonists at the $\beta(2)$ -Adrenergic Receptor. *J. Biol. Chem.* *285*, 36188–36198.
- Salazar, N.C., Chen, J., and Rockman, H.A. (2007). Cardiac GPCRs: GPCR signaling in healthy and failing hearts. *Biochim. Biophys. Acta - Biomembr.* *1768*, 1006–1018.
- Sankaranarayanan, S., De Angelis, D., Rothman, J.E., and Ryan, T.A. (2000). The Use of pHluorins for Optical Measurements of Presynaptic Activity. *Biophys. J.* *79*, 2199–2208.
- Sanman, L.E., van der Linden, W.A., Verdoes, M., and Bogoy, M. (2016). Bifunctional Probes of Cathepsin Protease Activity and pH Reveal Alterations in Endolysosomal pH during Bacterial Infection. *Cell Chem. Biol.* *23*, 793–804.
- Shen, Y., Rosendale, M., Campbell, R.E., and Perrais, D. (2014). pHuji, a pH-sensitive red fluorescent protein for imaging of exo- and endocytosis. *J. Cell Biol.* *207*, 419–432.
- Szent-Gyorgyi, C., Schmidt, B.F., Creeger, Y., Fisher, G.W., Zakel, K.L., Adler, S., Fitzpatrick, J.A.J., Woolford, C.A., Yan, Q., Vasilev, K. V, et al. (2008). Fluorogen-activating single-chain antibodies for imaging cell surface proteins. *Nat Biotech* *26*, 235–240.

- Takeda, Y., Yano, Y., and Matsuzaki, K. (2012). High-Throughput Analysis of Ligand-Induced Internalization of β 2-Adrenoceptors Using the Coiled-Coil Tag–Probe Method. *Anal. Chem.* *84*, 1754–1759.
- Tantama, M., Hung, Y.P., and Yellen, G. (2011). Imaging Intracellular pH in Live Cells with a Genetically-Encoded Red Fluorescent Protein Sensor. *J. Am. Chem. Soc.* *133*, 10034–10037.
- Thomas, J.A., Buchsbaum, R.N., Zimniak, A., and Racker, E. (1979). Intracellular pH measurements in Ehrlich ascites tumor cells utilizing spectroscopic probes generated in situ. *Biochemistry* *18*, 2210–2218.
- Wang, Y., Telmer, C.A., Schmidt, B.F., Franke, J.D., Ort, S., Arndt-Jovin, D.J., and Bruchez, M.P. (2015). Fluorogen activating protein-affibody probes: modular, no-wash measurement of epidermal growth factor receptors. *Bioconjug. Chem.* *26*, 137–144.
- Xu, Y., Rubin, B.R., Orme, C.M., Karpikov, A., Yu, C., Bogan, J.S., and Toomre, D.K. (2011). Dual-mode of insulin action controls GLUT4 vesicle exocytosis. *J. Cell Biol.* *193*, 643 LP-653.
- Yan, Q., Schmidt, B.F., Perkins, L. a., Naganbabu, M., Saurabh, S., Andreko, S.K., and Bruchez, M.P. (2015). Near-instant surface-selective fluorogenic protein quantification using sulfonated triarylmethane dyes and fluorogen activating proteins. *Org. Biomol. Chem.* *13*, 2078–2086.
- Yao, L., Fan, P., Jiang, Z., Mailliard, W.S., Gordon, A.S., and Diamond, I. (2003). Addicting drugs utilize a synergistic molecular mechanism in common requiring adenosine and Gi- β y dimers. *Proc. Natl. Acad. Sci. U. S. A.* *100*, 14379–14384.
- Yushchenko, D.A., Zhang, M., Yan, Q., Waggoner, A.S., and Bruchez, M.P. (2012). Genetically targetable and color-switching fluorescent probe. *Chembiochem* *13*, 1564–1568.

SUPPORTING INFORMATION:

Supplemental movies are available at: <https://cmu.box.com/s/djsnkfmt71x5o2c4enpu4ea4w0853xpc>

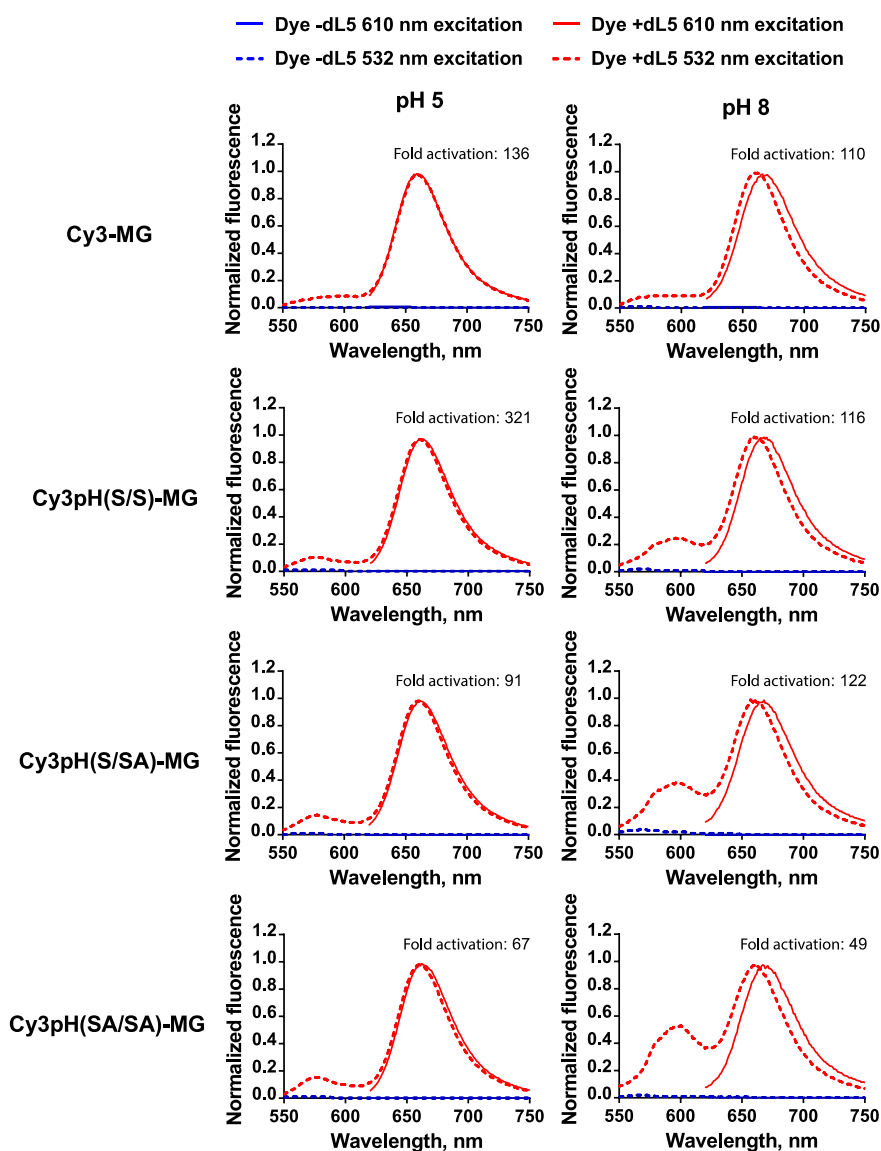


Figure S1. Dye activation with dL5 illustrated by emission spectra for dyes with or without protein (excitation at 610 nm (MG excitation) or 532 nm (Cy3 excitation)). Fold activation calculated as ratio of the integral emission at 660-700 nm range (common emission filter used for microscopy) with 610 nm excitation after correction for the sample absorption at the excitation wavelength. Dyes with 5-fold excess of dL5 were precomplexed in a pH 5 buffer and measured on a Quantamaster monochromator fluorimeter (Photon Technology International). Absorption of the samples was controlled to be lower than 0.1 on the excitation wavelength. The samples were excited at 530 nm and the emission scan was from 550 nm to 750 nm. The tandem dye only sample was also measured the same way and served as a control. **D.K. and S.S. collected data**

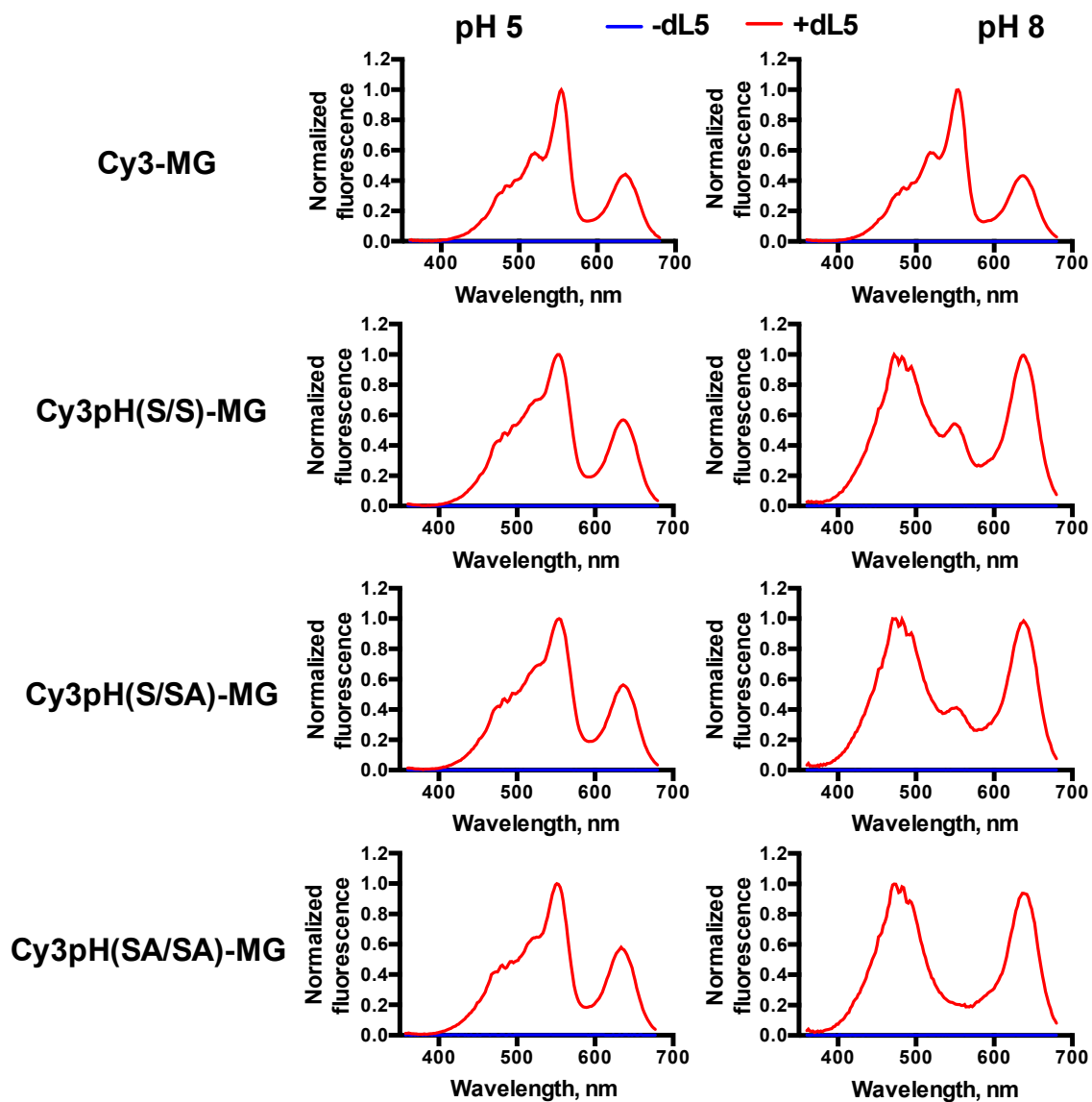


Figure S2. Excitation spectra of dyes and their complexes at different pH with emission collected at 690 nm. For this measurements, same samples as for the emission spectra (Supplemental figure 1) were used. Emission was collected at 690 nm with excitation scanned from 360 to 680 nm. Samples were measured on Quantmaster monochromator fluorimeter (Photon Technology International) with excitation correction. **D.K.** and **S.S** collected data.

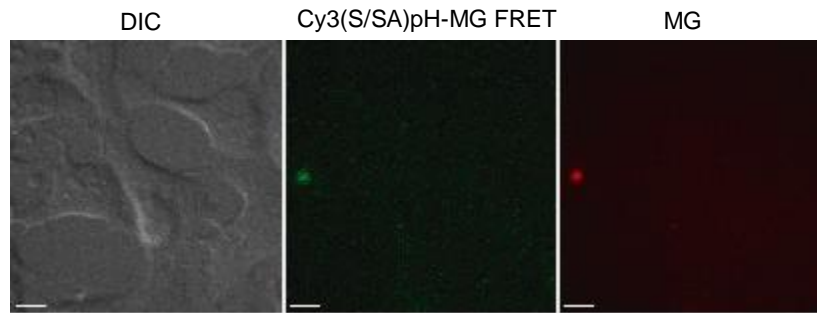


Figure S3. Cy3(S/SA)pH-MG dye is FAP specific. 500 nM Cy3sApH in HBSS was incubated with non-FAP expressing HEK293 cells for 15 min. Cell images were acquired on Andor revolution XD system spinning disk with a 60x, 1.49 TIRF objective (Nikon). Cy3(S/SA)pH-MG FRET: 560ex, 685/70 em. MG: 640ex, 680/75 em. Matched lookup tables. Scale Bar: 10 μ M.

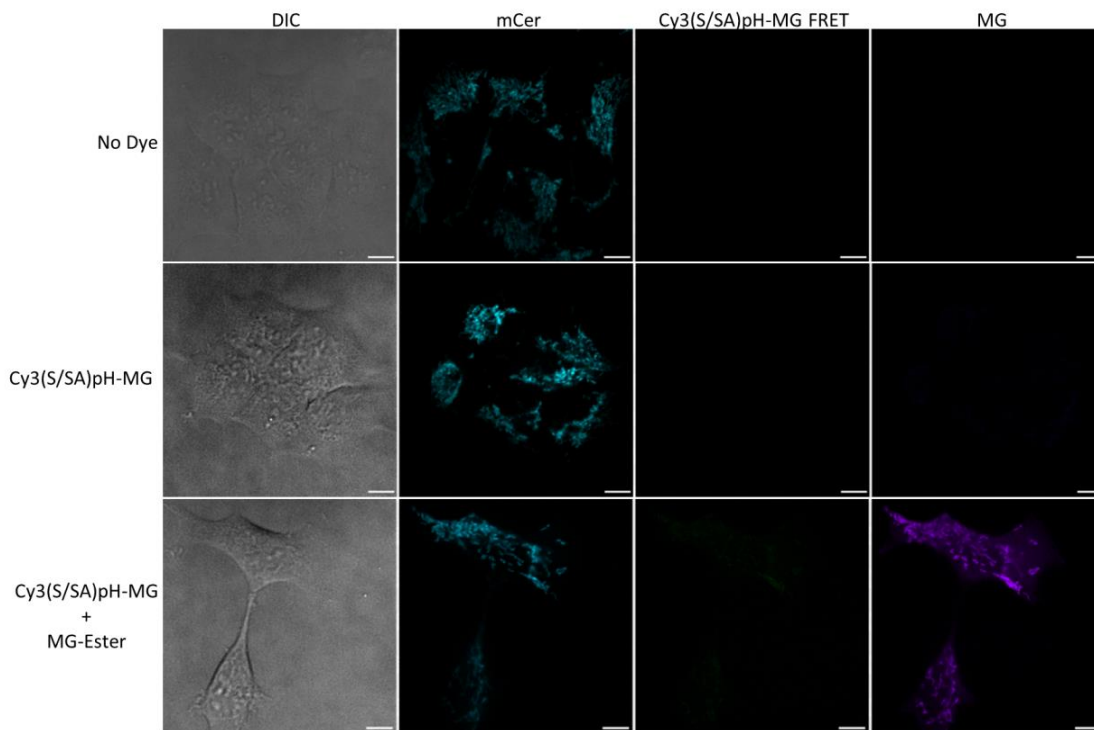


Figure S4. Cy3(S/SA)pH-MG dye is cell impermeable. Demonstrated pH probe cell exclusion through incubating 500 nM Cy3(S/SA)pH-MG dye in DMEM with HEK293 cells expressing FAP-mCerulean (mCer) tagged mitochondria. (Telmer et al., 2015) Top panel row is without any dye incubation, showing exclusively mitochondrial associated mCer fluorescence. Middle panel row is after 15 min incubation with 500 nM Cy3(S/SA)pH-MG dye, demonstrating no intracellular labeling of FAP-tagged mitochondria in either the FRET or MG channel. After Cy3(S/SA)pH-MG imaging, 500 nM cell permeable MG-Ester¹ was directly added and incubated for 15 min (last panel row). The presence of MG fluorescence and its colocalization with mCer, indicated that MG-ester labeled FAP-mitochondria.

Cell images were acquired on Andor revolution XD system spinning disk with a 60x, 1.49 TIRF objective (Nikon). mCer: 405 ex, 435/25 em. Cy3(S/SA)pH-MG FRET: 560ex, 685/75em. MG: 640ex, 680/75 em. Matched lookup tables. Scale Bar: 10 μ M.

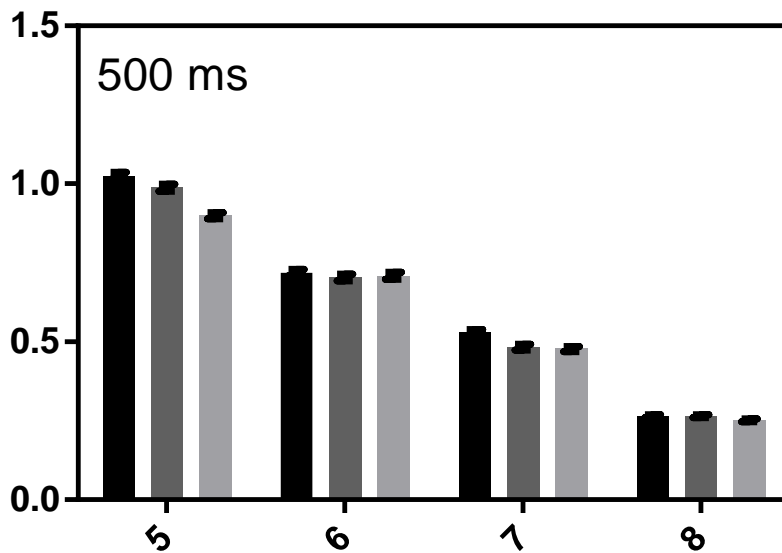
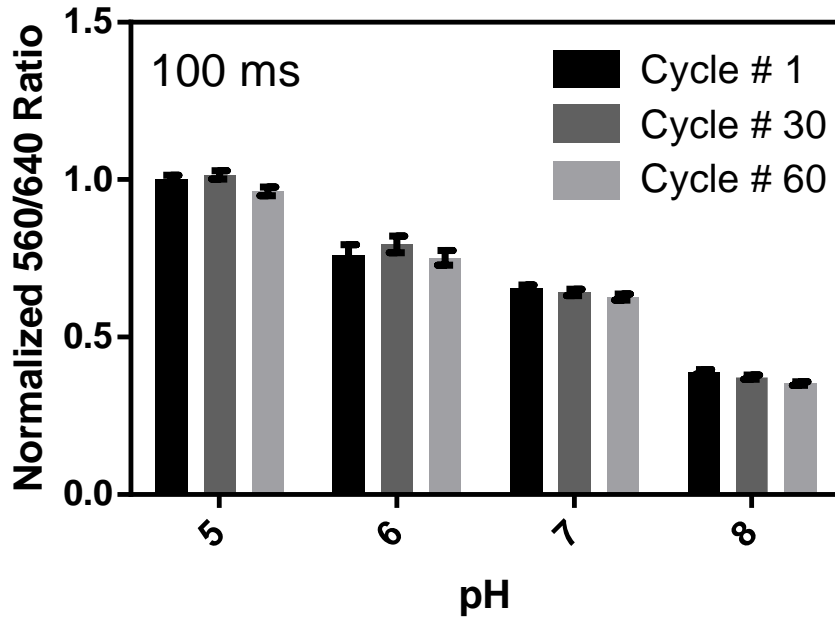


Figure S5: Photobleaching analysis of Cy3(S/SA)pH-MG when pH is clamped by nigericin. Following endocytosis and nigericin pH clamping, the cells were imaged for 60 cycles with an exposure time of 100 ms or 500 ms. In each cycle the sample was imaged with 640 nm and 560 nm excitation sequentially. The averaged 560/640 ratio at cycle #1, 30 and 60 was normalized to cycle #1 at pH 5 across the pH range. Data is expressed as the mean \pm S.E.M of 3 different fields of view. Cell images were acquired on Andor revolution XD system spinning disk with a 60x, 1.49 TIRF objective (Nikon). Cy3(S/SA)pH-MG FRET: 560ex, 685/75em. MG: 640ex, 680/75 em. Q.Y. collected data

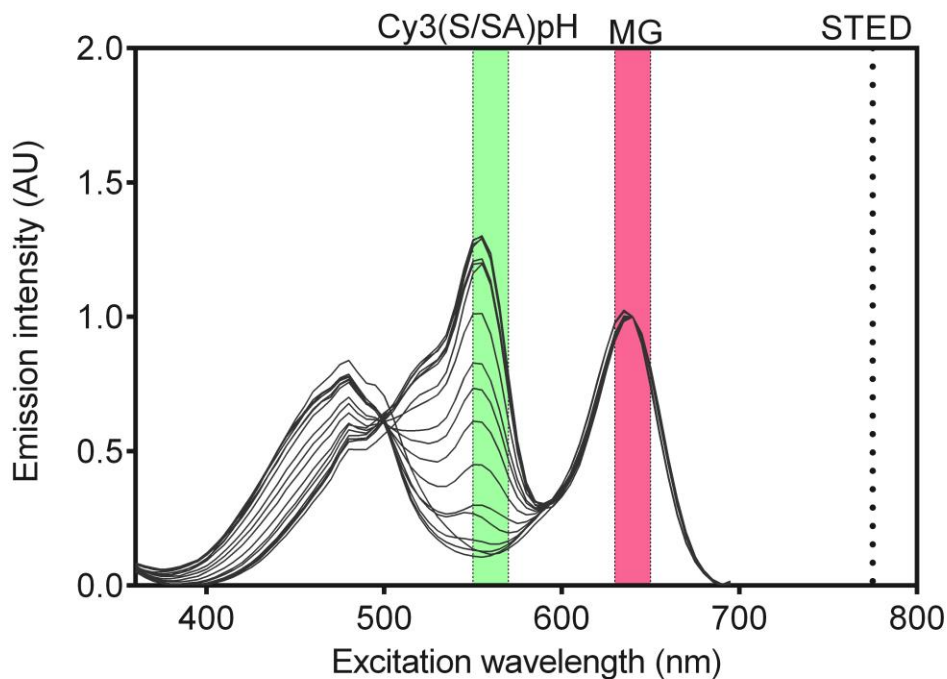


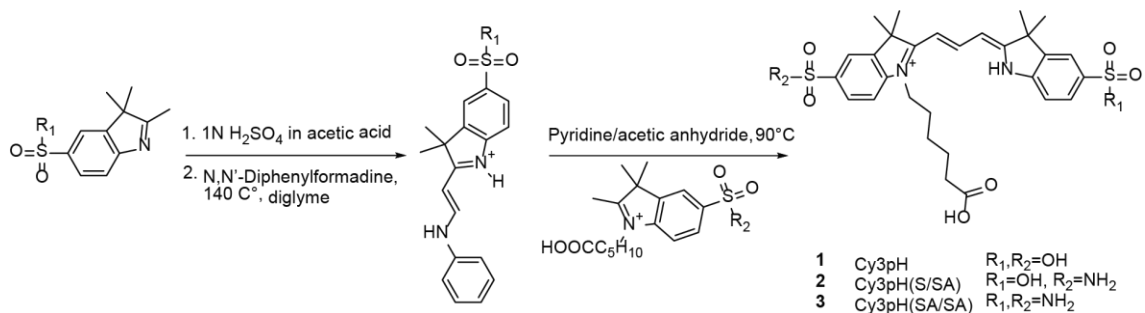
Figure S6. STED spectral depletion.

Chemistry Supplemental Information Section

Brigitte F. Schmidt designed and synthesized dyes

^1H NMR spectra were recorded at 500 MHz on a Bruker Avance instrument in MeOD-d_3 , DMSO-d_6 or D_2O as the solvent. Electrospray ionization mass spectrometry (ESI-MS) experiments were conducted on a Finnigan LCQ quadrupole ion trap mass spectrometer in positive ion mode using Xcalibur version 1.2.

Synthesis of the pH-sensitive Cy3 dyes



1-(5-Carboxypentyl)-2-((1*E*,3*Z*)-3-(3,3-dimethyl-5-sulfoindolin-2-ylidene)prop-1-en-1-yl)-3,3-dimethyl-3*H*-indol-1-ium-5-sulfonate (R₁=OH; R₂=OH); Cy3pH (1)

2,3,3-Trimethyl-3*H*-indole-5-sulfonic acid (240 mg, 1 mmol) was dissolved at 60°C in 1 mL of 1 M sulfuric acid in acidic acid. *N,N'*-Diphenylformamidine (590 mg, 3 mmol) dissolved in diethylene glycol dimethyl ether (diglyme) (3 mL) was added. The reaction mixture was heated to 140°C for 2 hrs. After cooling to rt the precipitate was filtered off. The solid was suspended in hot glacial acidic acid (10 mL) and hot filtered yielding the half dye, (*E*)-3,3-dimethyl-2-(2-(phenylamino)vinyl)-3*H*-indol-1-ium-5-sulfonate in 95 % yield.

¹H-NMR (MeOD/1 drop of NaOD): 7.69 (3H m, 1*H* bridge, 2*H* indolenine ring), 7.38 (1H,d, 2*H* indolenine ring), 7.30 (2H,m, phenyl ring), 7.10 (2H, m, phenyl ring), 7.0 (1H, t, phenyl ring), 5.39 (1H,d, bridge), 1.31 (6H,s, indolenine methyl groups). ESI M⁺ calcd. for C₁₈H₁₉N₂O₃S⁺ monoisotope 343.11 found 343.2.

1-(6-Carboxypentyl)-2,3,3-trimethylindoleninium sulfonic acid (354 mg, 1 mmol) was added to the half-dye and the mixture was dissolved in a 1:1 mixture of pyridine/ acetic anhydride (4 mL). The reaction mixture was heated to 90 °C under stirring for 1 hr. The reaction mixture was dropwise added to ether (20 mL). The precipitate was dissolved in 20 % ethanol / water, adding 1N sodium hydroxide until the color changed from red to orange. The dye was purified by MPLC on RP-18, eluent: ethanol/water/ 0.1% ammonia. ESI M⁺ calcd. for C₂₉H₃₃N₂O₆S₂⁺ monoisotope 601.29, found 602.3. Yield: 240 mg (40%)

¹H-NMR (D₂O) 8.56 (1H,dd,13.4 Hz), 7.90 (1H,s), 7.88 (1H,dd, 8.2 Hz, 1.6 Hz), 7.86 (1H,s), 7.83 (1H, dd, 8.2 Hz, 1.6 Hz), 7.37 (1H,d, 8.2 Hz), 7.25 (1H,d, 8.2 Hz), 6.43 (1H,d, 1.4 Hz), 6.20 (1H,d, 13.4 Hz), 4.14 (2H,t, 7.6 Hz), 3.59 (12H,s), 2.31 (2H, t, 7.4 Hz), 1.81 (2H,m), 1.73 (6H, s), 1.67 (2H,m), 1.55 (6H,s), 1.45 (2H,m).

(*Z*)-2-((*E*)-3-(1-(5-carboxypentyl)-3,3-dimethyl-5-sulfamoyl-3*H*-indol-1-ium-2-yl)allylidene)-3,3-dimethylindoline-5-sulfonate (R₁=OH; R₂=NH₂); Cy3pH(S/SA) (2)

1-(6-Carboxypentyl)-2,3,3-trimethylindoleninium sulfonamide (354 mg, 1 mmol) was added to the half dye, (*E*)-3,3-dimethyl-2-(2-(phenylamino)vinyl)-3*H*-indol-1-ium-5-sulfonate (342mg, 1mmol) and the mixture was dissolved in a 1:1 mixture of pyridine / acetic anhydride (4 mL). The reaction mixture was heated to 90 °C under stirring for 1 hr. The reaction mixture was dropwise added to ether (20 mL). The precipitate was dissolved in 20 % ethanol / water, adding 1 N sodium hydroxide until the color changed from red to orange. The dye was purified by MPLC on RP-18, eluent: ethanol/water/ 0.1% ammonia. ESI M⁺ calcd. for C₂₉ H₃₆N₃O₆S₂ monoisotope 601.29, found 602.3. Yield: 210 mg (35 %).

¹H-NMR (MeOD): 8.55 (1H,t, 13.5 Hz), 7.90 (1H,d,1.6 Hz) 7.88 (1H,dd, 8.4 Hz, 1.6 Hz), 7.86 (1H,d, 1.6 Hz), 7.82 (1H,dd, 8.2 Hz, 1.6 Hz), 7.37 (1H,d, 8.4 Hz), 7.24 (1H,d, 8.2 Hz), 6.42 (1H,d, 13.5 Hz), 6.19 (1H, d, 13.5 Hz), 4.14 (2H,t,7.2 Hz), 2.28 (2H, t, 7.2 Hz), 1.81 (2H, m), 1.75 (6H,s), 1.67 (2H,m), 1.55 (6H,s), 1.48 (2H,m).

6-(2-((1*E*,3*Z*)-3-(3,3-dimethyl-5-sulfamoylindolin-2-ylidene)prop-1-en-1-yl)-3,3-dimethyl-5-sulfamoyl-3*H*-indol-1-ium-1-yl)hexanoate (R₁=NH₂; R₂= NH₂); Cy3pH(SA/SA) (3)

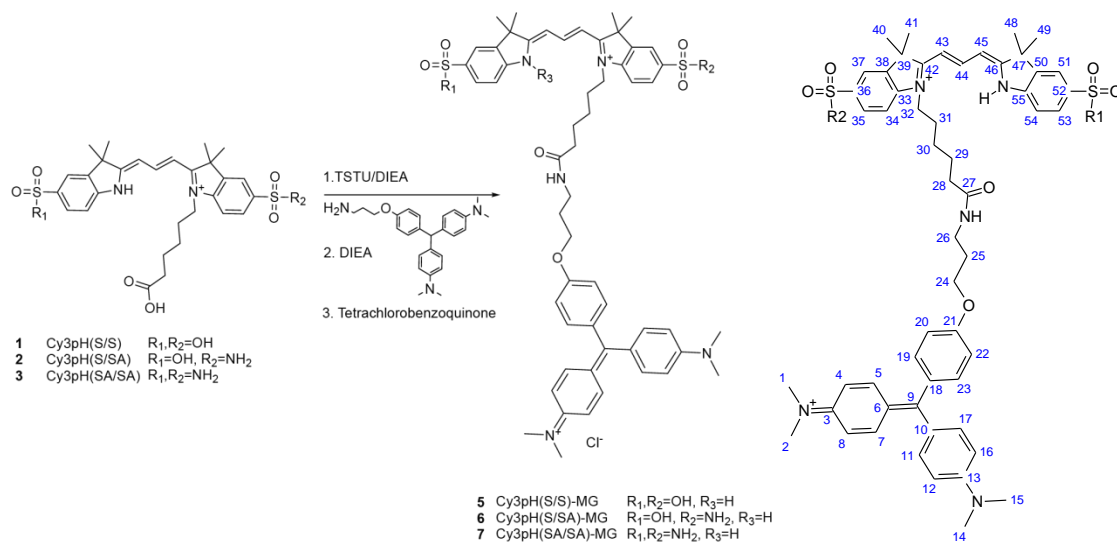
2,3,3-Trimethyl-3*H*-indole-5-sulfonamide (238 mg, 1 mmol) was dissolved at 60°C in 1 mL of 1 M sulfuric acid in acidic acid. *N,N'*-Diphenylformamidine (590 mg, 3 mmol) dissolved in diethylene glycol dimethyl ether (3 mL) was added. The reaction mixture was heated to 140°C for 2 hrs. After cooling to rt the precipitate was filtered off. The product was precipitated from the solution by the addition of ethyl acetate (6 mL). The solid was collected and

washed with ethyl acetate yielding the half dye in 80 % yield. ESI M⁺ calcd. for C₁₈H₂₀N₃O₂S⁺ monoisotope 342.13, found 342.1.

1-(6-Carboxypentyl)-2,3,3-trimethylindoleninium sulfonamide (354 mg, 1 mmol) was added and the mixture was dissolved in a 1:1 mixture of pyridine / acetic anhydride (4 mL). The reaction mixture was heated to 90 °C under stirring for 1 hr. The reaction mixture was dropwise added to ether (20 mL). The precipitate was dissolved in 20 % ethanol / water, adding 1 N sodium hydroxide until the color changed from red to orange. The dye was purified by MPLC on RP-18, eluent: ethanol/water/ 0.1% ammonia. ESI M⁺ calcd. for C₂₉H₃₆N₃O₆S₂ monoisotope 601.20, found 602.3. Yield: 150 mg (25 %).

¹H-NMR(MeOD 300 MHz) 8.25 (1H,dd, 14.6 Hz, 12.2 Hz), 7.89 (1H,d, 1.8 Hz), 7.88 (1H,dd, 7.3 Hz, 1.8 Hz), 7.80 (1H,dd, 8.3 Hz, 1.8 Hz), 7.77 (1H,d, 1.8 Hz), 7.51 (dd, 1H, 7.3 Hz, 1.8 Hz), 6.98 (d, 1H, 8.3 Hz), 3.83 (2H,t, 7.5 Hz), 2.19 (2H,t, 7.4 Hz), 1.75 (2H,m), 1.73 (6H,s), 1.70 (2H,m), 1.50 (2H,m), 1.47 (6H,s).

Synthesis of the pH-sensitive Cy3*-MG tandem dyes



Cy3pH-MG (R₁=OH; R₂=OH) (5)

Cy3pH in its basic form (60 mg, 0.1 mmol) was dissolved in 1 mL of dry DMF. TSTU (36 mg, 0.1 mmol) was added followed by DIEA (0.0175 ml, 0.1 mmol). The reaction mixture turns deep yellow and back to red as the active ester forms. After one hr at rt MG[H]-amine (40 mg, 0.1 mmol) dissolved in dry DMF (1 mL) was added followed by DIEA (0.0175 ml, 0.1 mmol). The reaction mixture was stirred at rt overnight. The reaction mixture was precipitated by the addition of ethyl acetate (15 mL). The organic layer was decanted and the residue washed with ethyl acetate followed by acetonitrile to remove any unreacted MG[H]-amine. The crude product was dissolved in a mixture of acetonitrile/methanol and heated to reflux. The product was oxidized by the addition of a hot solution of tetrachlorobenzoquinone (25mg, 0.01 mmol) in acetonitrile. The reaction mixture was refluxed for one hour. The solvent was removed and the residue was taken up in 20 % acetonitrile/water adding 1N sodium hydroxide until the color changed from purple to yellowish green. The mixture was separated by MPLC on RP-18, eluent: acetonitrile /water/ 0.1% ammonia. The product fractions were collected and adjusted to pH 7 with diluted hydrochloric acid. Yield: 45 mg (45%). ESI M⁺ calcd. for C₅₅ H₆₃ N₅ O₈ S₂ monoisotope 986.44 found 985.5.

¹H-NMR (DMSO-d₆ 500 MHz) 8.50 (1H, dd, H₄₄), 7.86 (1H, s, H₃₇), 7.73 (1H,s, H₅₁), 7.67 (1H,dd, H₃₅), 7.64 (1H,d, H₅₃), 7.37 (1H, d, H₃₄), 7.29 (2H,d, H₂₀, H₂₂), 7.28 (4H,d, H₅, H₇, H₁₁, H₁₇), 7.20 (1H,d, H₅₄), 7.19 (2H,d, H₁₉, H₂₃), 7.03 (4H,d, H₄, H₈, H₁₂, H₁₆), 6.39 (1H, d, H₄₃), 6.19 (1H, d, H₄₅), 4.14 (2H,t, H₂₄), 4.05 (2H,t, H₃₂), 3.23 (1H,t, H₂₆), 3.24 (12H,s, H₁, H₂, H₁₄, H₁₅), 2.08 (2H, t, H₂₈), 1.87 (2H, t, H₂₅), 1.70 (2H,m, H₃₁), 1.67 (6H,s, H₄₀, H₄₁), 1.56 (2H,m, H₂₉), 1.46 (6H,s, H₄₈, H₄₉), 1.34 (2H,m, H₃₀).

¹³C-NMR (DMSO-d₆ 125.75 MHz) 177.85 (C₄₆), 176.34 (C₉), 172.55 (C₂₇), 175.17 (C₄₂), 163.96 (C₂₁), 156.73 (C₃, C₁₃), 150.20 (C₄₄), 142.26 (C₃₃), 142.62 (C₅₅), 142.37 (C₅₂,C₃₆), 141.27 (C₃₈), 140.49 (C₅, C₇, C₁₁, C₁₇), 139.24 (C₅₀), 137.76 (C₂₀, C₂₃), 131.76 (C₁₈), 126.62 (C₃₅), 126.74 (C₅₃), 126.67 (C₆, C₁₀), 120.42 (C₃₇), 120.84 (C₅₁), 115.45 (C₁₉, C₂₃), 114.07 (C₄, C₈, C₁₂, C₁₆), 111.32 (C₅₄), 111.06 (C₃₄), 102.93 (C₄₃), 101.56 (C₄₅), 66.49 (C₂₄), 49.83 (C₄₇), 49.63 (C₃₉), 44.14 (C₃₂), 40.81 (C₁, C₂, C₁₄, C₁₅), 35.72 (C₂₈), 35.63 (C₂₆), 29.19 (C₂₅), 27.77 (C₄₀, C₄₁), 27.46 (C₃₁), 27.20 (C₃₀), 26.11 (C₄₈, C₄₉), 25.34(C₂₉).

Cy3pH(S/SA)-MG (R₁=OH; R₂=NH₂) (6)

Cy3pH(S/SA) in its basic form (60 mg, 0.1 mmol) was dissolved in 1 mL of dry DMF. TSTU (36 mg, 0.1 mmol) was added followed by DIEA (0.0175 ml, 0.1 mmol). The reaction mixture turns deep yellow and back to red as the active ester forms. After one hour at rt MG[H]-amine (40 mg, 0.1 mmol) dissolved in dry DMF (1 mL) was added followed by DIEA (0.0175 ml, 0.1 mmol). The reaction mixture was stirred at rt overnight. The reaction mixture was precipitated by the addition of ethyl acetate (15 mL). The organic layer was decanted and the residue washed with ethyl acetate followed by acetonitrile to remove any unreacted MG[H]-amine. The crude product was dissolved in a mixture of acetonitrile/methanol and heated to reflux. The product was oxidized by the addition of a hot solution of tetrachlorobenzoquinone (25mg, 0.01 mmol) in acetonitrile. The reaction mixture was refluxed for one hour. The solvent was removed and the residue was taken up in 30% acetonitrile/water adding 1N sodium hydroxide until the color changed from purple to yellowish green. The mixture was separated by MPLC on RP-18, eluent: acetonitrile/water/ 0.1% ammonia. The product fractions were collected and adjusted to pH 7 with diluted hydrochloric acid. Yield: 28 mg (28%). ESI M⁺ calcd. for C₅₅ H₆₅N₆O₇S₂ monoisotope 986.44 found 985.5.

¹H-NMR (MeOD 500 MHz) 8.62 (1H, dd, H44), 8.09 (1H, s, H37), 8.06 (1H,dd, H35), 7.94 (1H,s, H51), 7.89 (1H,d, H53), 7.47 (1H, d, H34), 7.39 (4H,d, H5, H7, H11, H17), 7.37 (2H,d, H20, H23), 7.34 (1H,d, H54), 7.18 (2H,d, H19, H23), 7.02 (4H,d, H4, H8, H12, H16), 6.42 (1H, d, H43), 6.36 (1H, d, H45), 4.20 (2H,t, H24), 4.10 (2H,t, H32), 3.41 (1H,t, H26), 3.33 (12H,s, H1, H2, H14, H15), 2.26 (2H, t, H28), 2.03 (2H, t, H25), 1.83 (2H,m, H31), 1.76 (6H,s, H40, H41), 1.72 (2H,m, H29), 1.58 (6H,s, H48, H49), 1.48 (2H,m, H30).

¹³C-NMR (MeOD 125.75 MHz) 180.51 (C46), 177.94 (C9), 174.68 (C27), 174.54 (C42), 164.22 (C21), 156.94 (C3, C13), 150.88 (C44), 146.35 (C33), 142.62 (C55), 142.37 (C52,C36), 141.42 (C38), 140.40 (C5, C7, C11, C17), 139.7 (50), 137.45 (C20, C23), 131.80 (C18), 129.58 (C35), 126.85 (C53), 126.81 (C6, C10), 122.31 (C37), 120.56 (C51), 114.64 (C19, C23), 113.06 (C4, C8, C12, C16), 111.82 (C54), 110.65 (C34), 103.35 (C45), 102.48 (C43), 66.00 (C24), 50.30 (C47), 48.97 (C39), 43.73 (C32), 39.42 (C1, C2, C14, C15), 35.89 (C26), 35.29 (C28), 28.69 (C25), 26.82 (C40, C41), 26.58 (C31), 25.82 (C30), 25.03 (C29), 24.59 (C48, C49).

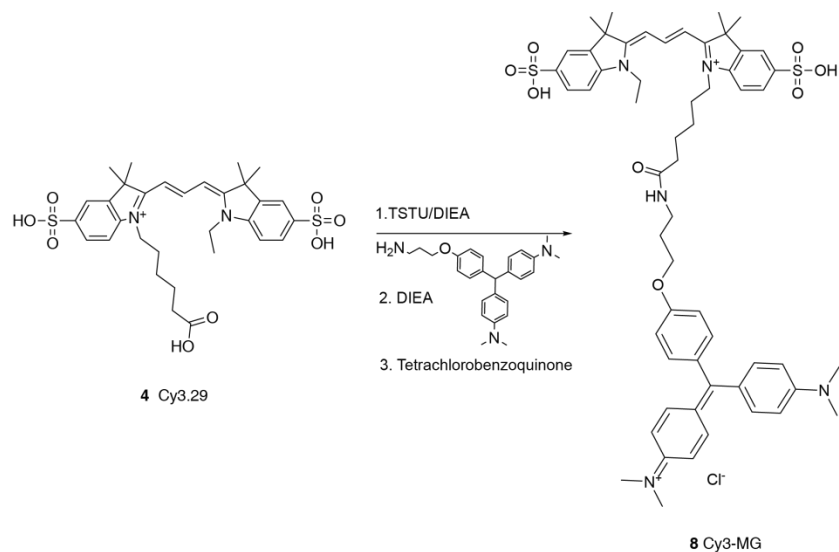
Cy3pH(SA/SA)-MG (R₁=NH₂; R₂=NH₂) (7)

Cy3pH(SA/SA) (60 mg, 0.1 mmol) was dissolved in 1 mL of dry DMF. TSTU (36 mg, 0.1 mmol) was added followed by DIEA (0.0175 ml, 0.1 mmol). The reaction mixture turns deep yellow and back to red as the active ester forms. After one hr at rt MG[H] amine (40 mg, 0.1 mmol) dissolved in dry DMF (1 mL) was added followed by DIEA (0.0175 ml, 0.1 mmol). The reaction mixture was stirred at rt overnight. The reaction mixture was precipitated by the addition of ether (15 mL). The organic layer was decanted and the residue was dissolved in 30% methanol/chloroform and purified on a short column of silica gel (eluent: methanol/chloroform). The product fraction was collected and concentrated. The product fraction was dissolved in acetonitrile and heated to reflux. The product was oxidized by the addition of a hot solution of tetrachlorobenzoquinone (25mg, 0.01 mmol) in acetonitrile. The reaction mixture was refluxed for one hour. The solvent was removed and the residue was taken up in 30 % acetonitrile/water. The mixture was separated by MPLC on RP-18, eluent: acetonitrile /water/ 0.1% trifluoroacetic acid. Yield: 20 mg (20%). ESI M⁺ calcd for C₅₅ H₆₇N₇O₆S₂ monoisotope 986.44 found 985.5.

¹H-NMR (MeOD 500 MHz) 8.65 (1H, dd, H44), 8.00 (1H, s, H37), 7.95 (1H,dd, H35), 8.03 (1H,s, H51), 8.00 (1H,d, H53), 7.39 (1H, d, H34), 7.41(4H,d, H5, H7, H11, H17), 7.37 (2H,d, H20, H23), 7.51(1H,d, H54), 7.19 (2H,d, H19, H23), 7.03 (4H,d, H4, H8, H12, H16), 6.32 (1H, d, H43), 6.49(1H, d, H45), 4.20 (2H,t, H24), 4.16 (2H,t, H32), 3.41 (1H,t, H26), 3.31 (12H,s, H1, H2, H14, H15), 2.26 (2H, t, H28), 2.03 (2H, t, H25), 1.86 (2H,m, H31), 1.79 (6H,s, H40, H41), 1.73 (2H,m, H29), 1.61 (6H,s, H48, H49), 1.48 (2H,m, H30).

¹³C-NMR (MeOD 125.75 MHz) 179.28 (C46), 8.04 (C9), 176.09 (C42), 174.51(C27), 164.25(C21), 156.96 (C3, C13), 151.39 (C44), 144.72 (C55), 144.39 (C33), 142.03 (C38), 140.42 (C5, C7, C11, C17), 140.79 (50), 140.0 (C52, C36), 137.46 (C20, C23), 131.82 (C18), 127.36 (C35), 127.30 (C53), 126.84 (C6, C10), 120.73 (C37),

120.24 (C51), 114.63 (C19, C23), 113.04 (C4, C8, C12, C16), 111.80 (C34), 111.30 (C54), 103.31 (C45), 102.40 (C43), 66.00 (C24), 49.91 (C47), 49.54 (C39), 44.01 (C32), 39.41 (C1, C2, C14, C15), 35.90(C26), 35.28 (C28), 28.70 (C25), 26.76 (C31), 26.69 (C40, C41), 25.03 (C30), 25.87 (C29), 24.88 (C48, C49).



Cy3-MG (R₁=OH; R₂=OH) (8)

Cy3.29 in its basic form (60 mg, 0.1 mmol) was dissolved in 1 mL of dry DMF. TSTU (36 mg, 0.1 mmol) was added followed by DIEA (0.0175 ml, 0.1 mmol). The reaction mixture turns deep yellow and back to red as the active ester forms. After one hr at rt MG[H]-amine (40 mg, 0.1 mmol) dissolved in dry DMF (1 mL) was added followed by DIEA (0.0175 ml, 0.1 mmol). The reaction mixture was stirred at rt overnight. The reaction mixture was precipitated by the addition of ethyl acetate (15 mL). The organic layer was decanted and the residue washed with ethyl acetate followed by acetonitrile to remove any unreacted MG[H]-amine. The crude product was dissolved in a mixture of acetonitrile/methanol and heated to reflux. The product was oxidized by the addition of a hot solution of tetrachlorobenzoquinone (25mg, 0.01 mmol) in acetonitrile. The reaction mixture was refluxed for one hour. The solvent was removed and the residue was taken up in 20 % acetonitrile/water adding 1N sodium hydroxide until the color changed from purple to yellowish green. The mixture was separated by MPLC on RP-18, eluent: acetonitrile/water/ 0.1% ammonia. The product fractions were collected and adjusted to pH 7 with diluted hydrochloric acid. Yield: 65 mg (64%).

ESI M⁺ calcd. for C₅₇H₆₉N₅O₈S₂²⁺ monoisotope 507.73 found 507.83

¹H NMR (500 MHz, DMSO-*d*₆) δ 8.35 (t, *J* = 13.4 Hz, 1H), 7.91 (t, *J* = 5.6 Hz, 1H), 7.82 (dd, *J* = 3.3, 1.6 Hz, 2H), 7.72 – 7.65 (m, 2H), 7.39 (t, *J* = 7.7 Hz, 2H), 7.31 (dd, *J* = 9.0, 3.4 Hz, 6H), 7.19 (d, *J* = 8.3 Hz, 2H), 7.06 (d, *J* = 9.0 Hz, 4H), 6.99 – 6.93 (m, 0H), 6.61 (d, *J* = 8.8 Hz, 0H), 6.58 – 6.50 (m, 2H), 4.17 (d, *J* = 9.8 Hz, 3H), 4.14 (d, *J* = 6.0 Hz, 1H), 4.09 (d, *J* = 8.2 Hz, 2H), 3.28 (s, 12H), 3.21 (d, *J* = 6.2 Hz, 2H), 2.85 (s, 1H), 2.51 (p, *J* = 1.9 Hz, 6H), 2.08 (t, *J* = 7.2 Hz, 2H), 1.86 (p, *J* = 6.5 Hz, 2H), 1.75 (d, *J* = 12.9 Hz, 1H), 1.69 (d, *J* = 3.3 Hz, 11H), 1.57 (q, *J* = 7.5 Hz, 2H), 1.37 (d, *J* = 6.3 Hz, 1H), 1.32 (t, *J* = 7.3 Hz, 3H).

SUPPLEMENTAL REFERENCES:

Telmer, C. A., Verma, R., Teng, H., Andreko, S., Law, L., and Bruchez, M. P. (2015) Rapid, specific, no-wash, far-red fluorogen activation in subcellular compartments by targeted fluorogen activating proteins. *ACS Chem. Biol.* 10, 1239–46.

Chapter III

High-content Surface and Total Expression siRNA Kinase Library Screen with VX-809 Treatment Reveals Kinase Targets that Enhance F508del-CFTR Rescue.

Published February 2018 in ACS Molecular Pharmaceutics

Reproduced in part with permission from High-Content Surface and Total Expression siRNA Kinase Library Screen with VX-809 Treatment Reveals Kinase Targets that Enhance F508del-CFTR Rescue. Lydia A. Perkins, Gregory W. Fisher, Matharishwan Naganbabu, Brigitte F. Schmidt, Frederick Mun, and Marcel P. Bruchez. *Molecular Pharmaceutics* 2018 15 (3), 759-767. Copyright 2018 American Chemical Society.

Author Contributions:

L.A.P designed and performed experiments, data analysis, and wrote the paper. G.W.F. performed siRNA transfections, kinase inhibitor dosing, and experiments. M.N. synthesized and characterized MGnBu dye. B.F.S. synthesized and provided MG-B-Tau dye. F.M. helped with performing experiments. M.P.B. designed experiments and wrote the paper.

ABSTRACT: The most promising F508del-CFTR corrector, VX-809, has been unsuccessful as an effective, stand-alone treatment for CF patients, but the rescue effect in combination with other drugs may confer an acceptable level of therapeutic benefit. Targeting cellular factors that modify trafficking may act to enhance the cell surface density of F508-CFTR with VX-809 correction. Our goal is to identify druggable kinases that enhance F508del-CFTR rescue and stabilization at the cell surface beyond that achievable with VX-809 corrector alone. To achieve this goal, we implemented a new high-throughput screening paradigm that quickly and quantitatively measures surface density and total protein in the same cells. This allowed for rapid screening for increased surface targeting and proteostatic regulation. The assay utilizes Fluorogen-Activating-Protein (FAP) technology with cell excluded and cell permeant fluorogenic dyes in a quick, wash-free fluorescent plate reader format on live cells to first measure F508del-CFTR expressed on the surface and then the total amount of F508del-CFTR protein present. To screen for kinase targets we used Dharmacon's ON-TARGET*plus* SMARTpool™ siRNA Kinase library (715 target kinases) with and without 10 μ M VX-809 treatment in triplicate at 37°C. We identified several targets that had a significant interaction with VX-809 treatment in enhancing surface density with siRNA knockdown. Select small-molecule inhibitors of the kinase targets demonstrated augmented surface expression with VX-809 treatment.

INTRODUCTION: Cystic Fibrosis Transmembrane conductance Regulator (CFTR) is finely controlled in its bioavailability at the apical surface of epithelial cells, where it plays a significant role as a chloride channel. Aberrant cellular trafficking and dysfunction of CFTR in the lung leads to decreased chloride transport, resulting in Cystic Fibrosis (CF) symptoms. These arise from a thickened mucus layer in lung epithelia, which causes airway obstruction, inflammation, chronic infection, and severe reduction in life expectancy. CF remains the most common fatal genetic disease among Caucasians.(Ratjen and Döring, 2003)

The disease is most frequently caused by the deletion of phenylalanine at position 508 of the CFTR gene (F508del-CFTR). F508del-CFTR is misfolded and becomes trafficking defective, where it is largely degraded by endoplasmic reticulum associated degradation pathways involving the proteasome.(Cheng et al., 1990) Rescuing trafficking to increase bioavailability would help restore anion channel function, where recovering only 30% of wild-type activity can provide a therapeutic benefit to CF patients.(Kerem, 2004) Partial rescue of F508del-CFTR trafficking to the plasma membrane (PM) has been shown with low temperature incubation that promotes proper folding of the channel, and through small molecule correctors, which can either act by direct participation in stabilizing CFTR conformation, or indirectly through interactions with quality control machinery or other cellular components involved in CFTR folding and trafficking. (Amaral and Farinha, 2013) F508del-CFTR that is rescued to the cell surface shows a moderate functional defect due to its inherent altered protein conformation and faces significant stability problems, where the peripheral protein quality control system redirects mutant CFTR from recycling endosomes towards degradation.(Okiyoneda et al., 2010) Hence, rescue of CFTR to the surface, combined with decreased degradation of rescued CFTR may present deliver improved therapeutic effects.

Identified correctors have been unsuccessful at achieving clinical relief as stand-alone treatments. The corrector, VX-809, promotes stabilization of the disrupted F508del-CFTR conformation, but that alone is insufficient for therapeutic effect.(Clancy et al., 2012) The combination of VX-809 and VX-770, a CFTR potentiator that increases channel activity at the PM, has been approved as a treatment strategy (Orkambi) for improving lung function in specific patient populations. Recently, two phase 3 clinical trials with VX-770 in combination with a different candidate corrector,VX-661, resulted in significant improvements in lung function.(Business Wire, 2015) However, there have been concerns regarding use of VX-770 for treatment of F508del-CFTR mutations because it appears to accelerate F508del-CFTR degradation from the PM after rescue with VX-809 or VX-661 correctors.(Cholon et al., 2015; Veit et al., 2014)

Repairing trafficking, the implicit defect of F508del-CFTR, has been a difficult objective for F508del-CFTR directed therapies. Currently, new-generation correctors, VX-152 and VX-440, are undergoing clinical development alone and in a triple combination with VX-661/VX-770. (Business Wire, 2017) Combinations of CFTR modulators have the potential to confer an acceptable therapeutic benefit.(Lin et al., 2010; Cholon et al., 2017) Despite VX-809's stand-alone clinical shortcomings and low therapeutic effect in combination with VX-770, it still remains an encouraging corrector since its discovery in 2011. A synergy-based small molecule screen for enhancing VX-809 correction efficacy was previously conducted to search for molecular correctors that restore F508del-CFTR structure stability that is not fully accomplished through VX-809 interaction alone. Identifying second-generation correctors can result in further rescue when applied with first generation correctors like VX-809.(Phuan et al., 2014)

Combinational therapies that utilize different possible methods of correction, have the potential to be the tipping point for a powerful treatment strategy for CF. Thus, identification of druggable kinase targets that, when inhibited, enhance the rescuing effect of VX-809 could lead to improved therapeutic strategies.

In screening for F508del-CFTR correction, kinases have been investigated through drug inhibition and RNA interference libraries.(Trzcinska-Daneluti et al., 2012;Trzcińska-Daneluti et al., 2015) However, such kinase centered high-throughput screens (HTS) have not been conducted in tandem with corrector treatment. Our goal is to develop an assay to identify druggable kinases that enhance F508del-CFTR rescue and stabilization at the cell surface beyond that achievable with VX-809 corrector alone at physiological temperature. We developed a screening method to rapidly and simply detect surface expression and total F508del-CFTR protein, independently assessing trafficking and proteostatic effects of each treatment.

A majority of F508del-CFTR corrector screens have been based on functional rescue. Such HTS activity assays include the yellow fluorescent protein based halide sensor, or the use of a voltage-sensitive membrane dye.(Pedemonte et al., 2011; Pedemonte et al., 2005; Van Goor and Straley, 2006; Trzcinska-Daneluti et al., 2009; Trzcinska-Daneluti et al., 2012; Trzcińska-Daneluti et al., 2015) In contrast, there have been several F508del-CFTR correction screens developed that measure rescued trafficking directly by detecting the presence of CFTR at the plasma membrane in non-permeabilized cells using immunodetection of epitope tags (HA and FLAG) with fluorescent antibody labeling, or quantifying horseradish peroxidase (HRP) tagged protein for surface specific luminescence.(Carlile et al., 2007; Botelho et al., 2015; Phuan et al., 2014) These surface-selective assays have several drawbacks, involving multiple wash steps and lengthy incubation periods, which limits processing speed and introduces potential variability. The HRP method allows interrogation of surface or total protein, in different assay wells, depending on permeabilization. There is a need for single well measurements of surface and total protein pools in a fast, no-wash whole-well format, consistent with high-throughput screening workflows.

A fluorogen-activating protein (FAP) based platform was previously introduced and validated as an alternative method for selective and sensitive F508del-CFTR surface fluorescence measurements.(Holleran et al., 2012a) More recently this platform was utilized for high-content imaging of F508del-CFTR detection.(Larsen et al., 2016) Here, we extended the FAP-F508del-CFTR platform to establish a new high-throughput screening paradigm that quickly and quantitatively measures surface expression and total protein at 37°C in a plate reader format, enabled by new quantum-yield matched cell permeant and cell-excluded dyes. Using this assay, we performed a siRNA screen targeting kinases to identify kinase targets that enhanced surface trafficking, and enhanced stability of F508del-CFTR. From these results, we identified targets that increased VX-809 mediated rescue, and several showed a significant positive interaction with VX-809. Plate reader results were recapitulated in high-throughput flow cytometry with individual siRNA treatments, and the influence of two identified target kinases were validated using specific inhibitors with single cell (flow cytometry) measurements. Specific kinase suppression resulted in significant and substantial increases in VX-809 mediated rescue at 37° C.

RESULTS:

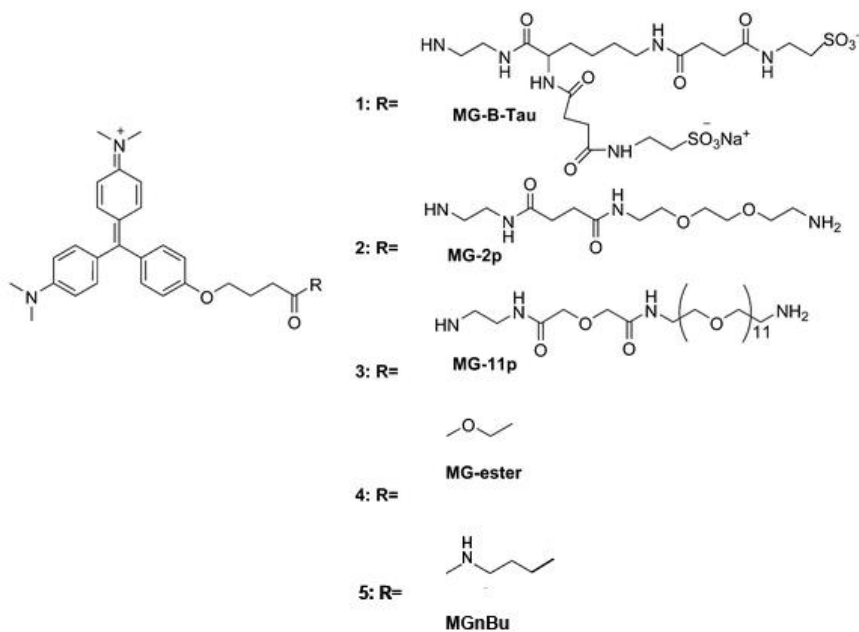
High-throughput assay development: *FAP-CFTR platform.* FAP technology is a fluorogenic labeling approach that uses high specificity binding to activate the fluorescence of a “dark” dye molecule. The FAP platform consists of a single chain antibody fragment, the size of GFP, fused to the protein of interest. The dL5** FAP complex has sub-nanomolar affinity binding towards Malachite Green (MG) based fluorogens. The fluorogenic MG analog dyes become fluorescent only once bound to the dL5**FAP, which eliminates the need for wash steps. This tool system is dynamic due to the ability to create different compositions of MG fluorogen analogs (Scheme 1), allowing for selective labeling of different subcellular pools of FAP fused proteins. (Szent-Gyorgyi et al., 2008a) F508del-CFTR and WT CFTR were fused with FAP (dL5**) at the N-terminus through an added membrane-spanning segment (PDGFR-TM, derived from pDisplay (Life Technologies, Inc)), and were stably expressed in HEK293 cells, illustrated in Figure 1. These constructs and cell populations have been previously established and validated. (Holleran et al., 2012b)

Cell surface protein and total protein labeling. With FAP-CFTR expressing cells, we used MG-B-Tau, a cell excluded sulfonated MG analog, as a method to label extracellular FAP-F508del-CFTR. MG-B-Tau has been reported previously as for its selective and rapid surface labeling. (Yan et al., 2015) After labeling and measuring surface protein, we are able to sequentially label intracellular protein and measure total protein in the same cells. Measuring both surface and total protein allows us to consider the % protein present at the cell surface. For labeling intracellular protein, MG-Ester has been the standard cell permeable dye commonly used in FAP technology. (Telmer et al., 2015) However, MG-Ester has a lower quantum yield in comparison to MG-B-Tau (Table 1). To achieve an accurate representation of cellular total protein, the cell excluded dye and cell permeable dye (both 640 nm ex/ 680 nm em) must have matched quantum yields and spectral properties. To label intracellular CFTR protein, we prepared and validated a new dye, MGnBu (Scheme 1, Scheme 2, Supplemental Scheme 1, Supplemental Figures 1-5), which has a similar quantum yield to MG-B-Tau. We screened various MG variants where the fluorogen had a different functional tail distal to the fluorogenic moiety, which structural studies indicated was oriented outside the binding cleft. (Szent-Gyorgyi et al., 2013) MGnBu, containing a butanamide linker through conjugating a n-butylamine functional group to the carboxylic acid on the MG fluorogen, showed a 50% increase in the quantum yield compared to MG-Ester and was identical in brightness and spectral properties to MG-B-Tau (Table 1). In addition, the overall positive charge of MGnBu causes the fluorogen to be cell-permeable. These properties, enhanced quantum yield and cell-permeability, make this dye an ideal cell-permeant chase reagent, allowing initial cell surface quantitation with the cell excluded MG-B-Tau, followed by total protein measurement by using a spectrally and quantum-yield matched cell-permeant dye to label remaining sites. The final complete dye-protein labeled cell reports total protein through measuring MG-B-Tau (surface) + MGnBu (inside) 680nm emission. Sequential reads are used to establish the relative fraction of protein at the surface and within intracellular biosynthetic and endocytic compartments. In addition, the amide moiety is less susceptible to cleavage by esterases or media conditions, and may be useful for more reliable labeling in complex specimens or thick tissues.

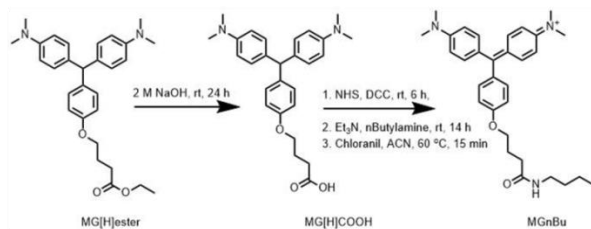
In addition to spectral equivalence, MG-B-Tau and MGnBu must also have equal brightness in cellular labeling. Their equivalent brightness permits sequential labeling with cell impermeant and cell permeant dyes to measure surface and total protein, as qualitatively demonstrated previously with two-color

fluorogen labeling.(Pratt et al., 2015) Flow cytometry based fluorescence measurements with HEK293 cells expressing FAP-WT-CFTR demonstrated the identical brightness of MG-B-Tau and MGnBu, and the comparable challenges with MG-ester. Cells were first measured for surface fluorescence by MG-B-Tau labeling, followed by remaining protein labeling with MG-ester for MGnBu. Sequentially labeled samples were compared to samples labeled exclusively with 500 nM MGnBu dye or 500 nM MG-Ester alone which labeled both surface and internal pools of protein, at a brightness indicative of the cell permeant dye (Figure 3). There was no significant difference between the two methods of measuring total protein using MGnBu, validating that in vivo the brightness of the two dyes are matched. However, MG-Ester showed a significantly reduced signal relative to the combined labeling, confirming that the higher intrinsic brightness of MG-B-Tau relative to MG-Ester compromises quantitative assessment of surface and total pools.

A measurable and quantifiable difference in surface expression of FAP-F508del-CFTR can be obtained using a whole-well plate-reader format assay with fluorogen detection. HEK293 cells expressing FAP-F508del-CFTR were plated in a 96 well high optical quality ibidi plate. The following day cells were treated with or without 10 μ M VX-809 for 24 hr at 27°C or 37°C. For surface labeling, 500 nM MG-B-Tau in HBSS was added to the cells followed immediately by fluorescence measurement on a plate reader (Figure 4). 37°C incubation with VX-809 treatment showed a small, but significant increase in fluorescence (~20%). As previously shown, 27°C incubation with VX-809 induced a dramatic increase in surface signal.



Scheme 1. Chemical structure of MG-B-Tau (1), MG-2p (2), MG-11p (3), MG-Ester (4), and MGnBu (5). Scheme adapted from Qi et al., 2015. MGnBu structure provided by Matharishwan Naganbabu



Scheme 2. Synthesis of MGnBu (5) Designed and synthesized by Matharishwan Naganbabu

Dye	Quantum Yield Φ_f	K_d (nM)
MG-B-Tau (1)	0.19	0.54 ± 0.04
MG-2p (2)	0.20	0.50 ± 0.35
MG-11p (3)	0.08	0.11 ± 0.02
MG-Ester (4)	0.12	0.42 ± 0.05
MGnBu (5)	0.20	0.40 ± 0.35

Table 1. Dye comparisons (1-5) with reported quantum yield and K_d . 1-4 dye data adapted from Yan *et al.*, 2015. And (5) provided by Matharishwan Naganbabu.

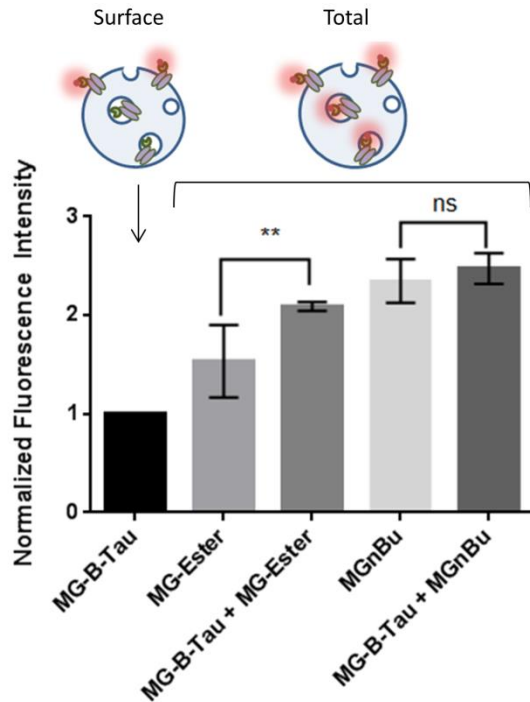


Figure 3. Cell permeable dye MGnBu is same quantum yield as the cell impermeable dye, MG-B-Tau, in FAP-WT-CFTR cells. Fluorescence signal is normalized to surface fluorescence (MG-B-Tau labeling). Total expression is shown in two different ways: 1) Measuring total expression through only labeling with cell permeable dyes, MG-Ester or MGnBu. 2) Sequential labeling with first 500 nM MG-B-Tau (surface) for 15 min followed by another 15 min incubation with 500 nM MGnBu or MG-Ester (intracellular). MGnBu, is same quantum yield as the cell impermeable dye, MG-B-Tau, at 37°C in FAP-WT-CFTR due to non-significant differences in labeling methods, however MG-Ester shows significant differences in the measurement of total protein. Data is expressed as the mean ± S.D. (4 replicates). One-Way ANOVA with multiple comparisons. ** $P \leq 0.01$; * $P \leq 0.05$; ns > 0.05 .

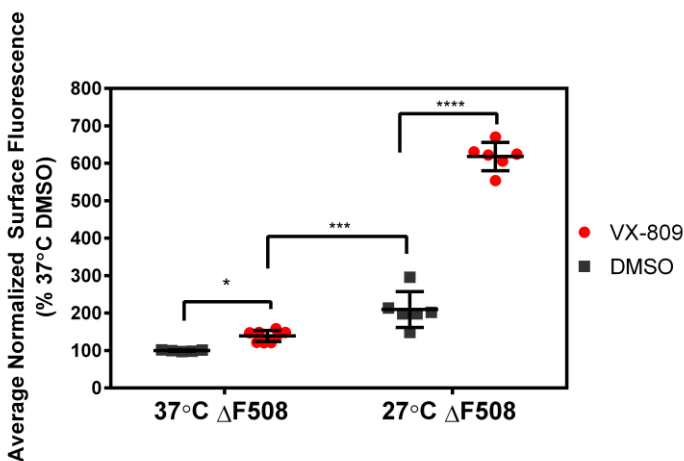


Figure 4. Measurable surface protein fluorescence differences with Δ F508-CFTR in a 96-well plate reader format. Cells were either incubated at 37°C and 27°C, with or without 10 μ M VX-809 for 24 hrs. Fluorescence was normalized to 37°C Δ F508-CFTR treated with vehicle control, DMSO. Data is expressed as the mean \pm S.D. of 6 replicates. One-Way ANOVA with multiple comparisons. **** $P \leq 0.0001$; *** $P \leq 0.001$; ** $P \leq 0.01$; * $P \leq 0.05$.

Hoechst 33342 nuclear stain was added to normalize for any potential differences in cell confluency across wells that may arise from transfection or the action of kinases on cell proliferation. Surface and total measurements were normalized to Hoechst stain. This high-throughput assay for conducting fluorescence measurements is illustrated and described in Figure 2. This simple plate reader-based, 1 hour assay, was applied as a method for quickly processing 96-well plates in a kinase knockdown screen using an siRNA library.

Identification of kinases whose repression promotes surface expression of Δ F508-CFTR beyond that of VX-809 alone: Using the high-throughput FAP based assay, we screened the Dharmacon ON-TARGETplus SMARTpool™ siRNA Kinase library (715 target kinases) with and without 10 μ M VX-809 treatment in triplicate at 37°C to determine surface and total cellular expression of the F508del-CFTR construct. Using this data, we identified kinase targets whose suppression results in increases of surface F508del-CFTR above the level obtained by VX809 alone.

SiRNA screen quality assessment. The quality control (QC) of the siRNA screen was assessed through strictly standardize mean difference (SSMD) score.(Zhang, 2011a, 2011b) This scoring method is favorable due to its ability to report consistent quality control results with positive controls that are not necessarily very strong. In our system, the positive control for transfection is siRNA that targets CFTR, with success resulting in a clear reduction in total fluorescence signal measured upon addition of MGnBu. The total amount of CFTR, however, is reduced due to the F508del mutation, and thus even with VX-809 treatment, total protein expression is low, making knockdown to background levels only a moderate change in total fluorescence. Our QC criterion was based off of a moderate control effect, assessing the VX-809 treated plate of a transfection pair, and using the CFTR siRNA wells as a positive control for total

protein knockdown and scrambled NC siRNA wells as a negative control. The siRNA kinase library was supplied in a 96-well format consisting of 9 plates total, where each library plate was utilized in true biological triplicate assays for both treatment conditions (with DMSO and VX-809). A plate passes QC if it has SSMD < -1 (good or excellent) quality. The QC results are presented in Figure 5, showing that all replicates passed our QC criterion for effective transfection.

Initial hit selection. Paired SSMD and mean fold change in CFTR surface expression were used to rank initial hits, identifying the kinase targets whose suppression increases surface expression of F508del-CFTR. The paired SSMD score was implemented from Zhang, 2011, and is ideal for processing RNAi screens with replicates. The SSMD score is the average log fold change penalized by variability. Similar to QC, a threshold of SSMD ≥ 2 (strong positive effect) was set to identify kinase target candidates whose knockdown increased CFTR surface levels. The SSMD score vs average log fold change of each target can be visualized in a flashlight plot (Figure 6) to show the spread of effect size and assay statistical quality.

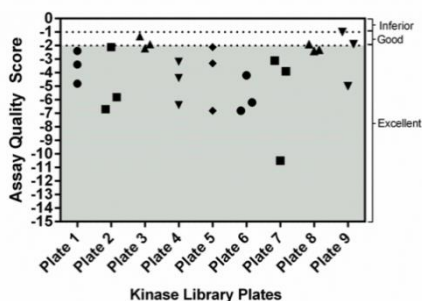


Figure 5. Quality assessment of transfection throughout siRNA screen. The assay quality scores for each 96-well library plate and their respective replicates. Thresholds for a moderate control: excellent: SSMD ≤ -2 , good: $-2 < \text{SSMD} \leq -1$, inferior: $-1 < \text{SSMD} \leq -0.5$, poor: $\text{SSMD} > -0.5$. Only one replicate of plate 9 borders between good and inferior at -1.

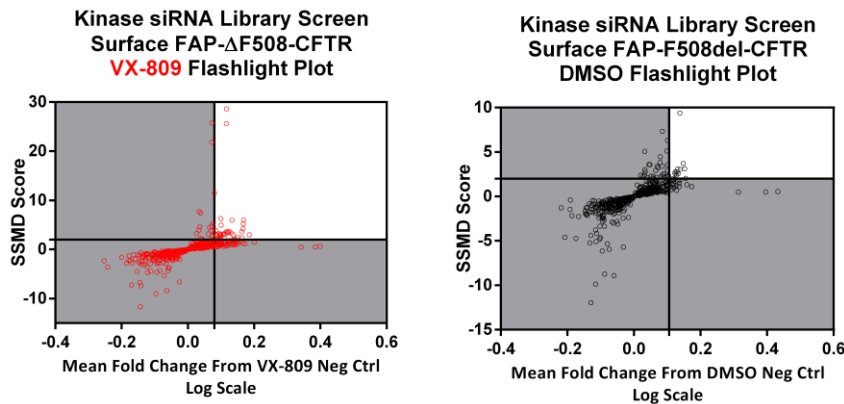


Figure 6. Flashlight plot thresholds of kinase screen surface florescence change. SSMD thresholds are set at 2 and the area below SSMD score 2 is greyed out. The negative control (non-targeted, scrambled siRNA) in each plot is represented at 0. The line on the mean fold change axis represents the threshold that yields a significant positive change from the neg. ctrl., the area below this threshold is greyed out. A) VX-809 flashlight plot where interesting targets are those above the visualized thresholds set from the VX-809 neg. ctrl. B) DMSO (vehicle treated) flashlight plot, shows that some siRNA treatments without VX-809 treatment may increase F508del-CFTR surface expression.

VX-809 + kinase targets above the selected threshold score were ranked based on their observed average % increase in surface expression from the VX-809 negative control. All hits that were significantly higher than the VX-809 negative control were selected (One-Way ANOVA, $P \geq .05$). The highest scoring, significant hits are shown in Figure 7. Surface signal of target-specific siRNA transfected cells treated with VX-809 are shown in red, and siRNA transfected cells treated with DMSO vehicle control are shown in black. The negative controls were treated with non-targeted, scrambled siRNA. The screen had a primary focus for identifying VX-809 + siRNA kinase target hits that increased surface CFTR expression significantly above VX-809 treatment alone. Any kinase target + VX-809 treatment that produced a significant interaction, where the combination is higher than the sum of their individual treatments, are identified alongside hits as P-value symbols in blue. We also assessed DMSO + siRNA kinase targets and classified hits compared to the DMSO negative control. These effects were generally weaker, suggesting that many may be below statistical significance, but targeting the FGFR4 kinase in both the VX-809 treated and DMSO-treated cell screens showed a significant increase in surface expression. These results are represented in Figure 8, depicting the distribution of these kinase targets.

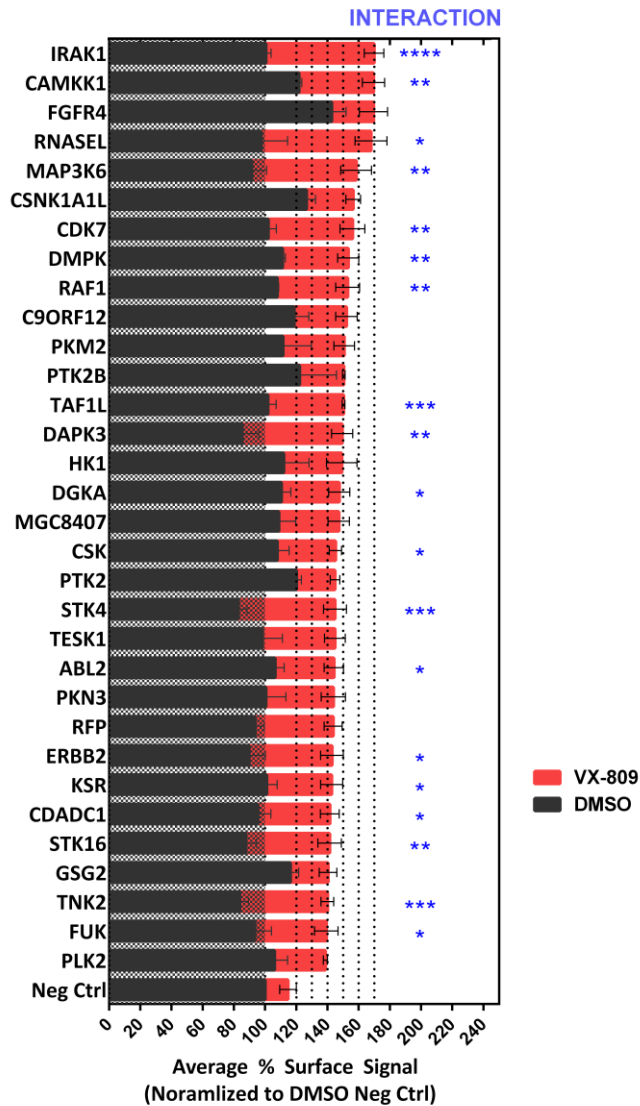


Figure 7. Ranked surface signal increase of identified kinase targets + VX-809 hits. SiRNA kinase targets + VX-809 with a score of SSMD ≥ 2 , and are significantly higher than VX-809 control (One-Way ANOVA, $P \geq .05$), are ranked based on their average % surface increase from DMSO negative control. SiRNA targets treated with VX-809 are shown in red, and targets treated with DMSO vehicle control are shown in black. Kinase targets in combination with VX-809 treatment that promote surface rescue, beyond VX-809 alone are shown with blue asterisks. Error bars are shown as mean \pm S.E.M. (3 replicates). Two-Way ANOVA for enhancing interaction (blue P-values). **** $P \leq 0.0001$; *** $P \leq 0.001$; ** $P \leq 0.01$; * $P \leq 0.05$.

715 siRNA Kinase Target Library

- 32 VX-809 + siRNA hits → 19/32 Enhancers
- 13 DMSO + siRNA hits
- 670 non-hits

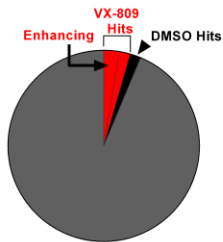


Figure 8. Pie-graph illustrating independent and overlapping hits. VX-809 + siRNA target hits are those showing a strong increase in surface expression from VX-809 negative control and DMSO + siRNA target hits are those showing a strong, significant increase in surface expression from DMSO negative control.

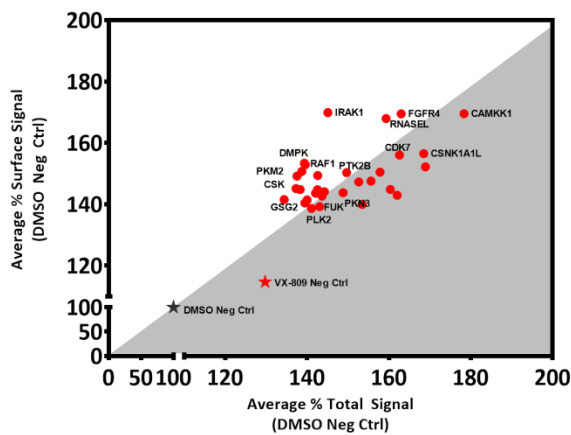


Figure 9. Average % surface vs. total signal in VX-809 treated siRNA kinase target knockdown. Average % surface and % total protein increase is normalized to F508del-CFTR DMSO negative control. Listing top VX-809 + siRNA % surface increase hits. Targets above the greyed are those that increased the amount of total protein expressed at the surface from DMSO negative controls. Mean values from screening (3) replicates are plotted.

Identified targets can be further evaluated by comparing surface vs total CFTR protein in respect to basal F508del-CFTR expression (Figure 9). The total protein measurements provide information on overall protein expression levels in addition to showing if hits shifted distribution of protein. Overall, the surface vs total protein plot shows a loose, positive linear trend. Targets above the diagonal may represent kinases whose inhibition would increase surface targeting of the F508del-CFTR protein without a concomitant increase in overall protein expression.

Select Kinase Target Validation: *Single siRNA CAMKK1 and RAF1 validation in flow cytometry.* Following the screen, the two kinases, CAMKK1 and RAF1 were selected for further validation. These targets were chosen based upon their significant enhancement of VX-809, and the availability of specific inhibitors. We confirmed the select kinase knock-down in the SMARTpool siRNA library by cherry picking those wells for transfection and performing immunofluorescence (supplemental figure 6). To demonstrate agreement with the plate reader results, which measures on a population scale, we performed confirmation experiments on a BD Accuri flow cytometer with Intellicyt HTFC for single-cell quantitative measurements. For flow-cytometry assays, after treatment, cells are plated on a 96-well plate and treated with 500 nM MG-B-Tau in HBSS for 15 min before measuring.

The initial validation experiment utilized single Dharmacon ON-TARGET^{plus} siRNA vs the SMARTpool siRNA used in the screening process. The individual siRNA from the pools were used to confirm the significant increase in surface expression upon siRNA knockdown of CAMKK1 and RAF1. The SMARTpool is composed of 4 siRNAs, and the 4 individual siRNA results are shown in Figure 10, assessed by flow cytometry. All four CAMKK1 siRNA targets and one siRNA targeting RAF1, combined with VX-809 significantly increased surface expression relative to the VX-809 scrambled siRNA control.

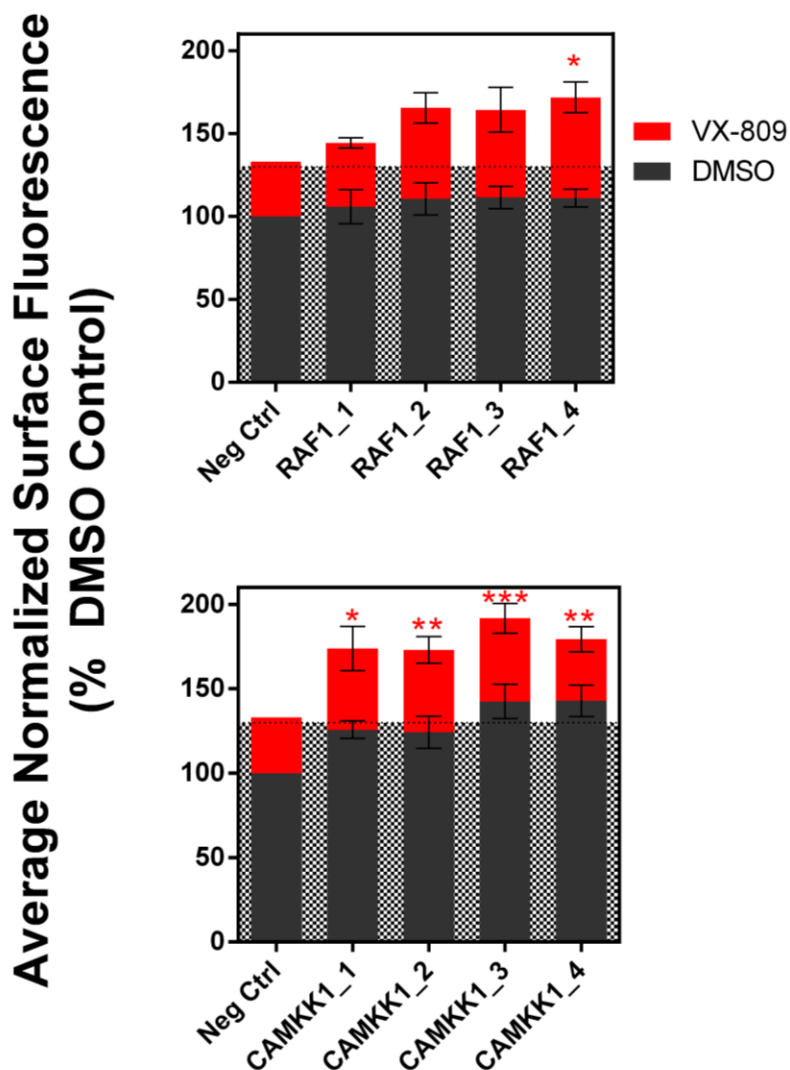


Figure 10. RAF1 and CAMKK1 single siRNA validation in flow cytometry. RAF1 and CAMKK1 single Dharmacon ON-TARGETplus siRNAs with or without VX-809 treatment. Measured surface CFTR fluorescence with a BD Accuri flow cytometer with Intellicyt HTFC. The greyed out region represents VX-809s average surface fluorescence. VX-809 + siRNA significance is shown from VX-809 negative control. Data shown as mean \pm S.E.M (3-4 replicates). One-Way ANOVA with multiple comparison for significant changes from VX-809 Neg. Ctrl (0 nM) (red P-values). *** $P \leq 0.001$; ** $P \leq 0.01$; * $P \leq 0.05$.

CAMKK1 and RAF1 drug inhibition validation in flow cytometry: Using an independent flow cytometry method, individual siRNAs showed agreement with screening results. Further validation was conducted with specific kinase inhibitors (Figure 11). For these studies, we used GW 5074, a drug that acts on Raf1, previously shown to enhance function of F508del-CFTR (Trzcinska-Daneluti et al., 2012) and STO-609 a known selective inhibitor of CAMKK1. Kinase inhibitor experiments were carried out via flow cytometry

(Figure 12). The flow cytometry fluorescence surface measuring assay produced confirmatory results. In combination with VX-809, the CAMKK1 inhibitor STO-609 and RAF1 inhibitor GW 5074 both showed a significant increase in surface signal from the VX-809 only control with a significant interaction.

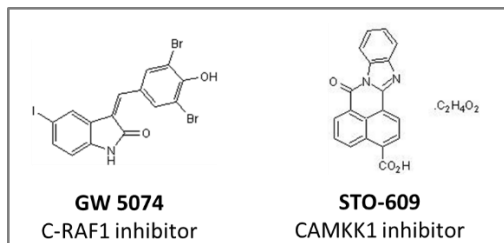


Figure 11. Chemical structures of inhibitors of two identified kinase targets, RAF1 and CAMKK1.

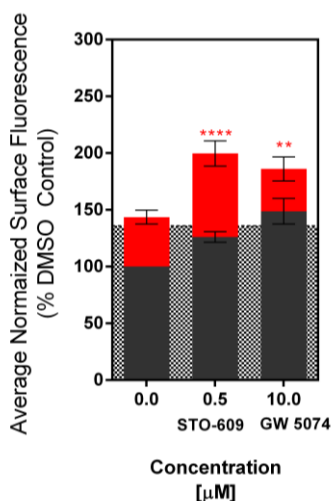


Figure 12. Measuring surface fluorescence changes using select kinase drug inhibitors with plate reader and flow cytometry method. Kinase inhibitors, GW 5074 and STO-609, with VX-809 treatment showed increase in surface fluorescence using a BD Accuri flow cytometer with Intellicyt HTFC. VX-809 + kinase inhibitor is shown normalized to DMSO treated control cells. The greyed out region represents VX-809s average surface fluorescence. Each drug showed significant interaction effects. Data shown as mean \pm S.E.M. (3 or more replicates). One-Way ANOVA with multiple comparison for significant changes from VX-809 control (0 nM) (red P-values). Two-Way ANOVA used for measuring interaction. ****P \leq 0.0001; **P \leq 0.01.

DISCUSSION: We have developed a new assay that selectively and quantitatively assesses the cell surface expression and overall protein content of membrane proteins in the same population of cells, and applied this assay to identify potential kinase targets that may enhance F508del- CFTR rescue to the plasma membrane in combination with VX-809 treatment. To determine overall total protein levels, we have introduced a new cell-permeant fluorogenic dye, MGnBu, that possesses the same quantum yield and spectral properties as the surface labeling dye, MG-B-Tau, to determine the ratio of surface exposed protein to total expressed protein. This assay utilizes a simple plate-reader format for accelerated screen processing, where surface and total protein measurements are readily transitioned to other instruments, such as flow cytometry or microscopy. The ability to readily collect complementary fluorescence measurements across different devices while using a single established labeling approach corroborates results readily. Through our developed screening assay, we identified several targets whose inhibition showed increased CFTR rescue with VX-809 treatment using a SSMD scoring metric. Of these hits, we used a Two-way ANOVA interaction test to determine targets that resulted in a significantly higher CFTR surface localization than either siRNA or VX-809 treatment alone, or the expected sum of the treatments. Kinase targets, CAMKK1 and RAF1, VX-809 enhancing effects were further validated using single siRNA knockdown and kinase inhibitors, and evaluated utilizing flow cytometric measurements. We have shown a high-throughput approach that uses both surface and total measurements that was applied to screening potential kinase targets that show an enhancement of VX-809 F508del-CFTR rescue. This platform could also be used for other cell surface protein trafficking related screens that require understanding the fraction of total protein at the surface and robust measurements to assess or control for proteostatic effects.

FUTURE DIRECTIONS: Investigating F508del-CFTR Post-Endocytotic Trafficking with VX-809 Correction.

While completing a high content screen for kinase targets that enhance VX-809s rescuing effect, we discovered a VX-809 induced atypical internalized F508del-CFTR localization pattern by confocal imaging. While a previous report suggested F508del-CFTR retention in early endosomal compartments with pulse-chase labeling methods, through our constitutive labeling of PM F508del-CFTR, we propose that VX-809 correction may also promote an irregular retrograde trafficking pathway after internalization that otherwise might have been too faint to observe by pulse-chase approaches.

WT CFTR that is endocytosed from the PM accumulates into early endosomes, where half is recycled quickly back to the surface, and the rest collects into slower recycling compartments. At steady state, 15-20% of CFTR is localized in these recycling compartments. From these pools, CFTR is not only trafficked to the cell surface, but can be trafficked elsewhere inside the cell. CFTR can be sent to late endosomes, where it can either undergo a degradation route, or trafficked to the trans-Golgi.(Farinha and Canato)

The F508del mutation resides in the nucleotide-binding domain 1 (NBD1) of the protein, and as a result of improper folding, the presentation of di-acidic ER exit motifs and di-arginine ER

retention/retrieval signals are altered, causing ER retention and even retrograde trafficking of mutant protein from the Golgi back to ER. VX-809 associates with the disrupted NBD1:CL4 interface of CFTR, aiding in stabilizing protein conformation, reducing quality control degradation, and increasing rescue to the PM, where F508del-CFTR remains on the surface for $T_{1/2} \sim 3$ hours.(Chiaw et al., 2011; Veit et al., 2014) Endocytosed VX-809 treated F508del-CFTR avoids MVB trafficking, and instead is confined into endosomal compartments with a reported pH of 6.31.(Veit et al., 2014) Yet, VX-809 correction is still not sufficient for fully recapitulating WT protein trafficking. While VX-809 helps stabilize protein conformation, its mechanism of action is not well understood, and does not stabilize NBD1 in itself. VX-809 treated F50del-CFTR may still have altered trafficking motifs, altered ER retention/exit signals, or its binding may also influence an alternate Post-PM trafficking itinerary.

METHODS:

Materials: Dulbecco's Modified Eagle's Medium (DMEM) was obtained from Hyclone (SH30022.01). OptiMEM reduced serum with no phenol red was from Thermo Fisher Scientific (11058201). Hanks Balanced Salt Solution (HBSS) with calcium and magnesium was from Life Technologies (14025134). High optical quality 96 well cell culture treated plates were obtained from Ibidi (89626). Poly-L-Lysine for coating 96 well plates was from Sigma (P4707). The ON-TARGET*plus* SMARTpool™ siRNA Kinase library, single ON-TARGET*plus* siRNAs (CAMKK1 and RAF1), DharmaFect1 transfection reagent (T-2001-02), the positive controls (ON-TARGET PLUS SMART POOL siRNA CFTR, L-006425-00-0005), and Negative controls (ON-TARGET Plus Non-targeting pool, D-001810-10) were from GE Healthcare Dharmacon. The kinase inhibitors were purchased from Cayman Chemicals and Selleck chemicals. VX-809 was purchased from Selleck chemicals. MG dyes were synthesized at Carnegie Mellon University and Hoechst 33342 cell stain was from Thermo Fisher Scientific.

Cell Line Generation and Cell Culture: Δ F508-CFTR and WT CFTR were fused with FAP (dL5**) at the N-terminus through an added membrane-spanning segment (Figure 1). The fusion constructs were made with a pBabeSacLac2 plasmid and expressed in HEK-293 cells for stable cell lines, described previously.(Holleran et al., 2012b) Clonal FAP expressing cell lines were generated by BD FACS Diva through selecting cells with the brightest fluorescence after MG-B-Tau dye surface labeling. The FAP-CFTR Δ F508 cell lines were sorted with the BD FACS Diva for the enrichment of highest responders to 24 hr treatment of 10 μ M VX-809 at 27°C. The enriched population was expanded and cryopreserved for use at the same passage for each screening experiment. HEK-293 cells were maintained in DMEM with 10% FBS, 100 units ml⁻¹ penicillin, and 100 μ g ml⁻¹ Streptomycin in a humidified atmosphere of 5% CO₂ at 37°C. Antibiotics were absent during transfection, and the 24hr incubation of VX-809/DMSO treatment. **G.F.W. maintained cell cultures**

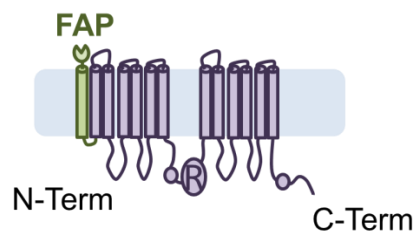


Figure 1. FAP-CFTR construct. An N-terminal fusion of the dL5** fluorogen activating protein with a PDGFR transmembrane spanning segment was used to express the FAP at the extracellular face of the plasma membrane.

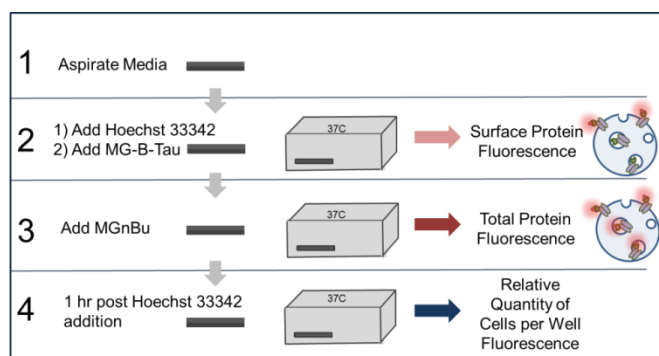


Figure 2. Stepwise plate reader fluorescence measurements

1. After plate treatment, the wells are aspirated.
2. 100 μ L of HBSS with Hoechst33342 (1 μ g/mL) are added to the wells. Immediately afterward, 50 μ L of MG-B-Tau is added to the plate at a final concentration of 500 nM. The plate is scanned on a M1000 Tecan Plate reader at 640/680 nm, 10 nm width, 250 gain, from the bottom, and 16 multiple reads of distinct areas in each well. The plate is scanned 3x.
3. 50 μ L of cell permeable dye, MGnBu, is added at a final concentration of 200 nM and incubated for 20 min at 37°C. Then scanned used the same parameters as step 2.
4. After an hour incubation with Hoechst 33342 (1 μ g/mL), the plate is scanned at 362/492 nm, 5 nm width, and with 150 gain.

HTS Plate Reader Surface and Total Expression Assay: *siRNA screen:* HEK-293 cells expressing FAP-F508del-CFTR were seeded at a density of 3×10^4 cells/well in a 96 well plate. Transfection was performed following Dharmacon's Library transfection protocol, using 25 nM siRNA. One-day post transfection, cells were transferred to two poly-L-lysine coated ibidi 96 well plates at 5×10^5 cells/well. Two days post transfection the media was treated with either 10 μ M VX-809 or DMSO for 24 hrs. After 24 hr incubation, cells were processed on a plate reader, described in figure 2. (Plating and transfection performed by G.F.W., Processing on plate reader done by L.A.P.)

Kinase drug target validation: Cell were plated at 5×10^5 cells/well in a poly-L-lysine coated ibidi 96 well plate and dosed with GW 5074 (RAF1) or STO-609 (CAMKK1) kinase inhibitors and were treated in combination with either DMSO or 10 μ M VX-809 for 24 hrs. After 24 hr incubation, cells were processed on a plate reader, described in figure 2. (Plating and dosing performed by G.F.W., Processing on plate reader done by L.A.P.)

Flow Cytometry: *Assessing relative brightness of MG fluorogens:* FAP-WT-CFTR cells were plated in 35mm dishes and grown to 80% confluency. Cells were incubated with 500 nM MG-B-Tau, MG-Ester, or MGnBu in PBS for 15 min, then suspended and analyzed for surface (MG-B-Tau) or total fluorescence via BD Accuri flow cytometer. For remaining cells/PBS/MG-B-Tau mix, 500 nM MGnBu or MG-Ester was added and incubated for 15 min to label intracellular protein, and then measured for total protein fluorescence.

SiRNA target validation: Cells were plated at 3×10^4 cells/well and dosed identical to the HTS plate reader method for siRNA screening, using single CAMKK1 and RAF1 siRNAs at 25 nM in a 96 well plate. After VX-809 24 hr incubation, media was removed and 100 μ L of cell stripper was added to detach cells and incubated for 20 min. Cell stripper was gently removed and 150 μ L of HBSS with 500 nM MG-B-Tau dye was added to suspend cells and transfer to a U-bottom 96 well plate where they were allowed to incubate for 15 min in dye before being read on an Intellicyt HTFC BD Accuri flow cytometer. (Plating and transfection performed by G.F.W., L.A.P. managed the Accuri)

Kinase Drug Target Validation: Cell were plated at 5×10^5 cells/well in a 96 well plate and dosed with GW 5074 (RAF1) or STO-609 (CAMKK1) kinase inhibitors and were treated in combination with either DMSO or 10 μ M VX-809 for 24 hrs. After VX-809 24 hr incubation, media was removed and 100 μ L of cell stripper was added to detach cells and incubated for 20 min. Cell stripper was gently removed and 150 μ L of HBSS with 500 nM MG-B-Tau dye was added to suspend cells and transfer to a U-bottom 96 well plate where they were allowed to incubate for 15 min in dye before being read on an Intellicyt HTFC BD Accuri flow cytometer. (Plating and dosing performed by G.F.W., L.A.P. managed the Accuri)

Data Analysis and Statistics: Hit scoring metrics were calculated according to established high-throughput RNAi screening data analysis and are described in the supplemental material.

Pre-Processing Screen Data

- Normalize fluorescence to Hoechst (cell count) and transform to log scale
- Remove intra-well outlier measurements
- Average intra-well measurements

Screen Hit Scoring Metrics Using Strictly Standardized Mean Difference (SSMD)

- Calculate SSMD based assay quality score for a moderate control
- Calculate paired SSMD score
- Threshold paired SSMD score based on strong effect (≥ 2)
- Calculate average % increase in surface and total protein
- Calculate siRNA kinase target + VX-809 hit interaction via Two-way ANOVA

ACKNOWLEDGEMENTS:

This work was supported in part by a pilot grant from the Cystic Fibrosis Research Center at University of Pittsburgh (5P30DK072506), the Shurl and Kay Curci Foundation, and NIH grant (R01EB017268). LAP was supported by a Presidential Fellowship at CMU. We would like to thank Gunnar Atli Sigurdsson for statistical advice, Professor Jon Jarvik for the FAP-CFTR cell line, and Professor Ray Frizzell for extensive discussion and advice about CFTR assays and trafficking.

REFERENCES:

- Amaral, M.D., and Farinha, C.M. (2013). Rescuing mutant CFTR: a multi-task approach to a better outcome in treating cystic fibrosis. *Curr. Pharm. Des.* *19*, 3497–3508.
- Botelho, H.M., Uliyakina, I., Awatade, N.T., Proença, M.C., Tischer, C., Sirianant, L., Kunzelmann, K., Pepperkok, R., and Amaral, M.D. (2015). Protein Traffic Disorders: an Effective High-Throughput Fluorescence Microscopy Pipeline for Drug Discovery. *Sci. Rep.* *5*, 9038.
- Carlile, G.W., Robert, R., Zhang, D., Teske, K. a, Luo, Y., Hanrahan, J.W., and Thomas, D.Y. (2007). Correctors of protein trafficking defects identified by a novel high-throughput screening assay. *Chembiochem* *8*, 1012–1020.
- Cheng, S.H., Gregory, R.J., Marshall, J., Paul, S., Souza, D.W., White, G.A., O’Riordan, C.R., and Smith, A.E. (1990). Defective intracellular transport and processing of CFTR is the molecular basis of most cystic fibrosis. *Cell* *63*, 827–834.
- Chiaw, P.K., Eckford, P.D.W., and Bear, C.E. (2011). Insights into the mechanisms underlying CFTR channel activity, the molecular basis for cystic fibrosis and strategies for therapy. *Essays Biochem* *50*, 233–248.
- Cholon, D.M., Quinney, N.L., Fulcher, M.L., Jr, C.R.E., Dokholyan, N. V, Randell, S.H., and Boucher, R.C. (2015). Potentiator Ivacaftor Abrogates Pharmacological Correction of Δ F508 CFTR in Cystic Fibrosis. *6*.
- Cholon, D.M., Jr, C.R.E., Gentsch, M., Hill, C., Hill, C., and Hill, C. (2017). fibrosis patients homozygous for the F508del-CFTR mutation.
- Clancy, J.P., Rowe, S.M., Accurso, F.J., Aitken, M.L., Amin, R.S., Ashlock, M. a., Ballmann, M., Boyle, M.P., Bronsveld, I., Campbell, P.W., et al. (2012). Results of a phase IIa study of VX-809, an investigational CFTR corrector compound, in subjects with cystic fibrosis homozygous for the F508del-CFTR mutation. *Thorax* *67*, 12–18.
- Farinha, C.M., and Canato, S. From the endoplasmic reticulum to the plasma membrane: mechanisms of CFTR folding and trafficking.
- Van Goor, F., and Straley, K. (2006). Rescue of DF508-CFTR trafficking and gating in human cystic fibrosis airway primary cultures by small molecules. *Am J Physiol Lung Cell Mol Physiol* *290*, 1117–1130.
- Holleran, J.P., Glover, M.L., Peters, K.W., Bertrand, C.A., Watkins, S.C., Jarvik, J.W., and Frizzell, R.A. (2012a). Pharmacological rescue of the mutant cystic fibrosis transmembrane conductance regulator (CFTR) detected by use of a novel fluorescence platform. *Mol. Med.* *18*, 685–696.
- Holleran, J.P., Glover, M.L., Peters, K.W., Bertrand, C. a, Watkins, S.C., Jarvik, J.W., and Frizzell, R. a (2012b). Pharmacological rescue of the mutant cystic fibrosis transmembrane conductance regulator (CFTR) detected by use of a novel fluorescence platform. *Mol. Med.* *18*, 685–696.
- Kerem, E. (2004). Pharmacologic therapy for stop mutations: how much CFTR activity is enough? *Curr. Opin. Pulm. Med.* *10*, 547–552.

Larsen, M.B., Hu, J., Frizzell, R.A., and Watkins, S.C. (2016). Simple image-based no-wash method for quantitative detection of surface expressed CFTR. *Methods* 96, 40–45.

Lin, S., Sui, J., Cotard, S., Fung, B., Andersen, J., Zhu, P., El Messadi, N., Lehar, J., Lee, M., and Staunton, J. (2010). Identification of synergistic combinations of F508del cystic fibrosis transmembrane conductance regulator (CFTR) modulators. *Assay Drug Dev. Technol.* 8, 669–684.

Okiyoneda, T., Barrière, H., Bagdány, M., Rabeh, W.M., Du, K., Höhfeld, J., Young, J.C., and Lukacs, G.L. (2010). Peripheral protein quality control removes unfolded CFTR from the plasma membrane. *Science* 329, 805–810.

Pedemonte, N., Lukacs, G.L., Du, K., Caci, E., Zegarra-Moran, O., Galiotta, L.J. V, and Verkman, A.S. (2005). Small-molecule correctors of defective DeltaF508-CFTR cellular processing identified by high-throughput screening. *J. Clin. Invest.* 115, 2564–2571.

Pedemonte, N., Zegarra-moran, O., and Galiotta, L.J. V (2011). High-Throughput Screening of Libraries of Compounds to Identify CFTR Modulators. *742*, 13–21.

Phuan, P.-W., Veit, G., Tan, J., Roldan, A., Finkbeiner, W.E., Lukacs, G., and Verkman, a. S. (2014). Synergy-based Small-Molecule Screen Using a Human Lung Epithelial Cell Line Yields F508-CFTR Correctors that Augment VX-809 Maximal Efficacy. *Mol. Pharmacol.* 42–51.

Pratt, C.P., He, J., Wang, Y., Barth, A.L., and Bruchez, M.P. (2015). Fluorogenic Green-Inside Red-Outside (GIRO) Labeling Approach Reveals Adenylyl Cyclase-Dependent Control of BK α Surface Expression. *Bioconjug. Chem.* 26, 1963–1971.

Ratjen, F., and Döring, G. (2003). Cystic fibrosis. *Lancet* 361, 681–689.

Szent-Gyorgyi, C., Schmidt, B.F., Creeger, Y., Fisher, G.W., Zakel, K.L., Adler, S., Fitzpatrick, J.A.J., Woolford, C.A., Yan, Q., Vasilev, K. V, et al. (2008a). Fluorogen-activating single-chain antibodies for imaging cell surface proteins. *Nat Biotech* 26, 235–240.

Szent-Gyorgyi, C., Schmidt, B.F., Schmidt, B. a, Creeger, Y., Fisher, G.W., Zakel, K.L., Adler, S., Fitzpatrick, J. a J., Woolford, C. a, Yan, Q., et al. (2008b). Fluorogen-activating single-chain antibodies for imaging cell surface proteins. *Nat. Biotechnol.* 26, 235–240.

Szent-Gyorgyi, C., Stanfield, R.L., Andreko, S., Dempsey, A., Ahmed, M., Capek, S., Waggoner, A.S., Wilson, I.A., and Bruchez, M.P. (2013). Malachite Green Mediates Homodimerization of Antibody VL Domains to Form a Fluorescent Ternary Complex with Singular Symmetric Interfaces. *J. Mol. Biol.* 425, 4595–4613.

Telmer, C.A., Verma, R., Teng, H., Andreko, S., Law, L., and Bruchez, M.P. (2015). Rapid, specific, no-wash, far-red fluorogen activation in subcellular compartments by targeted fluorogen activating proteins. *ACS Chem. Biol.* 10, 1239–1246.

Trzcinska-Daneluti, A.M., Ly, D., Huynh, L., Jiang, C., Fladd, C., and Rotin, D. (2009). High-content functional screen to identify proteins that correct F508del-CFTR function. *Mol. Cell. Proteomics* 8, 780–790.

Trzcinska-Daneluti, A.M., Nguyen, L., Jiang, C., Fladd, C., Uehling, D., Prakesch, M., Al-awar, R., and Rotin, D. (2012). Use of kinase inhibitors to correct Δ F508-CFTR function. *Mol. Cell. Proteomics* 11,

745–757.

Trzcińska-Daneluti, A.M., Chen, A., Nguyen, L., Murchie, R., Jiang, C., Moffat, J., Pelletier, L., and Rotin, D. (2015). RNA Interference Screen to Identify Kinases That Suppress Rescue of Δ F508-CFTR. *Mol. Cell. Proteomics* *14*, 1569–1583.

Veit, G., Avramescu, R.G., Perdomo, D., Phuan, P., Apaja, P.M., Borot, F., Szollosi, D., Wu, Y., Walter, E., Hegedus, T., et al. (2014). Some gating potentiators, including VX-70, diminish DeltaF508-CFTR functional expression. *Sci Transl Med* *6*, 1–33.

Xiaohua Douglas Zhang (2011). *Optimal High-Throughput Screening Practical Experimental Design and Data Analysis for Genome-Scale RNAi Research* (Cambridge University Press).

Yan, Q., Schmidt, B.F., Perkins, L. a., Naganbabu, M., Saurabh, S., Andreko, S.K., and Bruchez, M.P. (2015). Near-instant surface-selective fluorogenic protein quantification using sulfonated triarylmethane dyes and fluorogen activating proteins. *Org. Biomol. Chem.* *13*, 2078–2086.

Ye, F., Bauer, J. a, Pietenpol, J. a, and Shyr, Y. (2012). Analysis of high-throughput RNAi screening data in identifying genes mediating sensitivity to chemotherapeutic drugs: statistical approaches and perspectives. *BMC Genomics* *13 Suppl 8*, S3.

Zhang, X.D. (2011a). Illustration of SSMD, z Score, SSMD*, z* Score, and t Statistic for Hit Selection in RNAi High-Throughput Screens. *J. Biomol. Screen.* *16*, 775–785.

Zhang, X.D. (2011b). Illustration of SSMD, z score, SSMD*, z* score, and t statistic for hit selection in RNAi high-throughput screens. *J. Biomol. Screen.* *16*, 775–785.

Zhang, X.D., Ferrer, M., Espeseth, A.S., Marine, S.D., Stec, E.M., Crackower, M.A., Holder, D.J., Heyse, J.F., and Strulovici, B. (2007). The Use of Strictly Standardized Mean Difference for Hit Selection in Primary RNA Interference High-Throughput Screening Experiments. *J. Biomol. Screen.* *12*, 497–509.

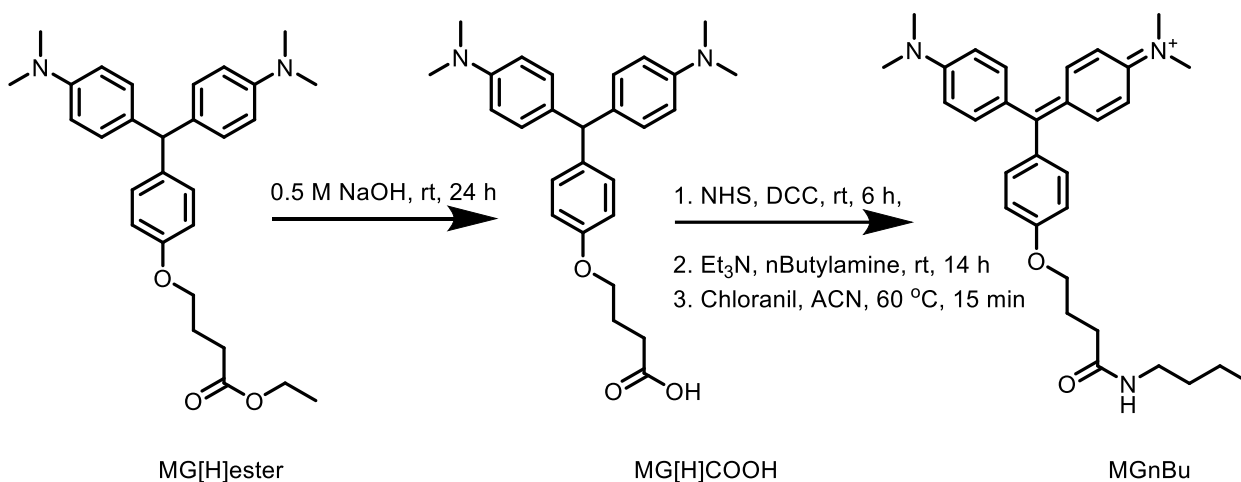
Two Phase 3 Studies of the Tezacaftor/Ivacaftor Combination Treatment Met Primary Endpoints with Statistically Significant Improvements in Lung Function (FEV1) in People with Cystic Fibrosis | Business Wire.

Vertex Announces Significant Progress in Its Development Efforts to Treat the Cause of Cystic Fibrosis in the Vast Majority of People with the Disease | Business Wire.

SUPPORTING INFORMATION:

Chemistry Supplemental Information Section

Synthesis and characterization of MGnBu by Matharishwan Naganbabu:



Scheme 1: Protocol for the synthesis of MGnBu from a previously reported MG precursor. MG[H]ester is first transformed to MG[H]COOH using a base, followed by the activation of terminal carboxylic acid, using NHS, DCC, and coupling using nButylamine to obtain MGnBu.

Synthesis:

To a solution of MG[H]ester (460 mg, 1 mmol, 1 eq.) in acetonitrile (10 mL), 0.5 M sodium hydroxide (2 mL) was added and the mixture was stirred overnight. ESI-MS of the mixture confirmed the ester cleavage. Subsequently, the solvent was removed *in vacuo* and the dry, solid MG[H]COOH was dissolved in anhydrous dichloromethane (5 mL). To this solution, NHS (127 mg, 1.1 mmol, 1.1 eq.) and DCC (227 mg, 1.1 mmol, 1.1 eq.), were added and stirred at room temperature. After 6 hours, a mixture of nButylamine (118 μL , 1.2 mmol, 1.2 eq.) and triethyl amine (181 μL , 1.3 mmol, 1.3 eq.) was added and stirred overnight (14 h) at room temperature. The mixture was filtered, dried, taken up in acetonitrile and boiled. To the boiling mixture, chloranil (245 mg, 1 mmol, 1 eq.) was added and stirred for 15 mins. The mixture was then cooled, filtered, dried and taken up in a mixture of 30%

acetonitrile in water (0.1 % TFA) for purification using reverse phase MPLC column. Yield: 72% (350 mg, 0.72 mmol)

¹H NMR (CD₃OD), 500 MHz: 0.95 (t, 3H, J = 7.3 Hz), 1.37 (m, 2H), 1.49 (m, 2H), 2.16 (t, 2H, J = 6.9 Hz), 2.44 (t, 2H, J = 7.3 Hz), 3.21 (t, 2H, J = 7.0 Hz), 3.34 (s, 12H), 4.21 (t, 2H, J = 6.2 Hz), 7.06 (d, 4H, J = 9.3 Hz), 7.19 (d, 2H, J = 8.7 Hz), 7.39 (d, 2H, J = 8.7 Hz), 7.45 (d, 4H, J = 9.15 Hz)

¹³C NMR (CD₃OD), 500 MHz: 12.69, 19.69, 25.03, 31.15, 31.93, 38.77, 39.40, 67.60, 113.00, 114.62, 126.92, 131.85, 137.48, 140.47, 157.01, 164.31, 178.36

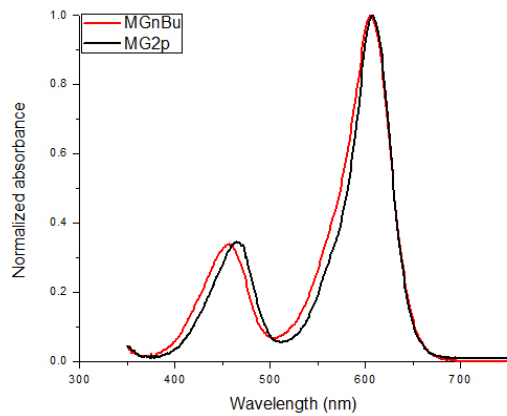
ESI-MS (positive mode, MeOH): expected: 486.31 obtained: 486.2

MGnBu Photophysical properties:

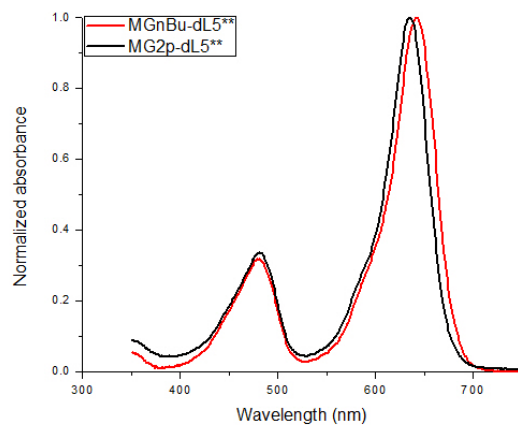
*The final dye solutions for spectroscopy and biological experiments were diluted from a 1000x stock solution in 1% acidic ethanol and prepared the same day of experiments.

Quantum yield: Quantum yield of the dyes were determined using MG2p-dL5** as a standard with a quantum yield of 20% in PBS 7.4. The fluorescence emission of dye-dL5** solutions containing the same O.D at 630 nm (λ_{ex}) in PBS 7.4 were obtained. The fluorescence spectra of the solutions were measured and the ratio of quantum yield of standard and unknown sample is: $F_x F_s = Q_x Q_s$ Where F – fluorescence intensity, Q – quantum yield; x – sample, s – standard

Absorbance spectra:



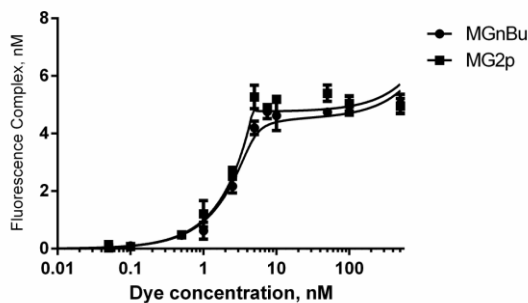
Supplementary Figure 1: Absorbance spectra of MGnBu and MG2p (3 μ M) in phosphate buffered saline (PBS) pH 7.4. Each dye was normalized to the wavelength corresponding to the highest optical density. The spectral profile of MG2p and MGnBu are similar. The extinction co-efficient of MG at 607 nm is 74,250 M⁻¹ cm⁻¹ in PBS 7.4.(Szent-Gyorgyi et al., 2008b)



Supplementary Figure 2: Absorbance spectra of MGnBu and MG2p (3 μ M) complexed with dL5** (15 μ M) in phosphate buffered saline (PBS) pH 7.4. Each dye-dL5** was normalized to the wavelength corresponding to the highest optical density. The spectral shift of MGnBu upon binding to dL5** is similar as MG2p-dL5** complex. The extinction co-efficient of MG – dL5** at 607 nm is 91,700 M⁻¹ cm⁻¹ in PBS 7.4.(Szent-Gyorgyi et al., 2013)

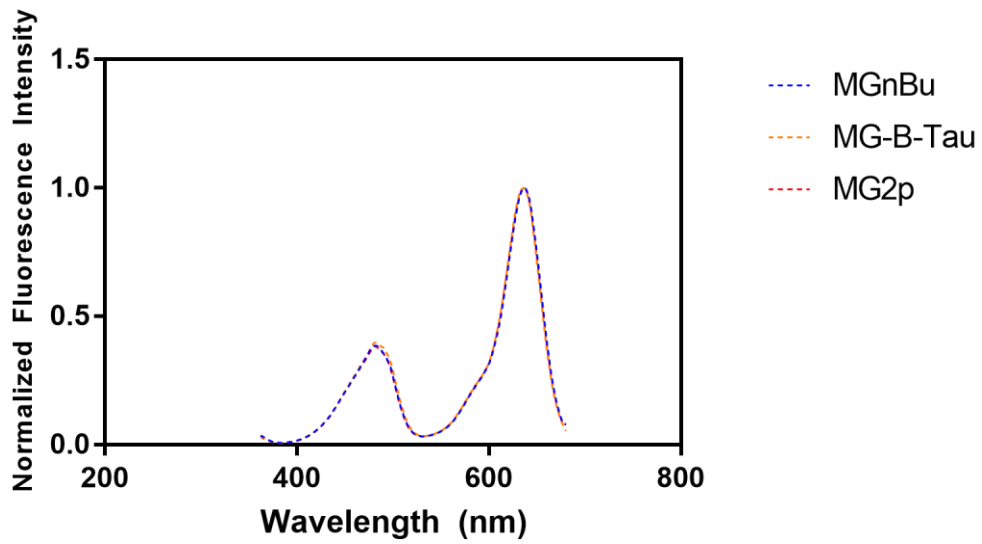
Binding affinity (Kd measurement): Binding affinity of MgNBu was determined by titrating it against a known concentration of dL5**. Triplicate fluorescence response was determined using a 96-well plate on a TECAN Infinite M1000 96-well plate reader fluorimeter using ex/em of 636 nm/664 nm. Analysis of fluorescence response was determined using a non-linear regression using One site – Total, accounting for ligand depletion. The model, originally used for radioactivity measurements was modified to fit fluorescence data by fixing the volume at 0.2 mL and SpecAct was set to 1.00 on GraphPad Prism 7.0 software, and the maximum fluorescent intensity was set to 5.0, representing the maximum concentration of complex that can be formed (based on 5 nM protein concentration). The ligand depletion model assumes that changes in complex formation are associated with complementary changes in free ligand and free receptor, and are a typical model for ligand-receptor interactions when one has to work at protein concentrations that are near the Kd value. The original formula and fitting can be found at:

http://www.graphpad.com/guides/prism/6/curve-fitting/index.htm?reg_one_site_total_depletion.htm

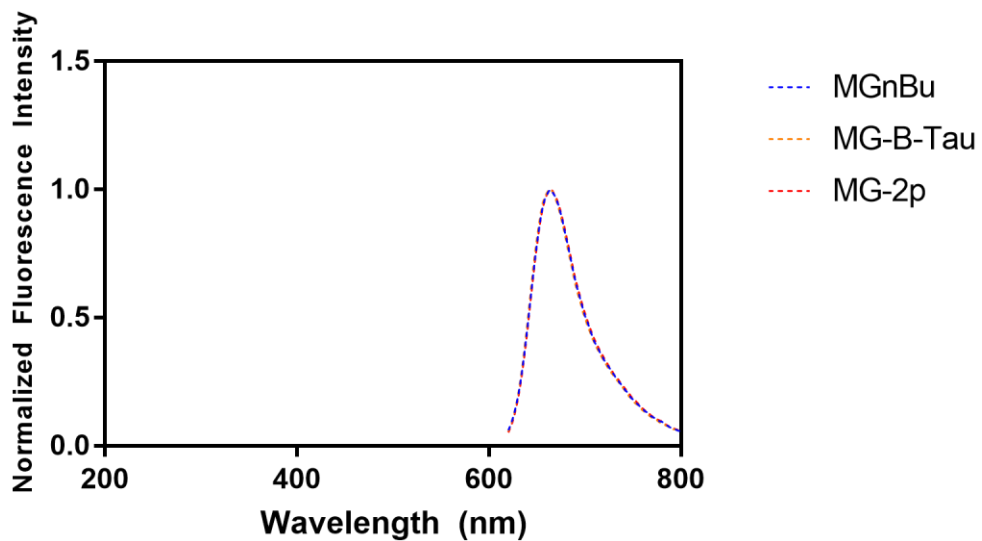


Supplementary Figure 3: Kd measurement of MGnBu and MG2p using purified dL5**. 5 nM dL5** was incubated with a serial dilution of 500 nM to 10 pM of the respective dye dissolved in phosphate buffered saline (PBS) pH 7.4. The dye fluorescence was subtracted from the dye-dL5** complex. MGnBu Kd (0.4 ± 0.35 pM); MG-2p Kd (0.5 ± 0.35 pM)

Excitation and emission spectra



Supplementary Figure 4: Excitation spectra was recorded using 1 μ M dye and 5 μ M dL5** in phosphate buffered saline (PBS) pH 7.4. λ_{em} was set to 700 nm. MGnBu was compared to MG-2p and MG-B-Tau. Normalization for the respective dye-dL5** was done by setting the λ of dye-dL5** with highest fluorescence intensity to 1.0.



Supplementary Figure 5: Emission spectra was recorded using 1 uM dye and 5 uM dL5** in phosphate buffered saline (PBS) pH 7.4. λ_{ex} was set to 600 nm to visualize direct excitation of MG-dL5** in MGnBu in comparison to MG-2p and MG-B-Tau.

-End of Chemistry Section-

Analysis and Statistics

Pre-processing data: All well measurements had the mean background fluorescence subtracted. The surface CFTR fluorescence signal and total fluorescence signal were normalized to the relative quantity of cells (Hoechst 33342 signal) per scanning point, 16 total, inside a well. All values were then transformed to log scale to achieve a normal distribution required for the subsequent statistical tests. For each well, the 16 intra-well values were subjected to outlier analysis using robust Z*Score testing to identify and exclude significant anomalies within a well. These irregular measurements could arise from technical error or small debris. The final well sample measurement was calculated by the interquartile mean of the intra-well values.

$$Z^*score = \frac{Y_i - \tilde{Y}_N(16 \text{ intra-well values})}{MAD(16 \text{ intra-well values})}$$

(1)

Y_i : value of point within a well

\tilde{Y}_N : median of 16 intra-well values

MAD : median absolute deviation of all 16 intra well measurements

SiRNA screen quality assessment: The quality control (QC) of the siRNA screen was assessed through strictly standardize mean difference (SSMD). (Xiaohua Douglas Zhang, 2011) This scoring method is favorable due to its ability to report consistent quality control results with positive controls that aren't necessarily very strong. In our system, our positive control is siRNA that targets CFTR, and the total amount of CFTR is reduced due to the F508d mutation. Even with VX-809 treatment, knockdown effect can be moderate in terms of total protein. Our QC criterion was based off of a moderate control effect assessing the VX-809 treated plate of a transfection pair, and using the

CFTR siRNA wells as a positive control for total protein knockdown and scrambled NC siRNA wells as a negative control. A plate passes QC if it has good or excellent quality.

$$SSMD\ QC = \frac{\bar{x}_p - \bar{x}_N}{\sqrt{S^2_p + S^2_N}} \quad (2)$$

\bar{x}_p : Sample mean of positive control

\bar{x}_N : Sample mean of negative control

S^2_p : Standard deviation of positive control

S^2_N : Standard deviation of Negative control

Hit selection: Paired SSMD and mean fold change in CFTR surface expression were used to evaluate hits.

⁴SSMD is the mean of differences (\bar{d}_i) divided by the standard deviation (S_i) of the differences between an siRNA and a negative reference. (Zhang, 2011b; Zhang et al., 2007) The SSMD score generated is the average fold change in log scale penalized by the variability of fold change on the log scale.

$$SSMD = \frac{\bar{d}_i}{S_i} \quad (3)$$

VX-809 treated plate: The median of the negative siRNA VX-809 treated NC of a plate was subtracted from each sample of the same plate. The mean difference and standard deviation of an siRNA was calculated from the plate replicates. To select for strong siRNA effects with VX-809, we used a hit threshold of 2 for the kinase library screen, which used 3 replicates per siRNA. The siRNAs that were above the threshold were ranked based on their average fold change from the median VX-809 NC.

Vehicle (DMSO) treated plate: Without any chemical or temperature correction, there is near zero surface fluorescence in the NC wells alone. These vehicle treated plates are more sensitive to small increases in surface signal, which can potentially arise from media evaporation at the edges. In the kinase library screen, the negative controls are positioned in the first column, making it important to be able to identify and counter this potential effect. The % difference between the median of the NC and the interquartile mean of the whole plate is determined. The interquartile mean is used only when there is a larger than 15% difference between the surface fluorescence of the negative controls and the interquartile mean of the plate. This large difference infers that the characteristic NC near zero signal was likely aggravated by possible edge effects, making it important to utilize the plate based normalization. Normalizing using most of the samples on the plate is powerful because

there are only very few instances where siRNA treatments promotes F508del-CFTR surface expression with DMSO alone. In addition, the large amount of samples in a plate promotes a more accurate measurement of the baseline surface signal.

The median of the negative control siRNA or interquartile mean of a DMSO treated plate was subtracted from each sample of the same plate. The mean difference and standard deviation of an siRNA was calculated from the plate replicates. To identify strong siRNA effects with DMSO, we used a hit threshold of 2 for the kinase library screen, which used 3 replicates per siRNA. The siRNAs that were above the threshold were ranked based on their average fold change from the median DMSO NC or plate interquartile mean. The primary purpose of the vehicle treated plate was to establish the effect of an siRNA without VX-809 to determine the interaction significance.

Interaction testing: Interaction was assessed using a linear model that included a siRNA-drug interaction effect. (Ye et al., 2012)

Surface Signal = siRNA(yes/no) + VX-809(yes/no) + siRNA*VX-809

(yes,yes) siRNA+VX-809

(yes,no) Vehicle siRNA

(no,yes) VX-809 NC

(no,no) Vehicle NC

A two-way, balanced (3 replicates per condition) ANOVA was performed in Graphpad prism 6 to test for significant interaction using the log fold change from DMSO NC (NC well median or interquartile mean of plate). Equal variance was confirmed using Levene's test in Minitab. However, due to the variable nature of siRNA knockdown efficiency between replicates and a bare minimum of replicates, there were instances where replicate variance was too broad to calculate significant interaction. To help mitigate variance between replicates in the VX-809 condition, where there is often some variability in the VX-809 treatment itself, the overall average of VX-809 NC log fold increase from the DMSO baseline surface expression of each transfection pair (VX-809 and DMSO treated plate of a single replicate) was used to rescale each replicate to the overall average.

Select siRNA kinase knock-down Immunofluorescence

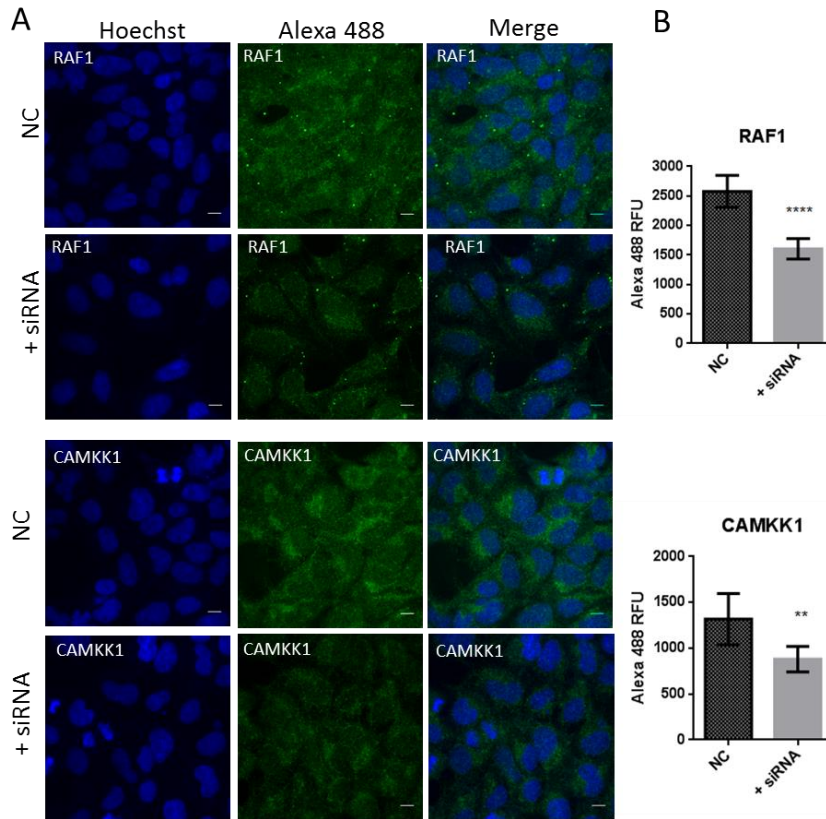
siRNA Transfection Method:

Cherry picked CAMKK1 and RAF1 siRNA from library and performed knockdown according to Dharmacon's Library transfection protocol, using same methods as those described in the manuscript.

Immunofluorescence 96 well imaging format:

Adapted from BD biosciences support protocols for bioimaging in 96 well plate.

Cell culture media was removed and 100 μ L of 37°C 4% PFA was added per well and incubated at room temperature for 10 minutes. After PFA incubation, PFA was removed and wells were washed with 100 μ L of PBS, followed by adding 100 μ L of 0.1% Triton X-100/ 4% FBS solution to wells for 1 hour at room temperature. Permeabilization/blocking solution was removed and incubated with either 50 μ L of Anti-RAF1 (abcam ab147435) (1:200 dilution) or Anti-CAMKK (abcam ab80066) (5 μ g/mL dilution) in 4% FBS for 1 hour at room temperature. Primary antibodies were washed off 3x with 100 μ L PBS. 50 μ L of secondary antibody, Goat Anti Rabbit IgG Alexa Fluor 488 (abcam ab15007) (1:500 dilution) was added to wells and incubated in dark at room temperature for 1 hour. After incubation, wells were washed 3x with 100 μ L PBS and then 200 μ L of PBS containing 2 μ g/mL of Hoechst 33342 was added. Plate was imaged on Andor Revolution XD system (Andor technology) with Yokogawa CSU-X1 spinning disk confocal unit (Yokogawa Industries). Cells were imaged with a 40x, .95 air objective (Nikon) with (488ex:525/50em) and (405ex:435/25em).



Supplementary Figure 6. SiRNA knock-down of CAMKK1 and RAF. A) Immunofluorescence imaging. Matched LUT between NC and + siRNA for each antibody. B) Measured mean Alexa 488 fluorescence intensity in cell ROIs \pm S.D. (7 ROIs/image). **** $P \leq 0.0001$; ** $P \leq 0.01$. Scale bar: 10 μ m. **G.W.F** performed siRNA transfections. **L.A.P** performed immunostaining, imaging, and data analysis.

SUPPPORTING INFORMATION REFERENCES:

Szent-Gyorgyi, C. *et al.* Fluorogen-activating single-chain antibodies for imaging cell surface proteins. *Nat Biotech* **26**, 235–240 (2008).

Szent-Gyorgyi, C. *et al.* Malachite Green Mediates Homodimerization of Antibody VL Domains to Form a Fluorescent Ternary Complex with Singular Symmetric Interfaces. *J. Mol. Biol.* **425**, 4595–4613 (2013).

Ye, F., Bauer, J. a, Pietenpol, J. a & Shyr, Y. Analysis of high-throughput RNAi screening data in identifying genes mediating sensitivity to chemotherapeutic drugs: statistical approaches and perspectives. *BMC Genomics* **13 Suppl 8**, S3 (2012).

Xiaohua Douglas Zhang. *Optimal High-Throughput Screening Practical Experimental Design and Data Analysis for Genome-Scale RNAi Research*. (Cambridge University Press, 2011). doi:Xiaohua Douglas Zhang,

Zhang, X. D. Illustration of SSMD, z score, SSMD*, z* score, and t statistic for hit selection in RNAi high-throughput screens. *J. Biomol. Screen.* **16**, 775–85 (2011).

Zhang, X. D. *et al.* The Use of Strictly Standardized Mean Difference for Hit Selection in Primary RNA Interference High-Throughput Screening Experiments. *J. Biomol. Screen.* **12**, 497–509 (2007).

CHAPTER IV

Lysosomal Protein FAP Construct Validation and Application

ABSTRACT: We introduce the development of a lysosomal protein trafficking platform based on fluorogen activating protein (FAP) technology. The proposed approach uses a lysosomal luminal fusion tag (FAP-LAMP1) and cell permeable MG-Coumarin FRET pH sensitive dye, BluR_{pH}, which can detect pulse-chase FAP-protein delivery to lysosomes and lysosomal proteolysis activity. The Bruchez lab is also fine-tuning a novel fluorogenic dye, AMG-Ester, which only binds FAP labeled proteins in acidic environments. The new AMG-Ester dye shows potential for specific lysosomal FAP labeling.

INTRODUCTION: Lysosomes play a critical role as the degradation center of eukaryotic cells. Biomacromolecules fated for degradation can be delivered to the membrane-bound organelle through multiple trafficking pathways, such as phagocytosis, endocytosis, or autophagic itineraries. The lysosome's acidic lumen possesses several types of proteases to break-down biological materials, which can be then recycled for reuse. The lysosomal membrane provides a station for transmembrane proteins that act as the central controllers. While a proportion of membrane associated proteins role still remains unknown, they have been found to conduct the formation and maintenance of the acidic organelle, and regulate the in and out trafficking of materials and lysosomal proteins.(Braulke and Bonifacino, 2009) In particular, the lysosomal membrane associated protein 1 and 2 (LAMP 1, LAMP2) constitutes 50% of the exhibited lysosomal membrane proteins.(Schoneberg et al., 1995; Schröder et al., 2007) Their full responsibilities are still unclear, but have been shown to be involved in motility and autophagic fusion events, and defective LAMP1 or LAMP2 trafficking causes autophagy disruption that is associated with neurodegenerative diseases.(Huynh et al., 2007; Eskelinen, 2006) Aberrant lysosomal trafficking can lead to a myriad of lysosomal storage disorders; Niemann Pick disease type C (NPC) is among the most represented examples. NPC is caused by an autosomal recessive genetic mutation in NPC1 or NPC2 genes, which results in NPC1 and/or NPC2 absence from the lysosome, where they function as cholesterol transporters. Without these lysosomal proteins, cholesterol accumulates in the late endosome and lysosomal compartments instead of being trafficked to their final destinations for cell use.(Liu et al., 2007; Repa and Mangelsdorf, 2000) Lysosomal dysfunction causes significant impairment that can cause devastating neurological and organ damage.(Wenger et al., 2003)

Studying the lysosomal machinery and developing new therapeutic strategies require rapid and dynamic methods that are capable of imaging, quantifying trafficking, and assessing proteolytic changes. Current lysosomal protein and acidic compartment labeling protocols can be time consuming, have limited applications, and technical caveats. LAMP1 is often used as a lysosomal marker due to its large

lysosome abundance. LAMP1 can be labeled with antibodies conjugated to fluorophores, but requires cell fixation, permeabilization, long incubations, and wash steps. Not only do these factors reduce the extent of the methods' application, they make it prohibitive in terms of time and cost as a high-throughput approach. Fluorescent protein (FP) tags attached to lysosomal proteins is a common method to visualize lysosomes. However, a FP tagged to a protein within the acidic, proteolytic lumen, or expressed on the luminal domain of a lysosomal membrane protein, such as LAMP1, may be cleaved or degraded, as well as fluorescently quenched.(Huang et al., 2014) The workaround is to either inhibit lysosomal degradation, or to label the cytosolic side of LAMP1, hindering experimental capabilities. Another important factor to consider is the potential impact of overexpressing FP tagged LAMP1. Promoting a large production of the tagged protein of interest may cause additional fluorescent signal in other non-lysosomal compartments due to increased amounts in the production and trafficking pathways, or alter organelle dynamics entirely by overexpressed protein interactions.(Costantini and Snapp; Snapp et al., 2003) Alternatively, fluorescent dyes can be used for marking acidic compartments, but also encounter challenges with photostability and cytotoxicity. There are many different lysosomal dyes commercially accessible, but the most commonly used is lysotracker.(Pryor, 2012) LysoTracker functions through a fluorophore associated with a weak base that becomes protonated at low pH, turning on its fluorescence. Once protonated it cannot passively exit the acidic compartment, thereby allowing specific acidic compartment signal. The dye itself exhibits rapid photobleaching and has an alkalinizing effect, which raises the pH of lysosome and causes a decline in fluorescence.(Pierzyńska-Mach et al., 2014) Another method utilizes fluorescent dextrans for observing lysosomal trafficking and labeling. Dextrans are resistant to lysosomal degradation and can be conjugated with a fluorophore that is unaffected by pH. Dextrans can also be attached to a designed pH biosensor complex. These probes are cell impermeable, being trafficked via cell fluid-phase uptake. Loading cells with dextrans uses a pulse-chase approach, following a pool of dextrans through endosomal trafficking and ultimately attaining a concentrated fluorescent signal in the lysosome. While these probes are extremely valuable in research, background signal can be high from dextran binding with glass surfaces.(Pryor, 2012) Most semisynthetic probes do not function in low pH environments due to chemical ligation requirements and need for nucleophilic attack in bond-forming reaction at the active site, requiring new technical labeling developments. Fluorogen activating protein (FAP) technology presents a new labeling scheme that uses a fluorogenic approach for labeling proteins of interest (POI). FAP is a small antibody fragment that specifically binds to malachite green (MG) dye, and only once bound to MG, the FAP-dye complex becomes fluorescent.(Szent-Gyorgyi et al., 2008) The specific POI labeling and capability to utilize different types of MG derivative dyes makes this an attractive method of assessing lysosomal protein trafficking and proteolysis activity. Here we present a new luminal-oriented lysosome incorporated FAP-LAMP1 tag and cell permeable MG-Coumarin FRET-based pH sensitive dye, BluRpH, which reports delivery to late endosomes and signal decay in lysosomes by independent ratiometric fluorescent measurements of protein-dye complex and the proximal pH. In addition, we demonstrate a new acid-dependent fluorogenic dye for specific lysosomal FAP-protein labeling.

RESULTS:

LAMP1 was chosen to create a new lysosomal FAP tools paradigm as LAMP1 is a traditionally used lysosomal marker and has high lysosomal expression, and LAMP1's cytosolic tail is necessary and sufficient for lysosomal trafficking. (Rohrer et al., 1996; Peters et al., 1990; Obermüller et al., 2002) Due to this feature, the luminal domain could be completely removed and replaced with a 26 kDa FAP tag, dL5**. Cheryl A. Telmer developed these probes using a G4S (G4S?) glycine-serine linker, which also can reduce the risk of tag cleavage, as 5-10 gly-ser residues are more prone to cleavage by lysosomal proteases.(Huang et al., 2014) The construct design is shown in figure 1 and sequence information in is the methods section.

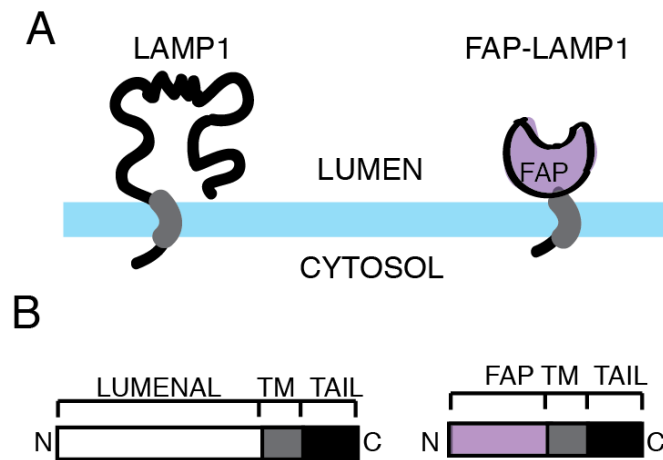


FIGURE 1. FAP-LAMP1 construct design. A) Illustration of LAMP1 construct. B) Diagram of domains. For the generation of the FAP-LAMP1 construct, overlap PCR was used to construct the transmembrane domain and cytoplasmic tail for Human LAMP1 (NM_005561.3). This fragment was cloned into pcDNA3.1-kappa-myc-dL5-G4S using AgeI and XhoI.(Telmer et al., 2015) Sequence information is provided in the methods. **Designed and created by Cheryl Telmer.**

FAP-LAMP1 was transfected into HEK293 cells (Yi Wang and Sue Andreko) and imaged for colocalization with other lysosomal markers to confirm its lysosomal presence. FAP-LAMP1 was labeled with cell permeable dye MG-ester(Telmer et al., 2015), and the lysosome was labeled by either lysotracker green or Rab7-GFP co-transfected cells. Pearson's R coefficient was used to determine colocalization with setting a threshold of $\geq .4$ as significant. However, imaging showed minimal observed colocalization with either of these markers. Initial imaging was previously done by Haibing Teng and Sue Andreko (data not shown).

LAMP1 is trafficked from the trans-golgi network (TGN) to early endosomes and then delivered to late endosomes and lysosomes.(Cook et al., 2004) The developed FAP-LAMP uses a cytomegalovirus (CMV) promoter for high expression, which can cause a large accumulation of signal in the biosynthetic pathway, particularly within the TGN. To determine where FAP-LAMP1 is localized, we used immunofluorescence with various antibodies for endosomal trafficking protein markers to identify which compartment the construct may be localized to. Immunolabeling used rabbit primary antibodies from the

endosomal marker antibody sampler kit from cell signaling (#12666), followed by secondary immunofluorescent labeling with an Alexa 488 dye anti-Rabbit conjugate. The endosomal kit included: early endosome (EEA1, clatherin, caveolin, and Rab 5), late endosome/lysosome (Rab 7), and recycling endosomes (Rab 11). We also used antibody markers for golgi (anti-giantin was kindly provided by the Lindstedt lab) and the endoplasmic reticulum (anti-PDI was kindly provided by the Lee lab). Figure 2. shows the confocal images with different markers, however FAP-LAMP1 only showed a Pearson's R colocalization coefficient $\geq .40$ with the TGN marker, not early endosomal markers or Rab11.

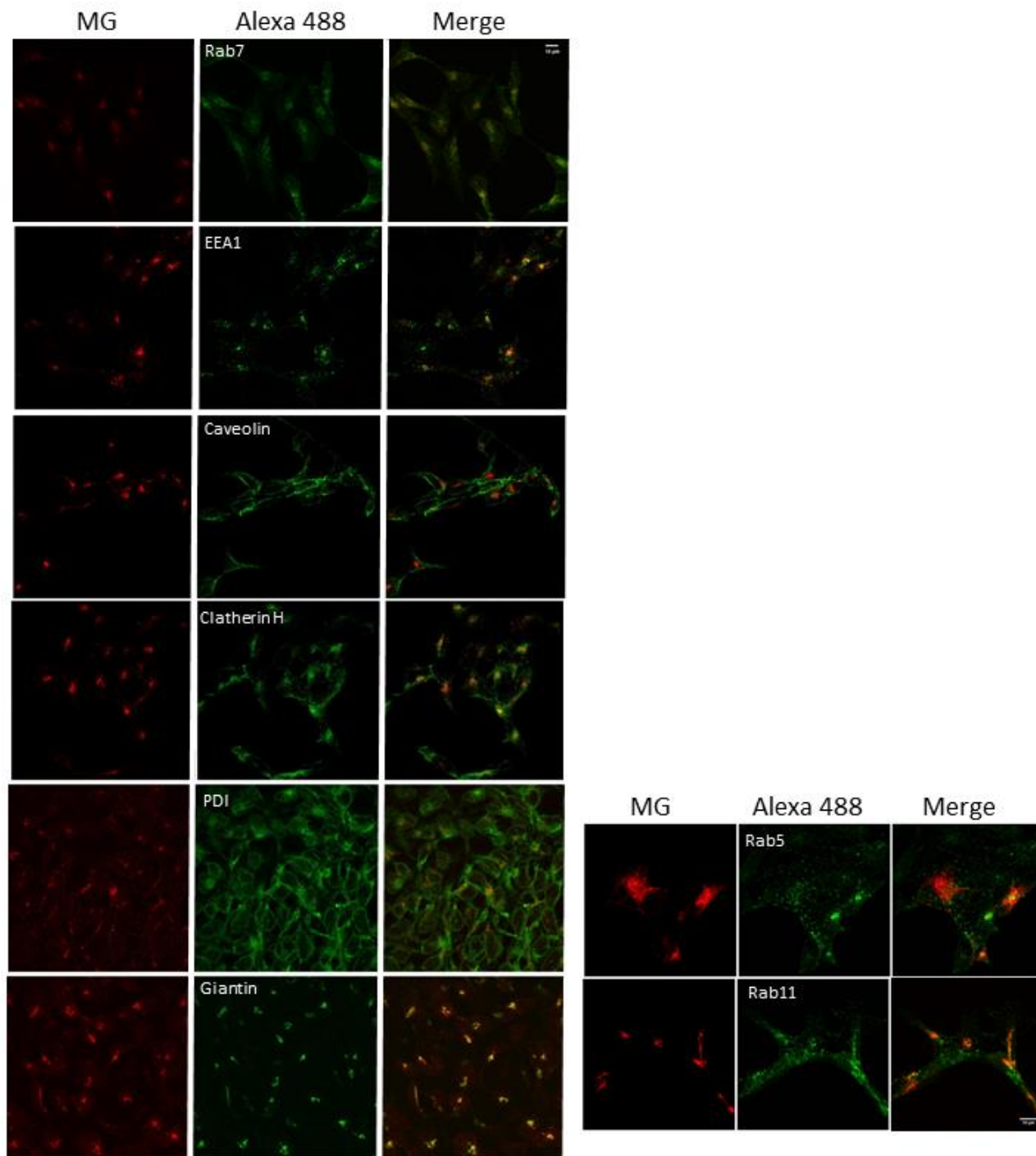


Figure 2. FAP-LAMP1 colocalization imaging. Rab7 marker showed low colocalization, $R=0.3$. PDI, EEA1, clathrin, Rab 5, Rab11 and caveolin also did not show significant colocalization. Golgi marker, giantin, colocalized with FAP-LAMP1 labeling, $R=0.52$. Scale bar 10 μm .

FAP-LAMP1's strong colocalization with the golgi marker suggests that most signal resides in its biosynthetic route, and an additional measure must be taken to achieve specific lysosomal signal. FAP technology gives us the ability to pulse-chase label LAMP1, thereby allowing a shift in fluorescence signal localization from the TGN to lysosome, as the labeled pool of protein is delivered to its final destination. LAMP1 traffics to the lysosome with a reported half-life of less than 1 hour.(Cook et al., 2004) We measured 1 and 4 hour time points after an initial 5 min labeling with MG-ester with washout, described in Figure 3a. Colocalization increased ($R > .40$) with Rab7, and continued to show colocalization with giantin until 4 hours post labeling, $R = .28$ (Figure 3b).

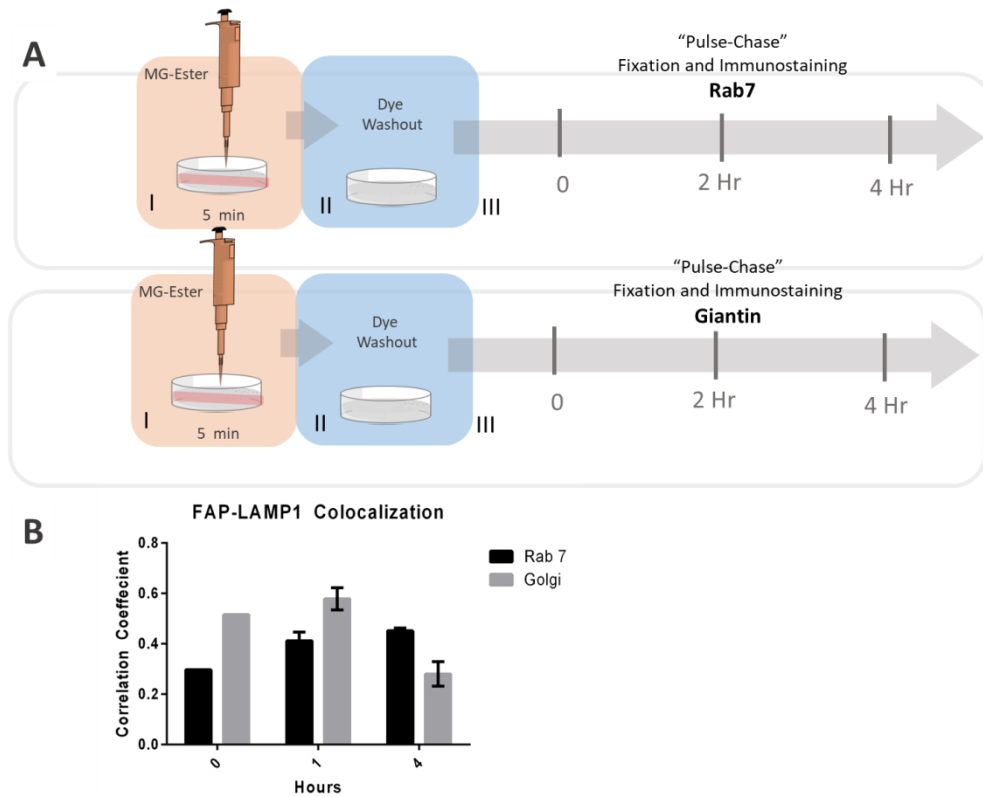


Figure 3. Pearson's coefficient of Rab 7 or Giantin colocalization with FAP-LAMP1 over pulse-chase time period of 1-4 hours. 1 and 4 hours results are average with S.D. error bars.

While we found increased lysosomal associated signal with pulse-chase labeling, signal had appeared to diminish over time (Figure 4a.). The decrease in signal led us to suspect that the FAP-dye complex was being degraded upon delivery into the lysosome lumen. Inhibition of lysosomal activity with 100 μ M chloroquine addition for a 12 hour incubation preserved MG-ester signal (Figure 4b).

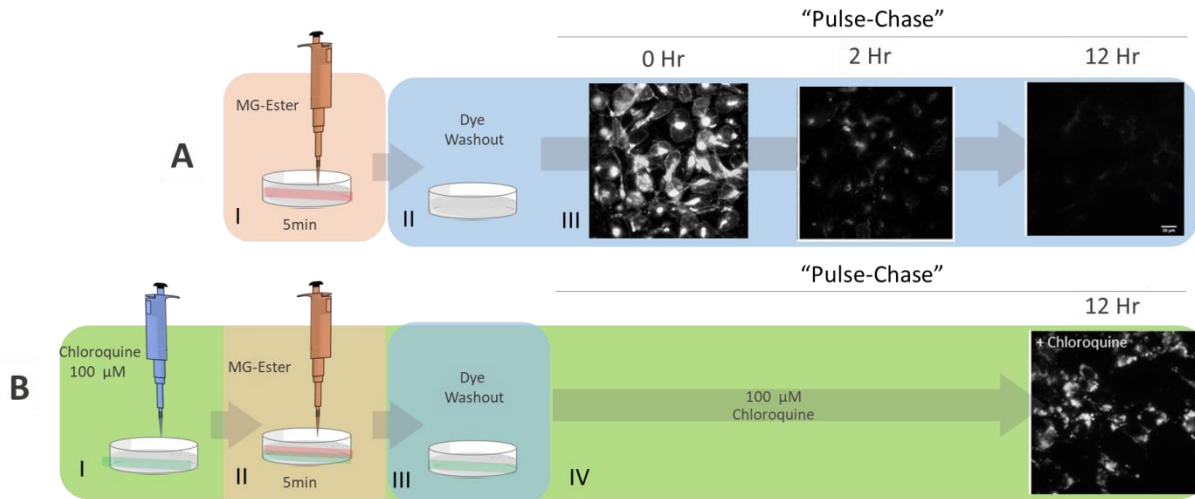


Figure 4. Showing the steps of 200 nM MG-Ester “pulse-chase” labeled FAP-LAMP1 and signal changes A) No lysosomal inhibition.

- I. 200 nM MG-Ester dye addition, 5 minute incubation.
- II. Dye washout.
- III. “Pulse-Chase” imaging period. 0 Hr, 2 Hr, and 12 Hr timepoints.

B) Lysosomal Inhibition

- I. Pre-treatment with 100 nM chloroquine Dye washout.
- II. 200 nM MG-Ester dye addition, 5 minute incubation.
- III. Dye washout.
- IV. “Pulse-Chase” imaging period showing 12 Hr timepoint. In presence of chloroquine.

Scale bar: 20 μm

To determine if observed FAP-LAMP1 signal was lysosomal, cells were treated with 100 μM chloroquine for 24 hrs and then labeled with MG-ester for 5 min then washed out. Fixation and Rab7 immunostaining immediately followed after time point 0, and 1.5 hours (Figure 5 a,b). Colocalization was observed for both time points, suggesting that inhibiting lysosomal degradation for a prior amount of time may be sufficient for effective lysosomal labeling.

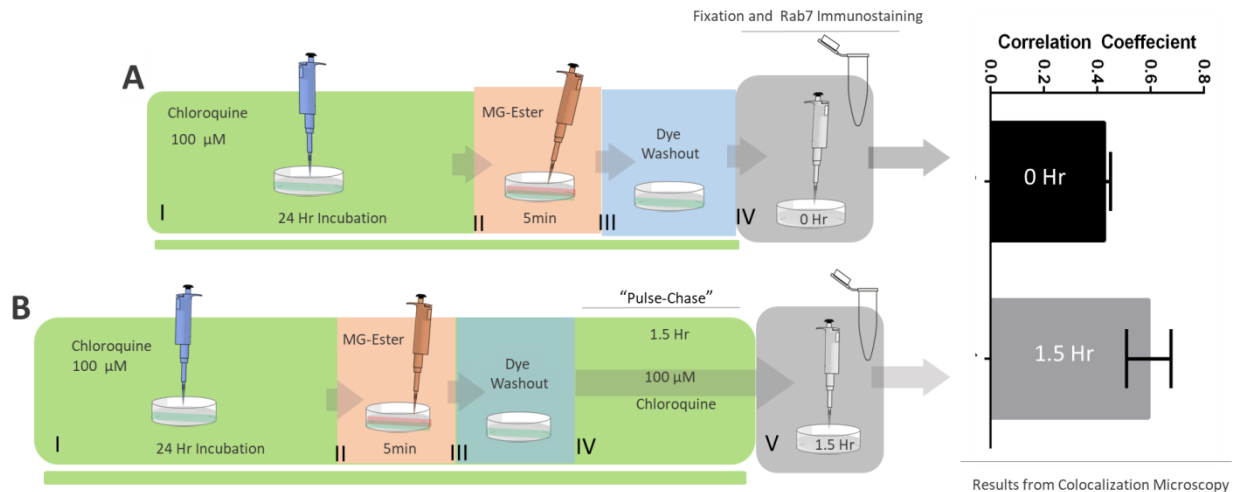


Figure 5. FAP-LAMP1 colocalization with Rab 7.

- A) No "Pulse-Chase", immediate fixation after dye washout
- I. Pre-treatment with 100 μ M chloroquine 24 Hr
 - II. 200 nM MG-Ester dye addition, 5 minute incubation.
 - III. Dye washout.
 - IV. Fixation and Rab7 Immunostaining, following by confocal imaging for FAP-LAMP1 colocalization

Graph on right shows 0 hr correlation coefficient. 0 hr R=.43. Data shown as average \pm S.D.

- B) No "Pulse-Chase", immediate fixation after dye washout
- I. Pre-treatment with 100 μ M chloroquine 24 Hr
 - II. 200 nM MG-Ester dye addition, 5 minute incubation.
 - III. Dye washout.
 - IV. "Pulse-Chase" 1.5 hr in presence of chloroquine.
 - V. Fixation and Rab7 Immunostaining, following by confocal imaging for FAP-LAMP1 colocalization

Graph on right shows 0 hr correlation coefficient. 0 hr R=.59. Data shown as average \pm S.D.

We observed a reproducible linear loss in fluorescence signal over time with FAP-LAMP1 trafficking from the TGN to the lysosome. This phenomenon was turned into a feature by measuring signal over time as an indicator of productive LAMP-1 trafficking, or lysosomal activity. This approach could be used as a unique advantage, as FP tags cannot be pulse-chase labeled.

This study describes the development of a new method using pulse chase FAP labeling with a cell-permeant pH sensitive fluorogenic “BluRpH” dye, developed by **Matharishwan Naganbabu**. The BluRpH dye contains a pH sensitive coumarin donor (Figure 7a highlighted in blue) that acts as an energy transfer donor to malachite green (MG) (Figure 7a highlighted in pink), with a pKa of 6.28. The MG conjugated, pH sensitive 6-chloro-7-hydroxycoumarin-3-carboxylic acid (405 nm excitation) is cell-permeable and transfers energy to malachite green’s 2ndary excitation band (482 nm) and emits at 680 nm. In contrast to the previously reported TRAPHIC dyes, for this BluRpH complex, lower pH will decrease the FRET channel’s signal. Figure 6 provides the excitation spectra for the BluRpH-dL5 complex, which has been adapted from Matharishwan Naganbabu’s thesis. Further in vitro details, such as synthesis and chemical properties can be requested (manuscript in preparation). Figure 7. Describes the methods used for measuring FAP-LAMP1 trafficking over time in different conditions. Figure 8b is a simple illustration of the LAMP1 trafficking pathway. BluRpH pulse-chase labeled FAP-LAMP1 signal changes depending on different conditions. Figure 8c,d shows FAP-LAMP1 trafficking with the anticipated fluorescent signal in the 405 ex pH sensitive coumarin FRET channel, and the 640 ex MG channel. Baseline trafficking shows a linear decline in fluorescence in both channels, presumably a result of FAP-degradation in the lysosome lumen. However, with 24 hr 100 μ M chloroquine inhibition, there is no decline in either channel signal, due to chloroquine raising pH, and thereby halting lysosomal proteases. The last condition, 21 μ M Leupeptin treatment for 4 hours, inhibits lysosomal activity, but preserves the lysosome’s acidic pH. With leupeptin, MG signal should remain stable over time, while 405-680 FRET channel signal should reduce over time, reflecting lysosomal acidification and delivery of FAP-LAMP1-BluRpH complex into acidic lysosomes. The conditions in Figure 8 were performed with live FAP-LAMP1 expressing HEK293 cell with confocal microscopy over time as described in Figure 7, and preliminary results are shown in Figure 9.

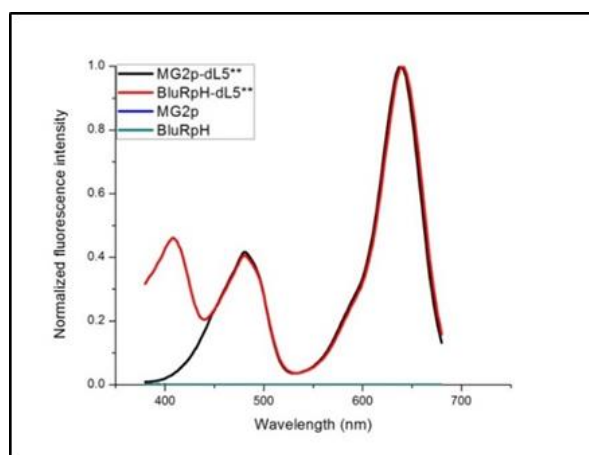


Figure 6. Steady-state fluorescence excitation spectra of BluRpH. Measurements were made using 1 μ M dye and 5 μ M FAP (dL5**) with a set emission wavelength of 700 nm. **Collected by Matharishwan Naganbabu.**

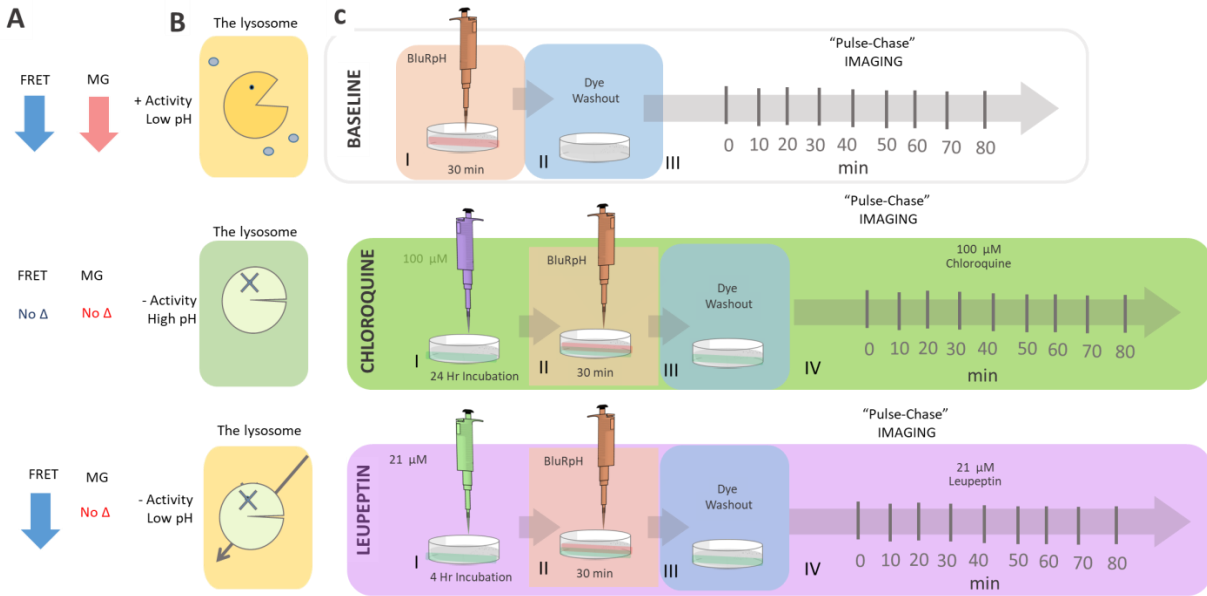


Figure 7. BluRpH labeled FAP-LAMP1 HEK293 signal over time in different conditions. A) Anticipated changes in FRET and MG signal over overtime in each condition. B) Pictorial display of lysosomal activity and pH. C) Description of methods in each condition.

Baseline:

- I. 500 nM BluRpH dye addition, 30 minute incubation.
- II. Dye washout.
- III. "Pulse-Chase" imaging period. 10 min timepoints for 80 minutes.

Chloroquine

- I. 100 μM chloroquine treatment for 24 hours.
- II. 500 nM BluRpH dye addition, 30 minute incubation.
- III. Dye washout.
- IV. "Pulse-Chase" imaging period in presence of chloroquine. 10 min timepoints for 80 minutes.

Leupeptin

- I. 21 μM Leupeptin treatment for 4 hours.
- II. 500 nM BluRpH dye addition, 30 minute incubation.
- III. Dye washout.
- IV. "Pulse-Chase" imaging period in presence of leupeptin. 10 min timepoints for 80 minutes.

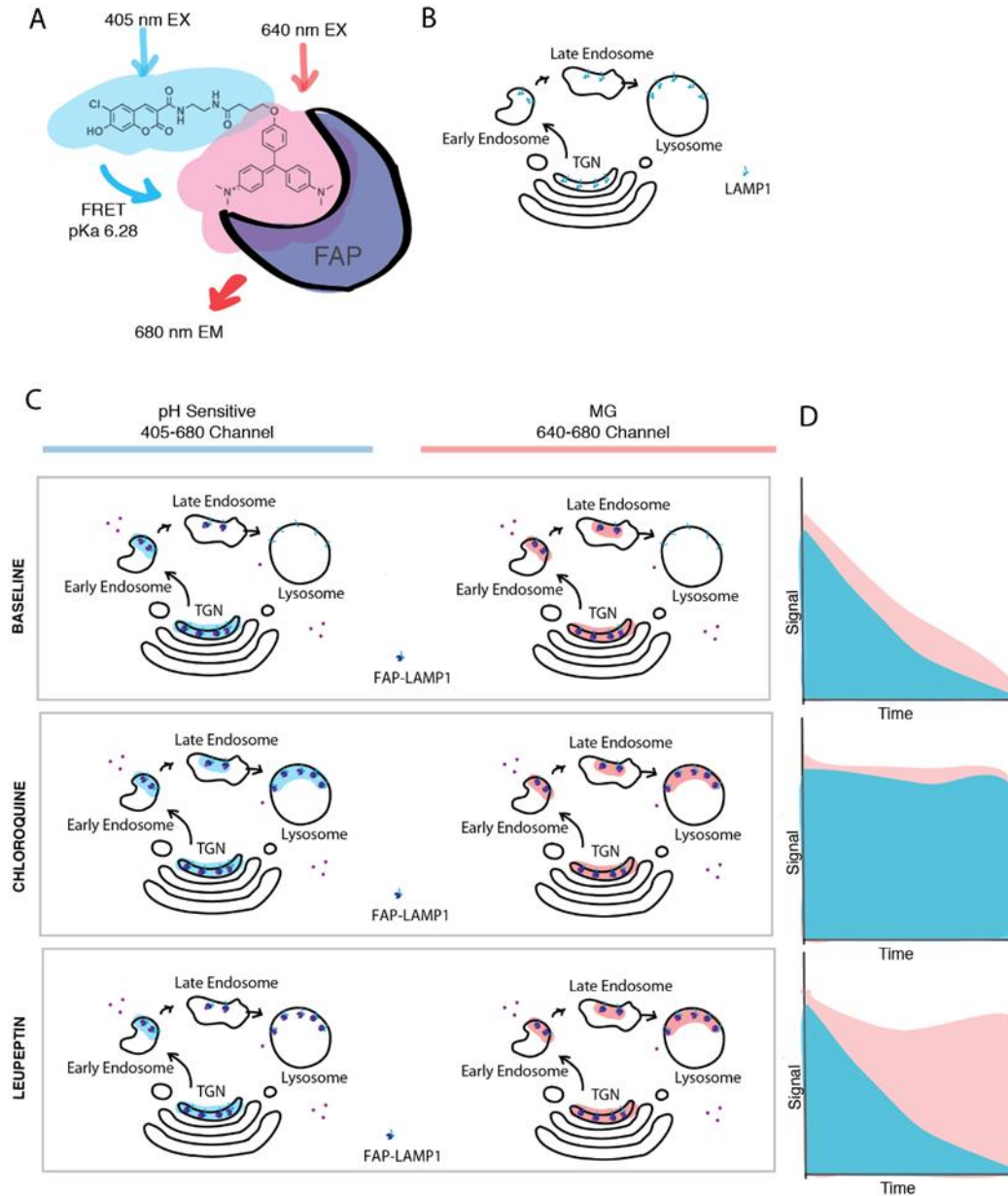


Figure 8. BluRpH and FAP-LAMP1 complex trafficking. A) BluRpH dye uses a pH sensitive coumarin donor (highlighted in blue) that acts as an energy transfer donor to MG (highlighted in pink), resulting in a cell-permeable, ratiometric pH sensor fluorogen. pH sensitive FRET channel: 405 ex/ 680 em. MG channel: 640 ex/ 680 em. B) LAMP1 trafficking itinerary. C) FAP-LAMP1 trafficking with anticipated fluorescence in the 405 ex pH sensitive coumarin FRET channel, and the 640 ex MG channel in different conditions, baseline, 24 hr 100 μ M Chloroquine, and 4 hr 21 μ M Leupeptin. D) Example FRET (blue) and MG (pink) signal over time in each condition.

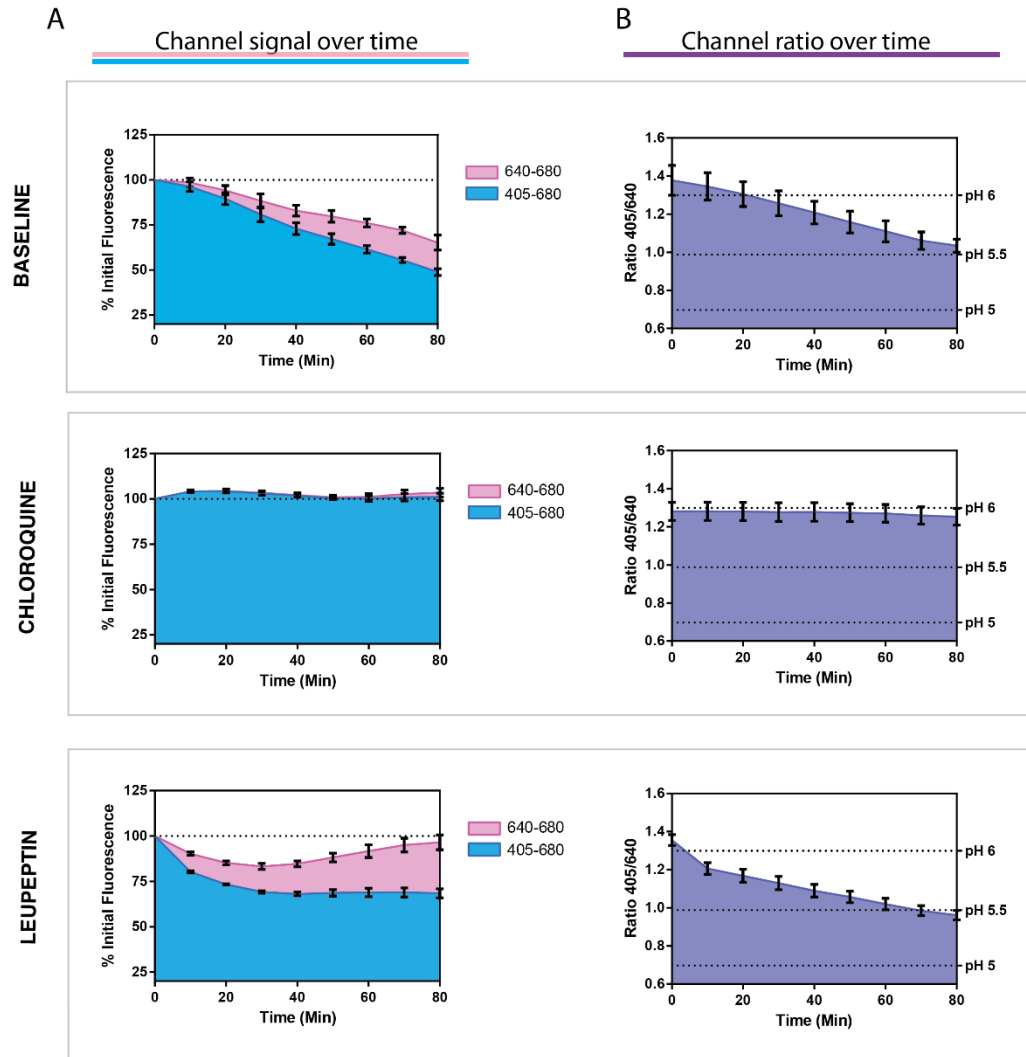


Figure 9. BluR_{pH} labeled FAP-LAMP1 HEK293 signal over time with lysosomal inhibition. A) % initial fluorescence intensity in 405-690 pH sensitive FRET channel and 640-680 MG channel over time in different conditions (Baseline, 24 hr 100 μ M Chloroquine, and 4 hr 21 μ M Leupeptin B) ratiometric pH associated measurement over time. Determined ratio by dividing 405 coumarin FRET signal by 640 MG. Data is presented as average and error bars at S.E.M.

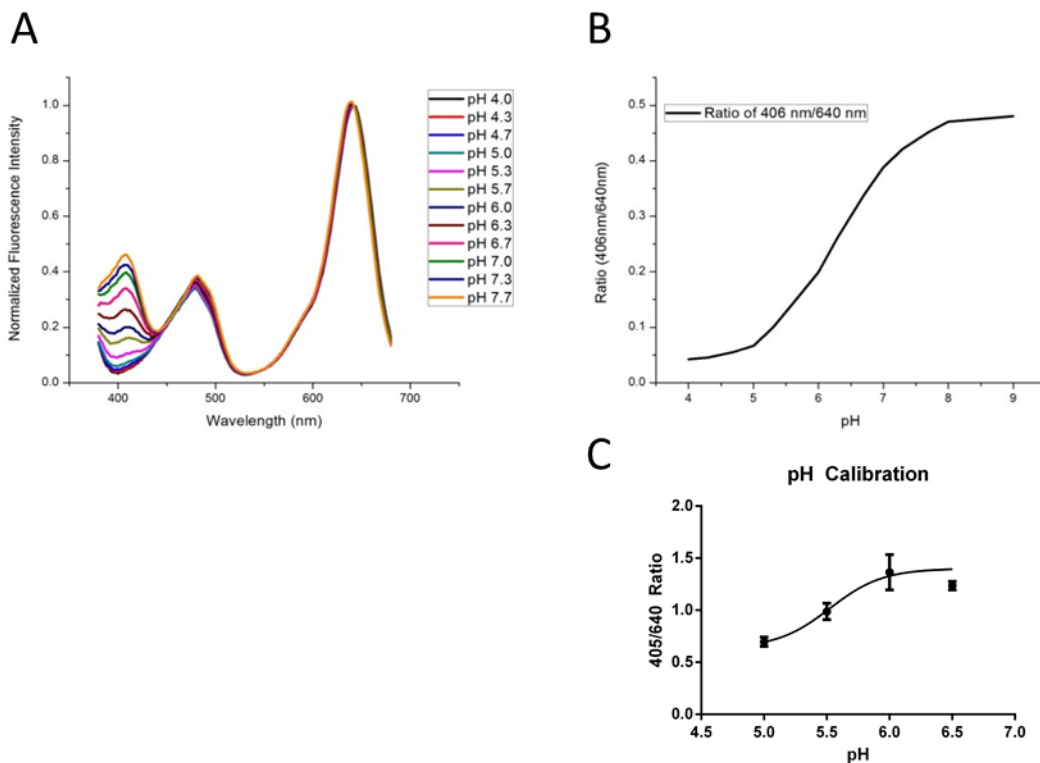


Figure 10. BluRpH pH calibration. A) In vitro excitation titration of BluRpH-dL5** in different pH buffers. B) In vitro ratio of 406 nm/640 nm plotted against pH. C) in vivo ratio 405/640 nm plotted against pH. A,B figures adapted from [Matharishwan Naganabu](#) thesis.

Figure 9a results are similar to what was proposed in Figure 8d. Baseline shows a strong linear decrease in fluorescence in both channels. The baseline linear correlation coefficients are 640-680 $R^2=0.80$; 405-680 $R^2=0.91$. Chloroquine prevented any loss in signal as anticipated with raised pH. By only inhibiting proteolysis with leupeptin incubation, 405-680 signal resembled more of an exponential decay trend, and MG signal fluctuated. The fluctuation could be due to Zeiss red channel autofocus changes at these time points, however more experimental replicates are required overall. To measure trafficking related pH changes over time, we divided the pH sensitive signal by MG signal for a ratiometric pH report. The ratiometric signal was pH calibrated in vitro and in vivo with the nigericin clamping method using different pH solutions (Figure 10). (Chow and Hedley, 2001) Figure 9b demonstrates the pH changes in each condition over time. All graph time point 0 hr measurements start \sim pH 6. Baseline had a linear decrease in pH, suggestive of forward trafficking from biosynthetic into acidic compartments, and leupeptin treatment also exhibits a similar trend, however it was only half a unit pH change in both conditions. Introducing longer time point measurements might show when majority of signal is in $<$ pH 5 lysosomal compartments. Albeit, baseline may never report \leq pH 5 measurements due to quick loss of signal in lysosomal compartments. In figure 9b., chloroquine treatment shows no changes in pH.

Recently another chemist in the Bruchez lab, [Dmytro Kolodieznyi](#), developed a new dye (an azetidiny-modified MG-ester analog, AMG-ester, 640 ex/680 em). AMG-ester could be used to eliminate

the need for lysosomal inhibition or dye washout. Because of changes in the carbinol-chromophore equilibrium, the AMG-ester probe is almost completely decolorized at neutral and basic pH, and colorized in acidic conditions. In colorized form is only when it can bind to FAP. While we found that MG-ester, BluRpH, and a new permeable dye, MGnBu, only exhibits significant lysosomal colocalization after lysosomal inhibition, or with pulse-chase labeling to decrease the pool visible in the biosynthetic pathway, this is not the case with AMG-ester. With a 1 hour incubation of 800nM AMG-ester, FAP-LAMP1 was colocalized with LysoTracker green (Figure 9). Further studies will assess colocalization with giantin labeling to determine if there is any significant labeling of FAP-LAMP1 in the biosynthetic pathway. This new dye is ideal for specific lysosomal FAP-LAMP1 labeling without needing additional steps. Future work will involve AMG-ester pulse-chase labeling to see if the dye signal also decreases overtime, indicating FAP degradation further. Initial experiments and planning were done together with Dymtro, but he is now independently continuing this project.

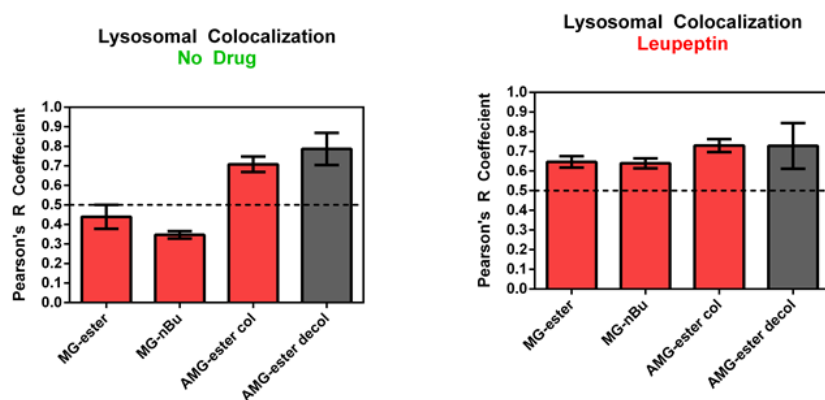


Figure 11. FAP-LAMP1 colocalization with lysotracker green with different cell permeable dyes. FAP-LAMP1 expressing cells were labeled for one hour in the presence of 800 nM of the respective dye: MG-ester, MGnBu, and AMG-Ester colorized or decolorized. Colorized AMG-ester is stock dye in acidic suspension, whereas decolorized dye has been previously suspended in a neutral solution at a known concentration. Only AMG-ester is highly colocalized with LysoTracker green without any drug treatment. Treating cells for 4 hours with 21 μ M leupeptin promoted lysosomal colocalization with MG-ester and MGnBu. Data is presented as average and error bars at S.D.

DISCUSSION AND FUTURE DIRECTIONS: We have established FAP-LAMP1 as a new construct to the inventory of FAP tagged proteins. The combination of BluR_{pH} and FAP-LAMP1 could be applied for measuring trafficking efficiency from TGN to lysosome, or as a prospective tool for observing lysosomal activity through fluorescence decay. FAP-LAMP1 can also be used as a lysosomal marker with sufficient prior lysosomal activity inhibition. This has been just one example of a potential fluoromodule approach. AMG-ester can also be used as a tool for simplified, specific acidic lysosomal labeling.

The Bruchez lab has another tagged lysosomal construct created by Cheryl Telmer. The lysosomal associated protein (LAP) also only requires the cytoplasmic peptide domain, allowing for the FAP tag to replace the luminal tail. Unlike LAMP1, LAP has a more complex and longer trafficking time frame. FAP-LAP is more difficult to validate due to being trafficking to the cell surface, where it goes through several rounds of recycling, and can remain at the plasma membrane for 4-5 hours before being delivered to the lysosome. (Braun et al., 1989) Future work with LAP will be to establish the construct's trafficking itinerary and considering its use as a tool for investigating lysosomal trafficking. We can take advantage of its temporary surface expression by labeling FAP-LAP with the cell impermeable ratiometric pH sensor probe, Cy3(S/SA)pH-MG (Perkins et al., 2018), that could measure trafficking through pH changes.

METHODS:

Plasmid and Cell Line Generation: For the generation of the FAP-LAMP1 construct, overlap PCR was used to construct the transmembrane domain and cytoplasmic tail for Human LAMP1 (NM_005561.3). This fragment was cloned into pcDNA3.1-kappa-myc-dL5-G4S using AgeI and XhoI (Telmer et al. 2015.)

Construct sequence information:

DNA sequence

```
gaggagtgtctgctggacgagaacagcatgctgatccccatcgctgtgggtggtgccctggcggggctggcctcatcgtcctcatcgccctacctcgtc  
ggcaggaagaggagtcacgcaggctaccagactatctag
```

Protein sequence

EECLLDENSMLIPIAVGGAL

AGLVLIVLIAYLVGRKRSHA

GYQTI*

Cheryl Telmer created the construct and Yi Wang generated the HEK293 cell line through transfecting HEK293 cells with – the construct followed by drug selection (1 mg ml⁻¹ puromycin, Invitrogen) and FACS enrichment of MG-ester stained cells (Becton Dickinson FACS Vantage flow cytometer. Excitation: 633 nm; emission: 685/35 nm).

Cell Culture: FAP-LAMP1 expressing HEK293 cells were cultured in Dulbecco's Modified Eagle Medium. Cultures were supplied with 10% fetal bovine serum and incubated at 37 °C in 5% CO₂.

MG-ester labeled FAP-LAMP1 colocalization with lysosome: cells plated on coverslips were labeled with cell permeable MG-ester dye (200 nM) in a pulse chase manner followed by glass slide immunostaining.

Cells were washed with PBS and then fixed with 4% PFA for 30 minutes. After fixation, cells were washed 2x with PBS, then incubated in blocking + permeabilization solution (.1% Triton X and 1% FBS in PBS) for 1 hour at room temperature. After incubation, cells were either labeled with primary monoclonal giantin (1:400), PDI (1:500, from the cell signaling endosomal marker antibody sample kit (#12666): Rab7 (1:100), EEA1 (1:200), clathrin H (1:50), caveolin (1:400), Rab5 (1:200), Rab11 (1:100) antibodies (Molecular Signaling) in blocking solution for 1 hour. After primary incubation, cells were washed 3x with PBS and then incubated with secondary antibody anti-rabbit Alexa 488 (1:1000) (abcam) in blocking solution for 30 minutes (Also with Hoechst stain) and washed 3x with PBS. Coverslips were mounted to slides and kept at 4°C. Slides were imaged with LSM 880 confocal (Zeiss) using a PlanApo 63x, 1.40 NA objective. Rab5 and Rab11 images were collected on Andor Revolution XD system (Andor technology) with a Yokogawa CSU-X1 spinning disk confocal unit (Yokogawa Industries). Cells were imaged with a 60x, 1.49 TIRF objective (Nikon). Colocalization was measured in Imaris.

Initial Investigation with MG-ester signal decay and chloroquine rescue: Cells were plated on Mattek dishes (MatTek Corp.) and dosed with 100 μM chloroquine for designated hours, before being labeled with 200 nM MG-ester for 5 min + dye washout. Imaging was done on wide field NikeTiE using a 40x .95 NA objective.

BluRph labeled FAP-LAMP1 imaging and imaging Analysis:

500 nM BluRph was incubated with cells in Mattek dishes (MatTek Corp.) for 30 min prior to imaging. After incubation, dye was washed out and replaced with Opti-MEM (Invitrogen). Imaged 5 different fields in presence of 5% CO₂ in 37 °C, humidity chamber for 80 min on Zeiss LSM 880 confocal using a PlanApo 63x, 1.40 NA objective. Used average fluorescence for whole frame image.

pH Calibration with Nigericin Clamping in Vivo: Nigericin calibration buffers contained 140 mM KCl, 5 mM α -D-glucose, 2 mM $\text{CaCl}_2 \cdot 2\text{H}_2\text{O}$, 1 mM MgCl_2 and the pH (pH 5 to pH 8) of the mixture was adjusted using 20 mM MES and 20 mM Tris base, where MES and Tris base were added in different ratios to generate different pH buffers. (Chow and Hedley, 2001) Cells were treated with the calibration buffer with 10 μM Nigericin (Sigma) for 10 min prior to imaging with 500 nM BlurpH

pH Calibration in Vitro: Excitation Spectra: Dyes with 5-fold excess of dL5 were precomplexed in pH buffers from pH 5 to pH 9 keeping sample absorption below 0.4 at main absorption peaks. Excitation scan was performed from 400 nm to 680 nm with the emission recorded at 710 nm and measured on a TECAN Infinite M1000 fluorescence plate reader.

AMG-ester labeled FAP-LAMP1 imaging: Cells were plated in an 8-well slide chamber (ibidi), and wells were dosed with either 800 nM MG-ester, MGnBU, and AMG-Ester colorized or decolorized for 1 hour before imaging with lysotracker green in HBSS. For leupeptin treatment, cells were plated in an 8-well slide chamber, and wells were treated with 21 μM leupeptin for 4 hours before being labeled with each dye for 1 hour prior it imaging with Lysotracker green in HBSS. Imaging was done on Andor Revolution XD system (Andor technology) with a Yokogawa CSU-X1 spinning disk confocal unit (Yokogawa Industries). Cells were imaged with a 60x, 1.49 TIRF objective (Nikon). Colocalization was measured using Imaris.

In Vitro BlurpH Excitation Spectra: 1 μM dye and 5 μM dL5**. Emission wavelength was set to 700 nm. spectra have been normalized to the peak with the highest fluorescence intensity. Matharishwan Naganbabu

REFERENCES:

- Braulke, T., and Bonifacino, J.S. (2009). Sorting of lysosomal proteins. *Biochim. Biophys. Acta - Mol. Cell Res.* 1793, 605–614.
- Chow, S., and Hedley, D. (2001). Flow Cytometric Measurement of Intracellular pH. *Curr. Protoc. Cytom.* 1–10.
- Cook, N.R., Row, P.E., and Davidson, H.W. (2004). Lysosome associated membrane protein 1 (Lamp1) traffics directly from the TGN to early endosomes. *Traffic* 5, 685–699.
- Costantini, L.M., and Snapp, E.L. *Fluorescent Proteins in Cellular Organelles: Serious Pitfalls and Some Solutions.*
- Eskelinen, E.-L. (2006). Roles of LAMP-1 and LAMP-2 in lysosome biogenesis and autophagy. *Mol. Aspects Med.* 27, 495–502.
- Huang, L., Pike, D., Sleat, D.E., Nanda, V., and Lobel, P. (2014). Potential pitfalls and solutions for use of fluorescent fusion proteins to study the lysosome. *PLoS One* 9, e88893.
- Huynh, K.K., Eskelinen, E.-L., Scott, C.C., Malevanets, A., Saftig, P., and Grinstein, S. (2007). LAMP proteins are required for fusion of lysosomes with phagosomes. *EMBO J.* 26, 313–324.
- Liu, B., Xie, C., Richardson, J.A., Turley, S.D., and Dietschy, J.M. (2007). Receptor-mediated and bulk-phase endocytosis cause macrophage and cholesterol accumulation in Niemann-Pick C disease. *J. Lipid Res.* 48, 1710–1723.
- Obermüller, S., Kiecke, C., von Figura, K., and Höning, S. (2002). The tyrosine motifs of Lamp 1 and LAP determine their direct and indirect targeting to lysosomes. *J. Cell Sci.* 115, 185–194.
- Peters, C., Braun, M., Weber, B., Wendland, M., Schmidt, B., Pohlmann, R., Waheed, A., and Figura, K. Von (1990). necessary and sufficient for targeting to lysosomes *S* . 9, 3497–3506.
- Pierzyńska-Mach, A., Janowski, P.A., and Dobrucki, J.W. (2014). Evaluation of acridine orange, LysoTracker Red, and quinacrine as fluorescent probes for long-term tracking of acidic vesicles. *Cytom. Part A* 85, 729–737.
- Pryor, P.R. (2012). *Analyzing lysosomes in live cells* (Elsevier Inc.).
- Repa, J.J., and Mangelsdorf, D.J. (2000). The Role of Orphan Nuclear Receptors in the Regulation of Cholesterol Homeostasis. *Annu. Rev. Cell Dev. Biol.* 16, 459–481.
- Rohrer, J., Schweizer, A., Russell, D., and Kornfeld, S. (1996). The targeting of lamp1 to lysosomes is dependent on the spacing of its cytoplasmic tail tyrosine sorting motif relative to the membrane. *J. Cell Biol.* 132, 565–576.

Schoneberg, T., Liu, J., and Wess, J. (1995). Plasma membrane localization and functional rescue of truncated forms of a G protein-coupled receptor. *J Biol Chem* 270.

Schröder, B., Wrocklage, C., Pan, C., Jäger, R., Kösters, B., Schäfer, H., Elsässer, H.-P., Mann, M., and Hasilik, A. (2007). Integral and Associated Lysosomal Membrane Proteins. *Traffic* 8, 1676–1686.

Snapp, E.L., Hegde, R.S., Francolini, M., Lombardo, F., Colombo, S., Pedrazzini, E., Borgese, N., and Lippincott-Schwartz, J. (2003). Formation of stacked ER cisternae by low affinity protein interactions. *J. Cell Biol.* 163, 257–269.

Szent-Gyorgyi, C., Schmidt, B.F., Creeger, Y., Fisher, G.W., Zakel, K.L., Adler, S., Fitzpatrick, J.A.J., Woolford, C.A., Yan, Q., Vasilev, K. V, et al. (2008). Fluorogen-activating single-chain antibodies for imaging cell surface proteins. *Nat Biotech* 26, 235–240.

Telmer, C.A., Verma, R., Teng, H., Andreko, S., Law, L., and Bruchez, M.P. (2015). Rapid, specific, no-wash, far-red fluorogen activation in subcellular compartments by targeted fluorogen activating proteins. *ACS Chem. Biol.* 10, 1239–1246.

Wenger, D.A., Coppola, S., and Liu, S.-L. (2003). Insights Into the Diagnosis and Treatment of Lysosomal Storage Diseases. *Arch. Neurol.* 60, 322.

CHAPTER V

Down the Road

On the Drug Discovery Route

Seeing the Results

Most of the drugs available only modify the activity of target cell surface proteins. (Bleicher et al., 2003) There is an unmet market for novel therapeutic strategies that can specifically address diseases that arise from trafficking defects and strategies that modulate dysfunctional activity through manipulating bioavailability at the cell surface. Drug discovery has been akin to searching a big black box, where researchers hope to find a compound or target, a “hit,” that has a desirable effect on a specific disease state. One of the most common methods of detecting a target effect is through using tools to measure changes in protein activity. Such activity screens are efficient in comparison to tools that measure the fraction of protein expression at the cell surface, which are labor-intensive and time-consuming. *We have addressed these limitations through developing tools that allow fast, specific fluorescent labeling, which can readily measure the fraction of protein at the cell surface.*

The early stages of drug discovery are centered on identifying a protein target or pathway, that when inhibited or activated produces a therapeutic effect in a disease state. *This identification stage often occurs in academia, and our lab has been focused on building FAP assay platforms as a foundation for generating lists of protein target candidates.* I have described several examples of FAP systems that have been developed for addressing specific protein trafficking experimental needs. These platforms provide a proof-of-concept for FAP based assay strategies that can be easily scalable to screens, having both established basic test-bed assays and showing examples of designed HT protocols. These developed approaches are primed for being used full throttle in protein trafficking screens. Our lab has been able to conduct a small HT screens in-house, as MBIC has begun laying groundwork to grow as a HT core facility being equipped with, a HT Accuri flow-cytometer, plate readers, HTS Nikon imaging software with a Nikon widefield microscope, and VIAFLO multichannel semiautomatic pipettor. (Perkins et al.) We can extend our opportunities and technology use by participating in screening collaborations with other biomedical labs and facilities- and have already started, with the University of Pittsburgh School of Medicine adapting FAP technology to their own high content screening methods (Larsen et al., 2016). Sharp Edge Labs and SpectraGenetics, Inc. have also commercialized FAP technology and used their respective resources to develop tactics for protein trafficking HT screens relating to cystic fibrosis, lysosomal disorders, GPCRs, and Parkinson’s disease. Recently, Sharp Edge Labs has worked with Proteostasis Therapeutics, Inc. to provide CFTR cell surface measurements in a HT screen. (Giuliano et al., 2018) In the near future, both in academia and industry, we will be looking forward to an increase of HT screening publications that use fluorogen activating modules as key methods.

Potential Lab Studies on Protein Trafficking

This is an exciting time to be seeing the fruits of our labor from developed strategies and assays, and also to boost our own biological output. One potential avenue for the Bruchez lab is a proposed screening project that involves **identifying targetable proteins that can control the cell surface expression of select disease-associated cell surface protein classes (such GPCRs and ion channels) in order to develop potential drug targets.** (Figure 1.)

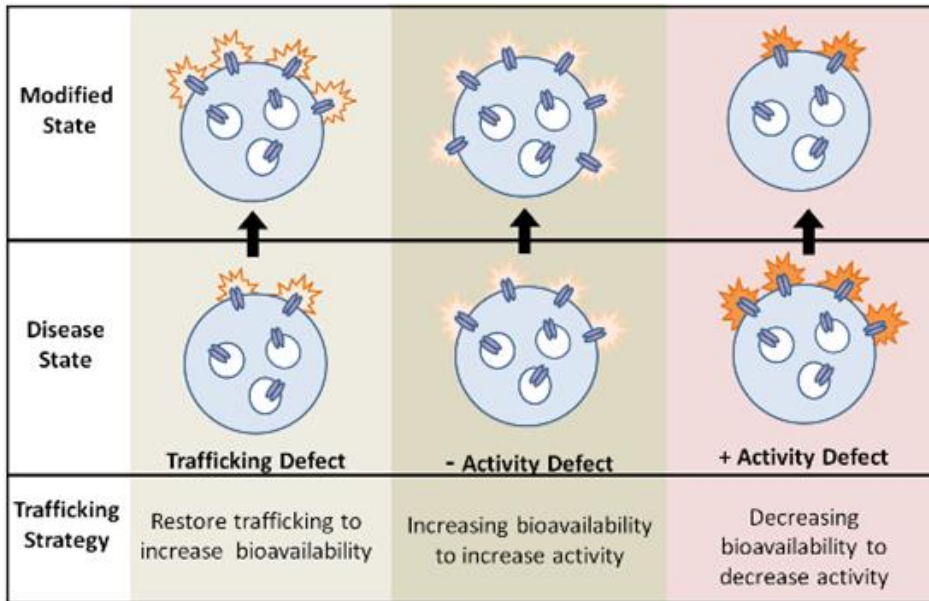


Figure 1. Therapeutic strategies targeting trafficking to treat specific disease states.

Ion Channels: With classical pharmacological approaches, drug targets have been difficult to find for ion channels due to the large potential for toxicity and unspecific blocking interactions with different ion channels, which can lead to serious complications.(Kaczorowski et al., 2008) **Instead of directly targeting ion channels to change their activity, we can seek to indirectly change their behavior through modulating surface expression.** The concept of changing trafficking in ion channels has been present for nearly a decade, when research revealed drugs that were designed to block Kv1.5 (hERG) current actually disrupted hERG trafficking to the cell surface. These “anti-arrhythmic” drugs were discovered to ultimately cause pro-arrhythmia due to causing a repolarization disorder like the hERG trafficking defect mutant.(Eckhardt et al., 2005) Despite these undesirable consequences, Schumacher et al. highlighted the potential avenue for manipulating anterograde or retrograde trafficking to safely modulate the acute surface expression of ion channels. (Schumacher and Martens, 2010) While our research will only highlight factors that decrease or increase cell surface expression of ion channels, there is potential for chemotherapeutics to target these factors and acutely change expression. For example, a target which can increase retrograde transport without affecting recycling would only induce a temporary change in surface density. With further validation of factors that modulate trafficking, those that are involved in the endosomal network may have an acute response.

GPCRS: Numerous approaches have been developed to improve GPCR bioavailability in heterologous cells. These approaches have included adding sequences to the N or C-terminus, deleting sequences that promote ER retention or induce protein misfolding, co-expressing other proteins to enhance trafficking, and treatment with compounds that act as pharmacological chaperones. (Dunham and Hall, 2009) Cell permeable pharmacologic chaperones have proven to be a powerful tool to enhance bioavailability due to their potential clinical application. These compound chaperones present therapeutic strategies for treating diseases associated with GPCR trafficking defects, analogous to corrector treatment in ion channel trafficking defective diseases. In addition, an exciting therapeutic opportunity is to use molecular chaperones to increase opioid receptors cell surface density to minimize desensitization, which would reduce drug tolerance and addiction. However, more studies are needed to conclude if pharmacological chaperone binding causes an antagonistic effect on GPCR activity at the cell surface and interferes with homo/heteromeric binding, which may affect function. (Petäjä-Repo and Lackman, 2014) *In this project, we would aim to accomplish the same goal of pharmacologic chaperones in encouraging plasma membrane expression, but through targeting the cells endogenous machinery.* Cell permeable pharmacologic chaperones have proven to be a powerful tool to enhance bioavailability due to their potential clinical application. These compound chaperones present therapeutic strategies for treating diseases associated with GPCR trafficking defects, analogous to corrector treatment in ion channel trafficking defective diseases. In addition, an exciting therapeutic avenue is to use molecular chaperones to increase opioid receptors cell surface density to minimize desensitization, which would reduce drug tolerance and addiction.

As previously mentioned, we have also started to include a new FAP construct to expand our protein trafficking measurement capabilities inside the cell for detecting lysosomal protein delivery. The overall development of a lysosomal based FAP platform may provide a new method for therapeutic drug screens for diseases caused by aberrant lysosomal trafficking, such as Niemann Pick C.

Adventuring into such screens would further broadcast the capability of FAP technology and contribute to adding potential drug targets on the list for therapeutic contenders for different diseases.

Advancing the Tools

There are different areas to grow, conquering current challenges that can turn into great opportunities.

- Discussed were difficulties with protein over-expression with FAP-LAMP1 by using a CMV promoter. Incorporating the new Clustered Regularly Interspaced Short Palindromic Repeats (CRISPR)(Cong et al., 2013) CRISPR-Cas9 would aid in making precise insertions of tagged proteins of interest and manage consistent stable cell-lines with suitable expression. This has been shown as an efficient, cheap, and successful approach with tagging the cytoskeletal protein, tubulin (*TubA1B*), with mEGFP and mEos 3.2. for super-resolution microscopy imaging. (Khan et al., 2017)
- The current developed dL5** MG dyes have subnanomolar Kds, taking hours for dye dissociation. Developing new dyes with higher Kds would be a powerful tool for creating dynamic assays and pulse-chase labeling strategies.
- The lab has recently developed a photosensitizer, light activated MG-2i reactive oxygen species (ROS) generating dye, that can exhibit cellular ablation.(He et al., 2016) In addition to cellular photoablation, I propose a rough idea that this platform, known as FAP-TAPs, use could also be used as a “phototrigger”.

Cancer nanomedicine utilizes drug delivery methods that rely on on-demand spatial and temporal release of chemotherapeutics from nanoparticle carriers. In particular, using external stimuli from either, light, heat, or magnetic field, to induce disruption of liposome membranes for drug release.(Puri and Anu, 2013) Phototriggerable synthetic lipids have been used as a method to destabilize liposomes. However, photosensitive lysosomes have been clinically limited by the activating light sources ability to penetrate biological tissues. FAP-TAPS use far-red excitation that improves the in-vivo applicability. A novel approach would be to create liposomes that comprise transmembrane FAPs and specific cell targeting features. In addition to the FAP-TAPs being a photodynamic therapy, this liposome complex could potentially be used as a drug carrier that will only release its contents based on the presence of dye and light, which would be designed to be specific to cancer cells and the surrounding area.

I have only presented a brief and narrow perspective of the many different directions the lab can take to advance the current toolbox. The group has interests in developing more super-resolution imaging techniques, using FRET pairs to detect specific protein localization/interaction and cell to cell contacts, and establishing a high-throughput synapse-specific detection paradigm. The development we should expect to see and produce is exciting as FAP tools are increasingly being used by different labs to address specific biological problems. The breadth of the technology potential presents many opportunities for several different future directions.

REFERENCES:

- Bleicher, K.H., Böhm, H.-J., Müller, K., and Alanine, A.I. (2003). Hit and lead generation: beyond high-throughput screening. *Nat. Rev. Drug Discov.* 2, 369–378.
- Cong, L., Ran, F.A., Cox, D., Lin, S., Barretto, R., Habib, N., Hsu, P.D., Wu, X., Jiang, W., Marraffini, L.A., et al. (2013). Multiplex genome engineering using CRISPR/Cas systems. *Science* 339, 819–823.
- Dunham, J.H., and Hall, R. a. (2009). Enhancement of the surface expression of G protein-coupled receptors. *Trends Biotechnol.* 27, 541–545.
- Eckhardt, L.L., Rajamani, S., and January, C.T. (2005). Protein trafficking abnormalities: a new mechanism in drug-induced long QT syndrome. *Br. J. Pharmacol.* 145, 3–4.
- Giuliano, K.A., Wachi, S., Drew, L., Dukovski, D., Green, O., Bastos, C., Cullen, M.D., Hauck, S., Tait, B.D., Munoz, B., et al. (2018). Use of a High-Throughput Phenotypic Screening Strategy to Identify Amplifiers, a Novel Pharmacological Class of Small Molecules That Exhibit Functional Synergy with Potentiators and Correctors. *SLAS Discov. Adv. Life Sci. R&D* 23, 111–121.
- He, J., Wang, Y., Missinato, M.A., Onuoha, E., Perkins, L.A., Watkins, S.C., St Croix, C.M., Tsang, M., and Bruchez, M.P. (2016). A genetically targetable near-infrared photosensitizer. *Nat. Methods* 13, 263–268.
- Kaczorowski, G.J., McManus, O.B., Priest, B.T., and Garcia, M.L. (2008). Ion channels as drug targets: the next GPCRs. *J. Gen. Physiol.* 131, 399–405.
- Khan, A.O., Simms, V.A., Pike, J.A., Thomas, S.G., and Morgan, N. V. (2017). CRISPR-Cas9 Mediated Labelling Allows for Single Molecule Imaging and Resolution. *Sci. Rep.* 7, 8450.
- Larsen, M.B., Hu, J., Frizzell, R.A., and Watkins, S.C. (2016). Simple image-based no-wash method for quantitative detection of surface expressed CFTR. *Methods* 96, 40–45.
- Perkins, L.A., Fisher, G.W., Naganbabu, M., Schmidt, B.F., Mun, F., and Bruchez, M.P. High-Content Surface and Total Expression siRNA Kinase Library Screen with VX-809 Treatment Reveals Kinase Targets that Enhance F508del-CFTR Rescue.
- Petäjä-Repo, U.E., and Lackman, J.J. (2014). Targeting opioid receptors with pharmacological chaperones. *Pharmacol. Res.* 83, 52–62.
- Puri, A., and Anu (2013). Phototriggerable Liposomes: Current Research and Future Perspectives. *Pharmaceutics* 6, 1–25.
- Schumacher, S.M., and Martens, J.R. (2010). Ion channel trafficking: a new therapeutic horizon for atrial fibrillation. *Hear. Rhythm* 7, 1309–1315.